

# **Controlled Branching of Industrially Important Polymers: Modeling and Multi-objective Optimization**

Anitha Mogilicharla

A Dissertation Submitted to  
Indian Institute of Technology Hyderabad  
In Partial Fulfillment of the Requirements for  
The Doctor of Philosophy



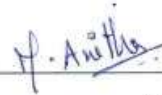
भारतीय प्रौद्योगिकी संस्थान हैदराबाद  
Indian Institute of Technology Hyderabad

Department of Chemical Engineering

August, 2014

## Declaration

I declare that this written submission represents my ideas in my own words, and where others' ideas or words have been included, I have adequately cited and referenced the original sources. I also declare that I have adhered to all principles of academic honesty and integrity and have not misrepresented or fabricated or falsified any idea/data/fact/source in my submission. I understand that any violation of the above will be a cause for disciplinary action by the Institute and can also evoke penal action from the sources that have thus not been properly cited, or from whom proper permission has not been taken when needed.



---

(Signature)

---

( Anitha Mogilicharla )

---

(CH10P003)

## Approval Sheet

This thesis entitled “Controlled Branching of Industrially Important Polymers: Modeling and Multi-objective Optimization” by Anitha Mogilicharla is approved Doctor of Philosophy from IIT Hyderabad.

  
Prof. Ravindra D Gudi

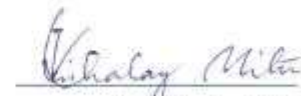
Examiner

  
Dr. Parag D. Pawar

Examiner

  
Dr. Saptarshi Majumdar

Adviser

  
Dr. Kishalay Mitra

Co-Adviser

  
Dr. Raja Banerjee

Chairman

## **Acknowledgements**

I take this opportunity to express my deep sense of gratitude to Dr. Saptarshi Majumdar and Dr. Kishalay Mitra for their constant inspiration, support and encouragement given to me. I would like to express my heartfelt thanks to them for their guidance and continuous support throughout my stay at IITH. Working on this project was an excellent opportunity for me.

I would like to thank my doctoral committee members, Dr. Vinod M Janardhanan, Dr. Sunil Kumar Maity, Dr. Parag Pawar and Dr. Raja Benerjee for their insightful comments and valuable suggestions. My special thanks to Prof. U. B. Desai (Director, IITH) for providing good research environment.

I consider myself fortunate to have nice friends at IITH. In fact it was their support, and love made that my stay memorable and delightful here. To list them is a Herculean task. Special thanks to Vandana, Naga Jyothi, Tinkle Chugh, Prateek Mittal, Vimala, Prasanna, Anindita, Pinaki, Utkarsh.

These words and space are not real tribute to the blessings and countless sacrifices of my parents. Whatever I am today it is their encouragement and unseen prayer of silence at God for me. My deepest gratitude goes to my husband S K V Prasad, for his support, patience and constant understanding, and to my daughter, Deetyasri, whose love are always my stimulus for life. I am very thankful to all my family members for their support.

Dedicated to

My Husband, S K V Prasad.

## Abstract

Long chain branching (LCB) in any polymerization is of profound importance. It helps in improving certain properties such as melt strength and strain hardening. Branched polymers are, therefore, having different characteristics than linear polymers. In addition to having good end use properties, they are well suited for various processing applications such as blow molding, thermoforming, extrusion coating etc. As real world applications demand different extents of branching of polymers for different applications, this study aims to perform an investigation for a controlled way of long chain branching of polymers with enhanced properties.

The main goal of this research is, therefore, three fold; viz. i) Finding the optimal process conditions for the desired combination of conflicting objectives, ii) Development of a kinetic model for long chain branched polypropylene system based on the available experimental data from open literature and simultaneously performing the multi objective optimization for the desired combination of conflicting performance objectives within experimental limits, and iii) Development of Kriging based surrogate model to replace the first principles based computationally expensive model to save execution time, while performing the multi objective optimization task for a highly non-linear, multi-modal search space.

First, a batch optimization study for the bulk polymerization of vinyl acetate has been considered to find optimal process conditions for imparting LCB in polymer architecture. A theoretical study has been conducted with a validated model to observe the effect of live radical concentration on long chain branching as this is an important factor for branching in polymer molecule via ‘chain transfer to polymer’ route. In order to obtain better polymer product in less time at various temperatures, a need was observed to perform a multi-objective optimization study as the selected objectives were conflicting in nature. Owing to the complex nature of moment based species balance equations and molecular weight distribution function, elitist non-dominated sorting genetic algorithm (NSGA II), a well-established multi-objective evolutionary algorithm, has been employed as an evolutionary optimization method to generate the Pareto optimal (PO) solutions. Objectives such as (i) minimization of

gel point conversion time, (ii) maximization of molecular weight and (iii) maximization of number average degree of branching ( $B_n$ ), can be simultaneously achieved, where the solutions were obtained within the experimental range of polydispersity index (PDI) and weight average molecular weight ( $M_w$ ) given in the open literature. Results show a wide range of process choices satisfying process objectives and constraints, both in low as well as high temperature regions.

Polypropylene (PP) is world's second largest industrial polymer and has potential to replace many non-biocompatible polymers in several applications. LCB in PP is one of the possible ways of customizing its properties for new applications. Unfortunately, to the best of our knowledge there is no validated mechanism for incorporation LCB in PP. Unlike polyethylene, PP is far difficult a candidate for LCB incorporation as well. In this thesis, a kinetic model has been proposed to describe the propylene polymerization process with long chain branching for a twin catalyst system to fit the experimental findings available in open literature for molecular weights, polydispersity index of atactic polypropylene, isotactic polypropylene and grafting density at different catalyst, cocatalyst concentrations. Kinetic parameters are estimated by real coded genetic algorithm (another evolutionary optimization technique) from the same set of experimental data. The validated model has the capability of predicting the branching density as a function of catalyst addition pattern, catalyst ratios and copolymerization time within experimental limits. Further, the validated model has been used to calculate the molecular weight long chain branching distribution. Parametric sensitivity study has also been conducted to analyze the effect of kinetic parameters on the long chain branching formation and other molecular properties of the polymer. Pareto optimal solutions for long chain branched polypropylene with the binary catalyst system are obtained by adapting non-dominated sorting genetic algorithm for a particular multi-objective setup. The optimization objective is to produce polymer having high molecular weight and grafting density (expressed as number of macromonomers per 1000 backbone monomer units) in minimum polymerization time. Addition amounts of two catalysts and cocatalyst, second catalyst addition time and total polymerization time are taken as decision variables with relevant process constraints (taken from experimental conditions and findings) that take care of model validity

over prescribed operating range. A wide variety of process choices have been obtained for the optimization set up which shows betterment in process performance.

Despite the established superiority in finding the global and well spread Pareto optimal (PO) points, the need of more numbers of function evaluations for population based evolutionary optimization techniques leads to a computationally demanding proposal. The case becomes more demanding when the function evaluations are carried out using a first principle based computationally expensive model, making the proposal not suitable for online usage of the application. In this work, a Kriging based surrogate model has been proposed to replace a computationally expensive model to save execution time while performing an optimization task. A multi-objective optimization study has been carried out for the bulk vinyl acetate polymerization with long chain branching using these surrogate as well as expensive models and Kriging PO solutions similar to those found by the first principle models are obtained with a close to 85% savings in function evaluations.



## Nomenclature

aPP	Atactic polypropylene
$b$	Number of branches per molecule
$B_n$	Number average degree of branching
$C_1^H$	Hydride activated complex
$C_2^{Me}$	Methylated catalyst activated complex
cat <sub>1</sub>	First catalyst concentration (mol/L)
cat <sub>2</sub>	Second catalyst concentration (mol/L)
cocat	Cocatalyst concentration (mol/L)
$D_n^j$	Dead polymer chains of length “n” belonging to generation j
$D_n^-$	aPP macromonomer concentration of chain length “n” (mol/L)
$DP_{n,m}$	Number average degree of polymerization of m <sup>th</sup> class polymer chains
$DP_{w,m}$	Weight average degree of polymerization of m <sup>th</sup> class polymer chains
GD	Grafting density
I , [I]	Initiator and initiator concentration, mol/l
iPP	Isotactic polypropylene
LHS	Latin hypercube sampling
$k_{i1}$	Initiation rate constant (L/(mol.min))
$k_\beta$	$\beta$ -H elimination constant (1/min)
$k_{\beta r}$	Reversible chain transfer to metal rate constant (L/(mol.min))
$k_{p1}$	Propagation constant for the first catalyst system (L/(mol.min))
$\alpha k_{lcb}$	Effective long chain branching rate constant (L/(mol.min))
$k_{a2}$	Activation rate constant for the second catalyst system(L/(mol.min))
$k_{i2}$	Initiation rate constant for the second catalyst system (L/(mol.min) )
$k_{p2}$	Propagation rate constant for the second catalyst system (L/(mol.min))
$k_{d2}$	Deactivation rate constant for the second catalyst system (L/(mol.min))
$k_{al}$	Chain transfer to cocatalyst for second catalyst system (L/(mol.min))

$k_{ri1}$	Re-initiation of hydride metal complex (L/(mol.min))
$k_d$	Initiator decomposition rate constant, $\text{min}^{-1}$
$k_{fm}$	Chain transfer to monomer rate constant, L/(mol.min)
$k_{fp}$	Chain transfer to polymer rate constant, L/(mol.min )
$k_{db}$	Terminal double bond rate constant, L/(mol.min)
$k_I$	Initiation rate constant, L/(mol.min)
$k_p$	Propagation rate constant, L/(mol.min)
$k_{tc}$	Termination by combination rate constant, L/(mol.min)
$k_{td}$	Termination by disproportionation rate constant,L/(mol.min)
[M]	Monomer concentration (mol/L)
MISO	Multiple input single output
$M_n$	Number average molecular weight, g/mol
$M_w$	Weight average molecular weight, g/mol
$P_n$	aPP live polymer of chain length ‘n’ (mol/L)
$P_n^j$	Live polymer chains of length “n” belonging to generation j
PDI	Polydispersity index
PO	Pareto optimal
$Q_{n,i}$	iPP copolymer of chain length “n” and “i” long chain branches (mol/L)
$R_{n,i}$	Dead iPP copolymer: Chain length “n” and “i” long chain branches (mol/L)
RAM	Random access memory
RMSE	Root mean square error
$R^2$	Coefficient of determination
$t_p$	Polymerization time (min)
T	Temperature, K
$W_i(n)$	Weight fraction of polymer population of $i^{\text{th}}$ class
$W_{\text{total}}(n)$	Overall weight fraction of polymer population
$\lambda_0$	Zero <sup>th</sup> moment of aPP live polymer (mol/L)
$\lambda_1$	First moment of aPP live polymer (mol/L)
$\lambda_2$	Second moment of aPP live polymer (mol/L)
$\mu_0^-$	Zero <sup>th</sup> moment of aPP macromonomer (mol/L)

$\mu_1^=$	First moment of aPP macromonomer (mol/L)
$\mu_2^=$	Second moment of aPP macromonomer (mol/L)
$\mu_0$	Zero <sup>th</sup> moment of live polymer (mol/L)
$\mu_1$	First moment of live polymer (mol/L)
$\mu_2$	Second moment of live polymer (mol/L)
$\nu_0$	Zero <sup>th</sup> moment of dead polymer (mol/L)
$\nu_1$	First moment of dead polymer (mol/L)
$\nu_2$	Second moment of dead polymer (mol/L)
$\mu_i^j$	i <sup>th</sup> moment of living polymer from j <sup>th</sup> generation (mol/L)
$\nu_i^j$	i <sup>th</sup> moment of dead polymer from j <sup>th</sup> generation (mol/L)
$\mu_{0,m}$	Zero <sup>th</sup> moment of live polymer of m <sup>th</sup> class (mol/L)
$\mu_{1,m}$	First moment of live polymer of m <sup>th</sup> class (mol/L)
$\mu_{2,m}$	Second moment of live polymer m <sup>th</sup> class (mol/L)
$\nu_{0,m}$	Zero <sup>th</sup> moment of dead polymer of m <sup>th</sup> class (mol/L)
$\nu_{1,m}$	First moment of dead polymer of m <sup>th</sup> class (mol/L)
$\nu_{2,m}$	Second moment of dead polymer m <sup>th</sup> class (mol/L)
$\Psi$	Correlation matrix for all observed data
$\psi$	Correlation matrix between new predicted point and old points
$\theta_m$	Spreading coefficient of correlation for monomer
$\theta_i$	Spreading coefficient of correlation for initiator
$\theta_t$	Spreading coefficient of correlation for temperature
$\sigma$	Standard deviation value
$\mu$	Mean value
$\hat{\mu}$	Optimum mean value for which likelihood is maximized

- $\hat{\sigma}$  Optimum standard deviation value for which likelihood is maximized
- $\Phi$  Cumulative distribution function
- $\phi$  Normal density function

# Contents

Declaration.....	<b>Error! Bookmark not defined.</b>
Approval Sheet .....	<b>Error! Bookmark not defined.</b>
Acknowledgements.....	iv
Abstract.....	vi
<b>Nomenclature</b> .....	<b>ix</b>
<b>1 Introduction</b> .....	<b>1</b>
1.1 Motivation.....	1
1.2 Research Objective .....	3
1.3 Organization of Thesis.....	4
<b>2 Literature review</b> .....	<b>6</b>
2.1 Branched polymers .....	6
2.2 Multi-objective Optimization .....	10
2.3 Surrogate Modeling .....	11
2.4 Tendency modeling .....	14
<b>3 Introduction to polymerization techniques, Methods and solver</b> .....	<b>15</b>
3.1 Polymer Theory .....	15
3.1.1 Molecular weight distribution .....	15
3.1.2 Architecture .....	16
3.1.3 Chain growth polymerization.....	17
3.2 Kinetic Scheme and Mathematical model .....	19
3.3 Methods to calculate MWD.....	21
3.3.1 Numerical Fractionation.....	21
3.3.2 Partition according to the number of branches.....	25
3.3.3 Fixed Pivot Technique.....	30
3.4 Solver.....	33
<b>4 Multi-objective Optimization of Bulk Vinyl Acetate Polymerization with Branching</b> .....	<b>35</b>
4.1 Introduction.....	35
4.2 Model.....	36
4.3 Optimization problem formulation .....	38
4.4 Results and discussion .....	44

4.4.1	Model validation.....	44
4.4.2	Optimization.....	47
4.5	Conclusion .....	51
<b>5</b>	<b>Modeling of propylene of polymerization with long chain branching.....</b>	<b>52</b>
5.1	Introduction.....	52
5.2	Model.....	53
5.3	Results and discussion .....	61
5.4	Conclusion .....	71
<b>6</b>	<b>Multi-objective Optimization of Long Chain Branched Propylene Polymerization .....</b>	<b>72</b>
6.1	Introduction.....	72
6.2	Problem Formulation and Optimization Procedure .....	73
6.3	Results and discussion .....	75
6.4	Conclusion .....	85
<b>7</b>	<b>Kriging surrogate based multi-objective optimization of bulk vinyl acetate polymerization with branching .....</b>	<b>86</b>
7.1	Introduction.....	86
7.2	Optimization problem formulation .....	87
7.3	Kriging Model development.....	88
7.4	Results and discussion .....	92
7.5	Conclusion .....	101
<b>8</b>	<b>Conclusions.....</b>	<b>102</b>
8.1	Conclusions.....	102
8.2	Future work.....	104
	<b>References.....</b>	<b>106</b>
	<b>List of publications.....</b>	<b>115</b>
	<b>Appendices.....</b>	<b>117</b>
	Appendix A.....	117
	Appendix B.....	126

# Chapter 1

## Introduction

### 1.1 Motivation

Branched polymers exhibit enhanced polymer processing properties as compared to their linear counterparts of similar molecular weight and this fact provides the former considerable edge over the latter for many practical applications. Branched polymers are characterized by high strain hardening, tensile strength, relaxation time and low density [1]. One such example is polypropylene (PP), which can be preferred over many other thermoplastics (that are currently in use but not bio-compatible) for applications which need light weight and reasonable thermal and chemical resistant properties. Branching in polypropylene, when possible to be introduced in controlled fashion, can have a large impact since PP is the second largest commercially important synthetic polymer in consumption after polyethylene. However, the polypropylene produced by the Ziegler-Natta and metallocene are highly linear [2]. Polymers produced by the former catalyst exhibit good processability due to the multiple active site behavior. But, it has lower mechanical properties [3]. Polymers produced by the latter one exhibit narrow molecular weight distribution (MWD) with good mechanical properties. Due to the poor shear thinning behavior of these polymers, processability is very difficult. After the discovery of constraint geometry metallocene catalyst, branched polyolefin synthesis was made possible due to its unprecedented control over the microstructure of the polymer [4-10]. The unique feature of this catalyst is that it incorporates the macromonomers in to the growing chain to create the branches. The lack of attention in the direct synthesis of long chain branched polypropylene (LCB PP) is due to the limited knowledge of embedded chemistry to produce the LCB PP [11]. To overcome this, various post reactor technologies, e.g. reactive extrusion [12] and electron beam irradiation [13], have been developed. LCB polymers prepared by these methods are complex and sometimes difficult to control the extent of branching in them. It

is also possible to increase the LCB levels by using the dual catalysts in the same reactor, where one catalyst is capable of forming macromonomers while the second catalyst in the reactor is incorporated as LCB on to the growing chain. This type of binary catalyst systems in a single reactor has shown to be effective for one step production of long chain branched polyethylene [14-15].

Though various experimental in situ polymerization techniques of synthesizing PP with branching are in progress [6, 10, 11, 16, 17], one of the theoretical approaches might be the modeling of LCBPP with a proposed mechanism which can validate experimental results and then using that validated model to optimize and control the extent of branching. Developing a mechanistic model for such a polymer system is going to be very helpful because in this process, the details of the system can be understood and the properties of the polymer can be controlled in a better manner. Calculation of molecular weight distribution (MWD) is very important for this kind of modeling of polymerization system as the MWD can be directly related to many of the properties of the polymer. The generic approach towards mechanistic modeling of polymerization system is to assume a kinetic mechanism, from which one can derive the net rate of formation of live and dead polymers. Calculation of the molecular properties dynamically inside the reactor leads to a very large set of ordinary differential equation - initial value problems (ODE-IVPs) to accommodate high degree of polymerization. Moment based modeling is generally applied to the live and dead polymers to reduce it to a lower order system. Next, the MWD can be calculated by fractionation of total polymer into various classes [18] based on the long chain branching (LCB) content (linear, LCB=1, LCB=2, etc.). With a model of such capability in place, the final aim is ideally to find out the optimal process conditions to get the desired combination of various objectives (e.g. simultaneous minimization of polymerization time, maximization of weight average molecular weight and number average degree of branching) obeying certain process and phenomenological constraints. Real life scenarios demand simultaneous attainment of number of above-mentioned objectives as opposed to single objective which can be conflicting to one another. A set of trade-off solutions, known as Pareto optimal (PO) solutions, can be obtained by solving the multi-objective optimization problem (MOOP). These PO solutions provide multiple alternatives, known as non-dominated solutions, to a decision maker from which a single solution can be chosen based on some additional information available at a higher level. Evolutionary optimization methods which have certain edges over their classical counter parts to find better quality PO solutions, are proven to be better candidates for solving several ill / well-behaved (e.g. convex as well as non-convex) MOOPs under different scenarios.



As mentioned earlier, evolutionary algorithms (EAs) are found to be very reliable and practical while seeking the solutions of a MOOP. On the one hand, these algorithms offer promise to find the global PO front in presence of several local ones, while the aspect of finding out a set of well spread PO solutions in the given objective space is the other strong edge these techniques have over their competitors (primarily the classical techniques) [19]. Despite the aforementioned distinctions, EAs, when used with the above-mentioned computationally expensive polymer models, requiring more time for each function evaluation. This will demand significantly long time to find the PO solutions, translating the approach to be less practical for real world online applications. The reason for high computational burden in these evolutionary algorithms is the repetitive function evaluations for each candidate solution, which cannot be avoided because these algorithms work with a population of solutions. The quality of the Pareto spread may be compromised if these functions evaluations are reduced by considering a budget cut in the population size [19]. One of the ways to reduce the computational burden might be to replace the computationally expensive model by another model or set of models that consume relatively less time, called meta-model or surrogate model [20-25]. The challenge lies in the fact of developing a surrogate model that has a reasonable balance of agility and reliability, an inherent trade off in any model building exercise while mimicking complex phenomena.

## **1.2 Research Objective**

The main objective of this thesis is to develop an experimentally validated kinetic model for the long chain branched polypropylene (LCBPP) system by using dual catalyst system and use the model for performing multi-objective optimization (MOO) for the desired combination of conflicting objectives. A critical review of literature reveals that

- Models of LCB for PP system with a proposed mechanism which can match experimental results is not available in the literature though few modeling efforts are reported without experimental validation.
- Use of experimentally validated models in optimizing operational process parameters while controlling the extent of branching, therefore, is even rarer.
- Reduction in execution time (i.e. for PVAc model) for the optimization formulation to make the application as a candidate for better online usage is not very ubiquitous.

In view of the above motivating factors, the specific research objectives of this work were:

- ❖ Perform multi-objective optimization for the desired combination of conflicting objectives by using evolutionary optimization method for the highly branched

polyvinyl acetate (PVAc) system which is manufactured by free radical polymerization. The system of PVAc has been chosen here as a test case for incorporating the phenomenon of branching because branching in PVAc is relatively well-understood and a large amount of validation data are available for this system.

- ❖ Develop a kinetic model to describe the branched polypropylene system with two single site catalysts, where one is capable of forming macromonomers, while the second one grafts these macromonomers into the growing chain to create branches and validate the same with experimental data.
- ❖ Perform MOOP to obtain the Pareto optimal solutions for the developed branched polypropylene system while handling several conflicting objectives by keeping the decision variables within the  $\pm 10\%$  experimental range to control the model extrapolation errors and analyze and compare the results with the existing literature data.
- ❖ Develop Kriging based surrogate models to partially or completely replace the original expensive model to reduce the number of function evaluations while performing MOOP by the evolutionary optimization technique.

### **1.3 Organization of Thesis**

This thesis consists of 8 chapters and is organized as follows:

Chapter 1 presents the introduction, research objectives and organization of thesis.

Chapter 2 contains the literature review of multi-objective optimization studies of various polymerization systems and kinetic modeling of branched polyvinyl acetate (PVAc) system. This is followed by the literature review on the branched polyolefin systems. Finally, it contains various surrogate based modeling techniques.

Chapter 3 discusses about the polymer basics, various types of chain growth polymerization and various methods to calculate the molecular weight distribution for the long chain branched polymers, i.e. numerical fractionation method, partition according to the number of branches and fixed pivot technique.

Chapter 4 describes the kinetic scheme adopted and the related modeling procedure to provide a link between the molecular architecture and polymer properties for the bulk free radical polymerization of vinyl acetate. Further, the simulation results of multi-objective optimization and its rationale behind the formulation of the problem is provided.

Chapter 5 discusses about the development of experimentally validated kinetic mechanism for the long chain branched polypropylene system by the binary catalyst system, where one catalyst responsible for forming macromonomers, while the second one copolymerizes the macromonomers to create branches into the growing chain.

Chapter 6 deals with the multi-objective optimization of long chain branched polypropylene system, which discusses the simulation results of multi-objective optimization to produce a polymer of high molecular weight and grafting density (number of macromonomers per 1000 backbone monomer units) in less polymerization time.

Chapter 7 describes the Kriging based surrogate model to replace a first principle based computationally expensive model (i.e. PVAc model) to save execution time while performing an optimization task. In the surrogate modeling exercise, Kriging models have been developed first for each of the objective functions and constraints one at a time. Pareto optimal solutions are compared with the original first principle model.

Chapter 8 deals with the concluding remarks of the thesis.

# Chapter 2

## Literature review

### 2.1 Branched polymers

The molecular architecture of a polymer determines various end use properties. For example, branched polymers are usually linked with improved processing characteristics, high melt strength and low melt flow index (MFI) [1] as compared to their linear counterparts. Branched polymers are also characterized by high strain hardening, tensile strength, relaxation time and low density [1]. As branched polymers are having different properties than linear ones, there has been some literature on manufacturing of different kind of branched polymers. For instance, Nagasawa *et al.* [26] performed detailed study on methods to manufacture specific branched polymers which include star and comb shaped polymers. Some examples for branched and linear free radical polymerization are extensively used in literature. For instance, kinetic modeling of poly (methyl methacrylate) is performed by Krajnc *et al.* [27] using tetraphenyl biphosphine as an initiator. In addition, work is there in literature using different types of initiator and monomers differ in number of functional groups. Kinetic modeling and experimental validation for hyperbranched polymerization of methyl methacrylate is performed by Simon *et al.* [28]. Keramopoulos *et al.* [29] gave example of poly(methyl methacrylate) using diffusion controlled free radical polymerization. Furthermore Achilias *et al.* [30] also performed study on diffusion controlled free radical polymerization of methyl methacrylate and styrene using different initiators. Low density polyethylene (LDPE) is largely used in literature as examples of branched polymers. Different kind of initiators, reactors and operating conditions are studied for polymerization of ethylene. High pressure polymerization of ethylene using continuous stirred tank reactor (CSTR) is performed by Pladis and Kiparissides [18]. Moreover, study also performed on modeling of LDPE in tubular and autoclave reactors by

Zhou *et al.* [31]. One other example is Poly vinyl acetate (PVAc), which is a highly branched thermoplastic polymer. It is manufactured by free radical polymerization of vinyl acetate and used as raw material for preparation of polyvinyl alcohol and polyvinyl acetate phthalate. PVAc is used as a film forming ingredient in water based paints and also known as wood glue. Since this structure-property relationship is of profound importance, it is necessary to examine the kinetics and the effect of process operating conditions on polymer molecular properties. There are several studies on the polymerization of vinyl acetate. Thomas [1] conducted batch experiments for polymerization of vinyl acetate at two different temperatures with different initiator conditions. The various properties such as molecular weight and number average degree of branching were calculated. Tobita *et al.* [32] used monte-carlo method to investigate the branching in batch polymerization process. There are also few studies on solution polymerization with different solvents. Solution polymerization using t-butanol is studied by Chatterjee *et al.* [33]. Timothy *et al.* [34] used different solvents for batch polymerization and investigated their effect on various properties of PVAc.

Molecular weight and long chain branching (MW-LCB) distribution is of great interest as it is directly related to the polymer properties. There are several methods in the literature to calculate this. Teymour and Campbell [35] gave numerical fractionation which can be applied in both pre and post gelation polymerization. In this method, polymer is divided into linear and branched chains. During the beginning of polymerization, linear polymer dominates and when a branch is added to the linear polymer, it is termed as first generation. If two first generation chains combine together, from that point it is considered as second generation and so on. Transition from one generation to other continues by geometric growth. In case, the terminal double bond reaction is assumed to be important, the assumption (i.e. geometric growth) in “Numerical Fractionation” method may not be valid. The main drawback of this method is that the branches may keep on adding without getting transferred to the next generation. Arzamendi and Asua [36] has modified the Numerical Fractionation method and applied to emulsion polymerization systems. Pladis and Kiparissides [18] developed a comprehensive model for the calculation of molecular weight long chain branching distribution in free radical polymerization, which is based on the fractionation of the entire polymer population based on the number of branches (i.e. classes). For each class, moment based modeling is applied for live and dead polymer chains to reduce the number of equations. From this technique, one can calculate average polymer properties like  $M_n$ ,  $M_w$ ,  $B_n$  etc. MWD is calculated for each class (i.e. having same

long chain branching (LCB)) by Wesslau distribution [18] using the above mentioned numerical technique (i.e. partition according to number of branches). The overall MWD is the weighed sum of MWDs of individual class. Here, the class number is increased by chain transfer to polymer reaction and reaction with terminal double bond as they increase long chain branching (LCB). In chain transfer to polymer reaction, internal radical is formed from dead polymer chain by hydrogen abstraction [37]. Monomer units present in the reactor attack the internal radical leading to formation of LCB. Meimaroglou *et al.* [38] compared the results between two-dimensional fixed pivot technique [39] and monte-carlo [32] in batch mode. In fixed pivot technique, two-dimensional sectional grid method is applied to solve the population balance equations. In this method, degree of polymerization and long chain branches per polymer chain were discretized into a number of two-dimensional finite elements. The resulting continuous discrete rate equations for live and dead polymer chains were solved to calculate average weight and branching in the polymer. Asteasuain *et al.* [40] used transform technique, probability generating function (PGF) to mass balances that describe free radical polymerization reactions. PGF balance equations are constructed and resulting transforms are inverted by using different methods to recover the complete molecular weight distribution. In the present work, method of moments is used to get the tractable set of equations from a high dimensional problem. Adopted model for batch free radical polymerization consists of stiff ordinary differential equations and is solved using LIMEX DAE [41] solver. Model is validated with experimental studies [1] and other numerical technique [18]. Numerical fractionation according to number of branches [18] is used to get the branching parameter and molecular weight-long chain branching distributions.

Significant numbers of experimental and theoretical studies have been conducted for various free-radical long chain branched systems. As another example, long chain branched polyethylene can be produced by free radical polymerization in a tubular reactor at high pressure and high temperature conditions [42]. In general, Zeigler Natta and metallocene catalysts are known to produce highly linear polymers. After the discovery of constraint geometry catalyst, branched polyolefins synthesis was made possible. The unique feature of constraint geometry metallocene is that it incorporates the macromonomers into the growing chain [6, 10, 16]. The lack of attention in synthesizing long chain branched polypropylene (LCB PP) is due to the limited knowledge of embedded chemistry to produce the LCB PP. To overcome this, various technologies, e.g. reactive extrusion [12] and electron beam irradiation [13] have been developed. LCB polymers prepared by these methods are

complex and sometimes the degree of branching of the resultant polymer is very difficult to control. Due to the advantage of metallocene technology, Weng *et al.* [6] have synthesized long chain branched isotactic polypropylene (iPP) by the incorporation of in situ vinyl terminated macromonomers. The experiments are conducted at low and steady propylene concentration to allow accumulation of macromonomers in the reactor so that the probability of incorporation of macromonomers to the growing polymer chain increases. Shiono *et al.* [10] copolymerized atactic polypropylene (aPP) macromonomer with propylene by an isospecific metallocene catalyst. They used *rac*-Me<sub>2</sub>Si(2-MeBenz[*e*]Ind)<sub>2</sub>ZrCl<sub>2</sub>, the best isospecific catalyst available for the incorporation of macromonomers, for this purpose. Ye and Zhu [16] produced LCB PP with isotactic back bones and atactic side chains using binary catalyst system. Here, the catalyst (1) produces vinyl terminated macromonomers (having terminal double bonds) and the catalyst (2) copolymerizes the polypropylene macromonomers with propylene. Under this mechanism the chains that have terminal unsaturation are inserted into the growing polymer chain to produce LCB PP. LCB PP has been produced by Paavola *et al.* [17] by using non-conjugated diene comonomers, where the diene monomer provides a reactive functional group along the backbone to ease branching. Polymers produced by this method exhibit broad molecular weight distribution with a polydispersity index value greater than 5. Langston *et al.* [11] produced long chain branched isotactic polypropylene by metallocene catalyst and T-reagent. They conducted experiment by the combination of *rac*-Me<sub>2</sub>-Si(2-Me-4-Ph-Ind)ZrCl<sub>2</sub>/MAO as catalyst and *p*-(3-butenyl)styrene as T-reagent. In the presence of hydrogen, T-reagent acts as comonomer as well as chain transfer agent. LCB PP produced by this method has branching density of the order of ~3.3 per 10000 carbon atoms. On the production of branched polyethylene, there has been considerable progress. Beigzadeh *et al.* [43] produced long chain branched polyethylene with binary metallocene catalyst system (2-ArN=C(Me))<sub>2</sub>C<sub>3</sub>H<sub>3</sub>N}FeCl<sub>2</sub>/MMAO (1) and *rac*-Me<sub>2</sub>Si(2-MeBenz[*e*]Ind)<sub>2</sub>ZrCl<sub>2</sub>/MMAO (2)) and observed the extent of long chain branching by varying the two catalysts in the reactor. Zou *et al.* [44] synthesized long chain branched polyethylene by homo polymerization of ethylene with nickel  $\alpha$ -diimine catalyst. They observed the influence of temperature and Al/Ni ratio on molecular weight and degree of long chain branching [44] in this work. Mathematical models have also been developed to explain long chain branched polyolefins. Mehdiabadi *et al.* [45] developed mathematical model for the general olefin polymerization in a series of two CSTRs, in which macromonomers produced in the first reactor is copolymerized with the propylene in the second reactor to produce PP with high LCB density. The Monte Carlo models have been

developed for branched polyolefins which are made with two single site catalysts [46]. Soares and Hamielec [47] developed a simple analytical expression to calculate molecular weight distribution of chain length and long chain branching of polyolefins in a steady state CSTR. Modeling study has been conducted by Zhu and Li [48] with the use of binary metallocene catalyst system to obtain highly comb-branched polymers in steady state CSTR and obtained an olefin polymer of narrow molecular weight distribution with a maximum polydispersity index of 2.25. By this catalyst systems, back bone and side chains provide a theoretical polydispersity index of 2 (Schulz-Flory distribution) [48] only. Yiannoulakis *et al.* [49] explained from comprehensive dynamic model for the construction of molecular weight long chain branching distribution by numerical fractionation technique for olefin polymerization. Iedema *et al.* [50] predicted branching densities and bimodal molecular weight distributions of polyethylene for mixed systems with a constrained geometry metallocene catalyst in a semi batch reactor by using Galarkin finite element method. Read and Soares [51] obtained the molecular weight and long chain branching distribution for polyolefins made with two single-site metallocene catalysts in a CSTR. A detailed review of mathematical models to explain the polymer microstructure with single site catalysts is given by Soares [52]. The validation of these models with experimental data is still to be done to satisfaction [52].

## **2.2 Multi-objective Optimization**

Multi-objective optimization techniques are excellent candidates to find out optimal solutions that are conflicting in nature, e.g. simultaneous attainment of maximum molecular weight and grafting density in less polymerization time in a polymerization set up. It is known that polymer with higher molecular weight can be obtained in higher polymerization time; on the contrary, the objective is to attain polymers with higher molecular weight in less time - there is the conflict. Moreover, to maintain the competitive advantage, it is more apparent that enterprises need to produce products in such operating conditions that solve multiple conflicting operating objectives simultaneously than attaining only one goal. Multi-objective optimization works are, therefore, gaining popularity to solve optimization problems in the polymerization domain, which are quite often conflicting in nature, over last few decades. The early efforts to solve multi-objective optimization problems in polymer reaction engineering go back to the works of Tsoukas *et al.* [53] and Fan *et al.* [54]. These studies are primarily based on the Pontryagin's maximization principle to find solutions to the optimal control problems where various single objective optimization based methods are used to transform the original multi-objective optimization problems to obtain the Pareto



optimal (PO) solutions. There are benefits of using evolutionary optimization methods for solving multi-objective optimization problems. These population based methods attack the multi-objective optimization problems using a vector approach where all objectives are considered simultaneously as opposed to the single objective optimization approaches for solving multi-objective optimization problems. Multiple numbers of well spread PO solutions can be obtained in single optimization run using these evolutionary approaches. One such earlier efforts is the multi-objective optimization study of optimal control of industrial nylon-6 semi-batch reactor [55], where evolutionary algorithms are shown to work better than conventional Pontryagin maximization principle [55] based approaches to solve multi-objective optimal control problems. In another example, Raha *et al.* [56] investigated the effect of NaOH addition as a catalyst in semi-batch mode for epoxy polymerization, which was otherwise considered as a batch operation. Detailed optimal control studies have been performed by Mitra *et al.* [57] and Majumdar *et al.* [58] with relevant process constraints to find out optimal addition profiles for various other reactants that further support semi-batch operation as compared to conventional batch process. As another example, Majumdar *et al.* [59] maximized the degree of polymerization and concentration of desired species in minimum polymerization time for the poly (propylene terephthalate) system with a titanium based catalyst using evolutionary algorithms. Mitra *et al.* [60] considered different alternatives for catalysts and carried out optimization study with various sets of process objectives with newly estimated kinetic parameters. Sundaram *et al.* [61] and Upreti *et al.* [62] studied optimal control for polymethylmethacrylate system using bi-functional initiator in a non-isothermal reactor. Multi objective optimization of an industrial low density polyethylene tubular reactor has been conducted by using genetic algorithm and its jumping gene adaptations [63]. Most of these literature show superiority of evolutionary methods to solve multi-objective optimization problems as compared to other classical optimization techniques for solving problems related to polymerization which is otherwise also shown for solving other chemical engineering multi-objective optimization problems. A thorough review of various such works from polymerization domain can be found in the literature [64-67].

### **2.3 Surrogate Modeling**

Evolutionary algorithms (EAs) [68-69] are found to be very reliable and practical while seeking the solutions of a multi-objective optimization problem. On the one hand, these algorithms give promise to find the global PO front in presence of several local ones, while the aspect of finding out a set of well spread PO solutions in the given objective space is the

other strong edge these techniques have over their competitors (primarily the classical techniques) [19]. Despite the aforementioned distinctions, EAs, when used with first principle based computationally expensive models, requiring more time for each function evaluation, demand significantly long time to find the PO solutions, translating the approach to be less practical for real world online applications. The reason for high computational burden in these evolutionary algorithms is the repetitive function evaluations for each candidate solution, which cannot be avoided because these algorithms work with a population of solutions. The Quality of the Pareto spread may be compromised if the numbers of functions evaluations are reduced [19]. One of the ways to alleviate the computational burden is to replace the first principle based computationally expensive model by another model or set of models that consume relatively less time, called meta-model or surrogate model [70]. The challenge lies in the fact of developing a surrogate model is that it has to have a reasonable balance of agility and reliability, an inherent trade off in any model building exercise while mimicking a complex phenomenon.

A detailed survey of fitness approximation of various techniques has been conducted by Jin [71]. An approximation can be achieved widely at three levels: problem approximation, function approximation and approximation at the level of the algorithms [20]. In problem approximation, the given problem itself is replaced by an easy-to-solve new problem [72]. In function approximation, an implicit or explicit function based black box model is formulated between inputs and outputs which can approximately capture the behavior of the original function and makes the system faster. Evolutionary approximation, the next in order, can be achieved in the algorithmic level of evolutionary routine. For instance, the fitness value of offspring children can be estimated by fitness value of their parents etc. [73]. The approach of function approximation has been emphasized here. There have been several techniques for function approximations in literature such as response surface [74], multivariate adaptive regression splines [75], Kriging [22-25], artificial neural networks [70], radial basis functions [76-77] and support vector regressions [75] to name a few.

The challenge lies here is how can we develop a high fidelity surrogate model with less number of function evaluations. It is, therefore, very important to use function evaluations carefully while building the surrogates so that the quality of the optimal solution is not compromised. In conventional optimization, this is known as model management [78] or evolution control in evolutionary computation [79]. There are several ways in literature for model management or evolution control. For example, function evaluation can be

completely replaced by surrogate model [78] or function evaluations can be used for a few generations (controlled generations) or for a few individuals in a population (controlled individually) and the rest using surrogate model [79-80]. Dellino *et al.* [23] compared the various metamodeling strategies in a case study of the design of a component of the injection system for compressed natural gas (CNG) engines, where Kriging surrogate has been used. Jin *et al.* [81] gave the framework for controlled evolution which guarantees the correct convergence while reducing the computational burden. Nain and Deb [70] used controlled generation approach, fixed number of expensive model calculations followed by fixed number of surrogate model usage, to use feed forward neural network model with an evolutionary algorithm for several multi-objective optimization case studies and observed the savings up to 50%. Mitra and Majumder [20] extended this approach by introducing automatic transition between surrogate and expensive model calculations while solving a multi-objective optimization study of iron ore induration process. Surrogates have found their usage in rolling rod product design where expensive finite element models (FEM) have been replaced by the combination of design of experiments (DOE) and response surface models (RSM) for multi-objective optimization study [82]. Li *et al.* [24] utilized the Kriging assisted multi-objective genetic algorithm (K-MOGA) and observed the Pareto with approximately 50% lesser number of function calls as compared to the conventional genetic algorithm. Here, some of the population points are evaluated by Kriging surrogate model instead of first principle model, based on criteria related to model accuracy. Li [25] developed an improved Kriging assisted multi-objective genetic algorithm (Circled Kriging MOGA, i.e. CK-MOGA) and concluded that CK-MOGA exhibited improved performance in terms function calls as compared to the K-MOGA. In an another study, Li *et al.* [83] compared various surrogate modeling techniques such as radial basis function, artificial neural network, Kriging, support vector regression and multivariate regression splines where the support vector regression is found to be the best in terms of robustness and accuracy while carrying out the optimization of a job shop design problem. Several works started surfacing in literature about surrogate associated multi-objective optimization for various applications, crashworthiness design [84], structural dynamics [85] and draw-bead design [86] etc. to name a few. Giri *et al.* [87] suggested building different models of varying structures using ANN and genetic programming before focusing on a particular parsimonious model considering the tradeoff between the model complexity and accuracy.

Kriging (Gaussian process regression) surrogate model has been used to replace the expensive model to reduce the computational burden due to its superior prediction accuracy

as compared to the other models [88]. Gaussian process based infill criteria such as expected improvement [22, 89] has been used to build the surrogate model. Chi *et al.* [90] used the NSGA II [19] to generate Pareto between prediction mean and uncertainty. These Pareto points are further clustered to give experimental data to be conducted for the next iteration.

#### **2.4 Tendency modeling**

A more exhaustive model, which focuses the estimation beyond the experimental range, is necessary. This model is also referred as “tendency modeling”. It is a non-linear, lower order, dynamic model that approximates the kinetic relationships of a process using the experimental data along with basic knowledge of the process [91-93]. The model structure and parameters are updated as more data becomes available.

# Chapter 3

## Introduction to Polymerization techniques, Methods and Solver

This chapter deals with the polymer theory and various methods to calculate the molecular weight distribution of branched polymer systems.

### 3.1 Polymer Theory

Polymers are high molecular weight materials formed by smaller repeating units called monomers. The molecular properties of the polymers are characterized in terms of molecular weight distribution (MWD), polydispersity index (PDI) etc. These molecular properties completely depend on the formulation (monomers, initiators, catalysts etc.), the polymerization technique (free radical, coordination etc.), reactor (i.e. batch, tubular reactor, CSTR etc.) and process conditions (temperature, time, concentration) [94]. For example, the catalyst design is the key to success of any industrial process for olefin polymerization. This is because the catalyst finally determines how the monomers will be linked in the polymer chain [94], eg. Polymers produced by the Ziegler-Natta catalyst exhibit good processability as compared to the metallocene due to the multiple active site behavior. Methods to calculate MWD are extremely important. Some of these methods are explained below

#### 3.1.1 Molecular weight distribution

Polymers consist of chains of various lengths and they are characterized by molecular weight distribution (MWD). Polymer properties strongly depend on MWD, e.g. mechanical strength of the polystyrene improves with increase in its molecular weight. Although the properties of the polymers strongly depend on the overall MWD, they can often be characterized by the average molecular weights based on number and weight.

Number average molecular weight:

$$M_n = \frac{\sum_{n=1}^{\infty} n(D_n + P_n)}{\sum_{n=1}^{\infty} (D_n + P_n)} \quad (3.1)$$

Weight average molecular weight:

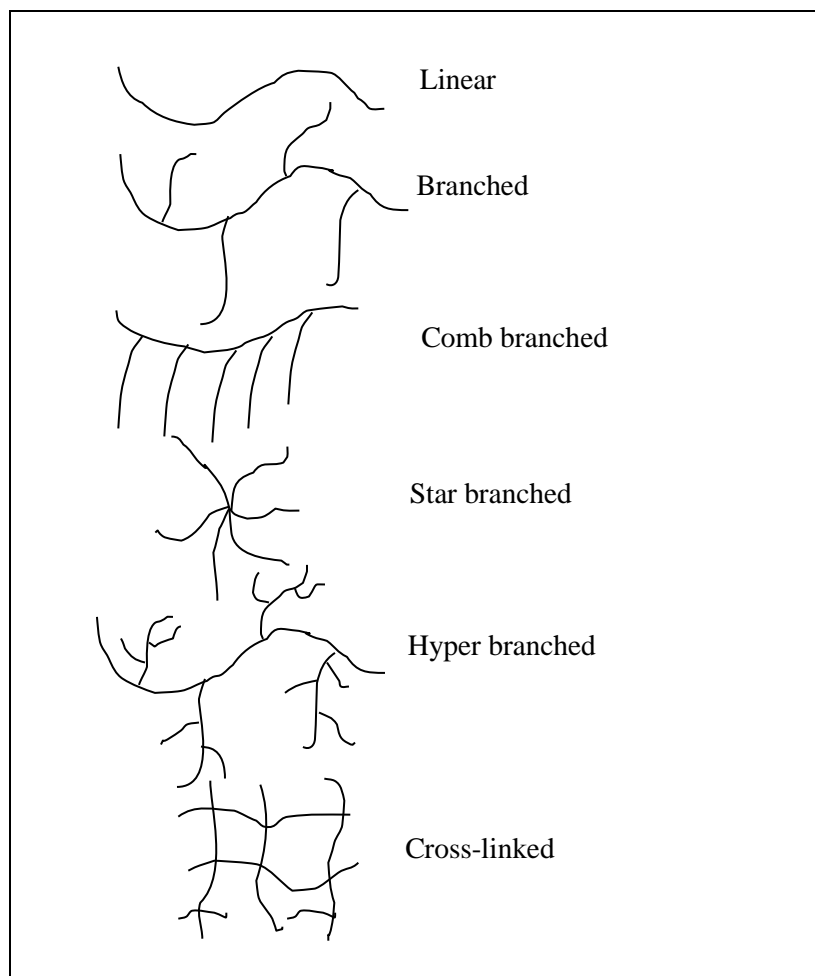
$$M_w = \frac{\sum_{n=1}^{\infty} n^2 (D_n + P_n)}{\sum_{n=1}^{\infty} n(D_n + P_n)} \quad (3.2)$$

Where  $P_n$  and  $D_n$  represent the number of moles of live and dead polymer chains of length  $n$  and  $w_m$  is the molecular weight of the monomer unit. Live polymer can have the capability to further grow, while the dead polymer cannot grow further. The ratio of weight average and number average molecular weights gives the value of polydispersity Index ( $PDI=M_w/M_n$ ). This value gives the idea of the broadness of the MWD. Since the structure property relationship is directly related to the complete MWD, the construction of MWD for branched polymer by various computational methods has been described in section 3.3.

### 3.1.2 Architecture

Polymers can be classified as linear, branched and cross-linked networks in terms of their architecture as shown in Table 3.1. In linear polymers, the monomer units are arranged in a linear fashion. Branched polymers include star like, comb like and hyper branched (extensive branching) polymers. In cross-linked polymers, polymer chains are linked together to form a three dimensional network.

Table 3.1: Polymer architectures [91]



### 3.1.3 Chain growth polymerization

In this polymerization, monomers can join active chains. Monomers contain carbon-carbon double bonds, e.g. propylene, ethylene, styrene etc. The chain activity can be commenced either by a catalyst or an initiator. According to the type of active center, chain growth polymerization [94] can be classified as:

- Free radical polymerization
- Coordination polymerization
- Anionic polymerization
- Cationic polymerization

#### Free radical polymerization

In free radical polymerization, active center is a free radical, which is formed from an initiator. Reaction proceeds by the addition of monomer units to the active end of the growing chain. The growth of these chains can be terminated by the transfer of the radical to

other compounds like monomer, chain transfer agent, polymer or/and bimolecular reaction between the radicals.

### **Coordination polymerization**

In this, a suitable catalyst is required for polymerization. Monomer units are inserted between the catalyst site and growing chain, for the reaction to proceed. Coordination polymerization catalysts include Ziegler-Natta, transition metal catalysts and metallocenes. The microstructural properties of the polymer can be well controlled by the type of the catalyst. For example, due to the multiple sites present in the catalyst like Ziegler-Natta catalysts, polymer of non-uniform properties can be produced.

### **Anionic polymerization**

It requires the initiators that provide the initiator anions. These anions will only attack those monomers, whose electrons can be moved in such a way that monomer anion results, e.g. cyclic monomers such as ethylene oxide, glycolide etc. In this polymerization kinetic mechanism, termination mechanism is not included because macroanions grow until all monomers in the reactor are polymerized. This is also called living polymerization. Polymers produced by this exhibits very narrow molecular weight distributions.

### **Cationic polymerization**

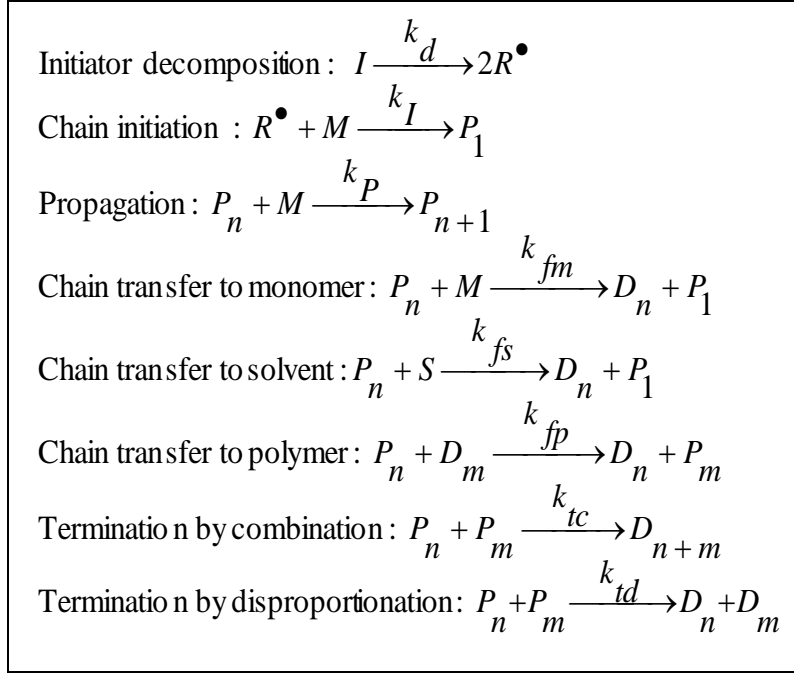
In cationic polymerization, carbenium salts produces cationic initiators, Lewis acids, react with monomer to give monomer cations. The monomers having electron donating groups can only participate in this type of polymerization, e.g.: isobutene.



### 3.2 Kinetic Scheme and Mathematical model

The reaction scheme considered in this section is taken from Butte *et al.* [95] (Table 3.2).

Table 3.2: Kinetic Mechanism



Where  $P_n$  and  $D_n$  represent live and dead polymer chains of length “n”. Net rates of formation of live and dead polymer chains can be derived from the above kinetic mechanism and are shown in Equations (3.3) and (3.4).

$$\begin{aligned} \frac{dP_n}{dt} = & \{k_I [R^\bullet] [M] + (k_{fm} [M] + k_{fs} [S]) \sum_{n=1}^{\infty} P(n) \} \delta(n-1) + k_p [P(n-1) - P(n)] [M] \\ & - (k_{fm} [M] + k_{fs} [S]) P(n) + k_{fp} [nD(n)] \left( \sum_{n=1}^{\infty} P(n) \right) - k_{fp} P(n) \sum_{n=2}^{\infty} nD(n) \\ & - k_{tc} P(n) \sum_{n=1}^{\infty} P(n) - k_{td} P(n) \sum_{n=1}^{\infty} P(n) \end{aligned} \quad (3.3)$$

$$\begin{aligned} \frac{dD_n}{dt} = & (k_{fm} [M] + k_{fs} [S]) P(n) + k_{td} P(n) \sum_{n=1}^{\infty} P(n) + \frac{1}{2} k_{tc} \sum_{y=1}^{n-1} P(n) P(n-y) \\ & + k_{fp} P(n) \sum_{n=2}^{\infty} nD(n) - k_{fp} nD(n) \sum_{n=1}^{\infty} P(n) \end{aligned} \quad (3.4)$$

Where  $\delta(x)$  is the Kronecker’s delta function. The above equations lead to a very large set of differential equations to describe the molecular properties in a polymerization reactor. A

lower order system of equations can be derived using the method of moments approach [18] instead of solving the above large set of equations (e.g. 40000) using following definitions as shown in Equations 3.5 - 3.6.

$$\mu_j = \sum_{x=1}^{\infty} x^j P(x) \quad (3.5)$$

$$\nu_j = \sum_{x=1}^{\infty} x^j D(x) \quad (3.6)$$

From the above definitions, 0<sup>th</sup>, 1<sup>st</sup> and 2<sup>nd</sup> moments of the live and dead polymers can be derived (Equations 3.7 to 3.12).

$$\frac{d\mu_0}{dt} = 2fk_d[I] - (k_{tc} + k_{td})\mu_0^2 \quad (3.7)$$

$$\begin{aligned} \frac{d\mu_1}{dt} = & 2fk_d[I] + k_p[M]\mu_0 - (k_{fm}[M] + k_{fs}[S])\mu_1 - (k_{tc} + k_{td})\mu_0\mu_1 \\ & + k_{fp}(\mu_0\nu_2 - \mu_1\nu_1) \end{aligned} \quad (3.8)$$

$$\begin{aligned} \frac{d\mu_2}{dt} = & 2fk_d[I] + 2k_p[M]\mu_1 - (k_{fm}[M] + k_{fs}[S])\mu_2 - (k_{tc} + k_{td})\mu_0\mu_2 \\ & + k_{fp}(\mu_0\nu_3 - \mu_2\nu_1) \end{aligned} \quad (3.9)$$

$$\frac{d\nu_0}{dt} = (k_{fm}[M] + k_{fs}[S])\mu_0 + (\frac{1}{2}k_{tc} + k_{td})\mu_0^2 \quad (3.10)$$

$$\frac{d\nu_1}{dt} = (k_{fm}[M] + k_{fs}[S])\mu_1 + (k_{tc} + k_{td})\mu_0\mu_1 - k_{fp}(\mu_0\nu_2 - \mu_1\nu_1) \quad (3.11)$$

$$\begin{aligned} \frac{d\nu_2}{dt} = & (k_{fm}[M] + k_{fs}[S])\mu_2 + (k_{tc} + k_{td})\mu_0\mu_2 + k_{tc}\mu_1^2 - k_{fp}(\mu_0\nu_3 - \mu_2\nu_1) \end{aligned} \quad (3.12)$$

The other rate equations for initiator, primary radical, monomer and solvent are shown below.

$$\frac{d[I]}{dt} = -k_d[I] \quad (3.13)$$

$$\frac{d[R^\cdot]}{dt} = 2fk_d[I] - k_I[R^\cdot][M] \quad (3.14)$$

$$\frac{d[M]}{dt} = -k_p[M]\mu_0 \quad (3.15)$$

$$\frac{d[S]}{dt} = -k_{fs}[S]\mu_0 \quad (3.16)$$

### 3.3 Methods to calculate MWD

Calculation of MWD of final product is very important since it can be directly used to calculate the end use properties. The MWD of a polymer is a record of the kinetic history of the reactions which occurred during the polymer buildup. Some of the methods to construct MWD of the polymer have been discussed in this section.

#### 3.3.1 Numerical Fractionation

This method was proposed by Teymour and Campbell [35]. In numerical fractionation method, the entire polymer population is divided into linear and branched generations. Again, the latter one is subdivided into various generations according to the geometric growth. In the beginning stage of polymerization, linear polymer dominates. If branching reaction occurs, this is referred to as first generation. Second generation will only occur when two first generation chains connect together forming a single molecule. This molecule will add more linear and first generation before it reacts to form the second generation member. Higher generations will come into existence only when there is a reaction between lower generation members. As the polymer molecule moves from one generation to the higher generation, the average size of polymer will grow geometrically. As the higher generation members react to form much larger polymer molecules finally, this leads to a generation of infinitely large molecule (i.e. formation of gels).

The overall moment equations for live and dead polymers have been shown in the previous section. Population balance equations for linear, first generation and  $i^{\text{th}}$  generation of live and dead polymers have been shown in Equations 3.17 to 3.22.

**Net formation for linear and branched live polymer:**

$$\frac{dP_n^0}{dt} = k_p[M](P_{n-1}^0 - P_n^0) - (k_{fs}[S] + k_{fm}[M] + k_{fp}v_1)P_n^0 - (k_{tc}\mu_0 + k_{td}\mu_0)P_n^0 + \delta\{(k_{fs}[S] + k_{fm}[M])\mu_0 + 2fk_d[I]\} \quad (3.17)$$

$$\frac{dP_n^1}{dt} = k_p[M](P_{n-1}^1 - P_n^1) - (k_{fs}[S] + k_{fm}[M] + k_{fp}v_1)P_n^1 - (k_{tc}\mu_0 + k_{td}\mu_0)P_n^1 + k_{fp}\mu_0(nD_n + nD_n^1) \quad (3.18)$$

$$\frac{dP_n^i}{dt} = k_p[M](P_{n-1}^i - P_n^i) - (k_{fs}[S] + k_{fm}[M] + k_{fp}v_1)P_n^i - (k_{tc}\mu_0 + k_{td}\mu_0)P_n^i + k_{fp}\mu_0 nD_n^i \quad (3.19)$$

**Net formation of linear and branched dead polymer:**

$$\frac{dD_n^0}{dt} = (k_{fs}[S] + k_{fm}[M] + k_{fp}v_1 + k_{td}\mu_0)P_n^0 + \frac{k_{tc}}{2} \sum_{s=1}^{n-1} P_s^0 P_{n-s}^0 - k_{fp}\mu_0 n D_n^0 \quad (3.20)$$

$$\frac{dD_n^1}{dt} = (k_{fs}[S] + k_{fm}[M] + k_{fp}v_1 + k_{td}\mu_0)P_n^1 + \frac{k_{tc}}{2} \sum_{s=1}^{n-1} P_s^1 P_{n-s}^0 - k_{fp}\mu_0 n D_n^1 \quad (3.21)$$

$$\begin{aligned} \frac{dD_n^i}{dt} = & (k_{fs}[S] + k_{fm}[M] + k_{fp}v_1 + k_{td}\mu_0)P_n^i + \frac{k_{tc}}{2} \sum_{s=1}^{n-1} P_s^{i-1} P_{n-s}^{i-1} - k_{fp}\mu_0 n D_n^i \\ & + k_{tc} \sum_{s=1}^{n-1} P_s^i \left( \sum_{j=0}^{i-1} P_{n-s}^j \right) \end{aligned} \quad (3.22)$$

The rate equations for the leading moments of the active and inactive chains for each generation can be derived from the above population balance equations.

#### Moment rates for linear live polymer chains:

$$\begin{aligned} \frac{d\mu_0^0}{dt} = & -(k_{fs}[S] + k_{fm}[M] + k_{fp}v_1)\mu_0^0 - (k_{tc}\mu_0 + k_{td}\mu_0)\mu_0^0 + \\ & (k_{fs}[S] + k_{fm}[M])\mu_0 + 2fk_d[I] \end{aligned} \quad (3.23)$$

$$\begin{aligned} \frac{d\mu_1^0}{dt} = & k_p[M]\mu_0^0 - (k_{fs}[S] + k_{fm}[M] + k_{fp}v_1)\mu_1^0 - (k_{tc}\mu_0 + k_{td}\mu_0)\mu_1^0 + \\ & (k_{fs}[S] + k_{fm}[M])\mu_0 + 2fk_d[I] \end{aligned} \quad (3.24)$$

$$\begin{aligned} \frac{d\mu_2^0}{dt} = & k_p[M](2\mu_1^0 + \mu_0^0) - (k_{fs}[S] + k_{fm}[M] + k_{fp}v_1)\mu_2^0 - (k_{tc}\mu_0 + k_{td}\mu_0)\mu_2^0 + \\ & (k_{fs}[S] + k_{fm}[M])\mu_0 + 2fk_d[I] \end{aligned} \quad (3.25)$$

#### Moment rates for first generation live polymer chains:

$$\frac{d\mu_0^1}{dt} = -(k_{fs}[S] + k_{fm}[M] + k_{fp}v_1)\mu_0^1 - (k_{tc}\mu_0 + k_{td}\mu_0)\mu_0^1 + k_{fp}\mu_0(v_1^0 + v_1^1) \quad (3.26)$$

$$\begin{aligned} \frac{d\mu_1^1}{dt} = & -(k_{fs}[S] + k_{fm}[M] + k_{fp}v_1)\mu_1^1 - (k_{tc}\mu_0 + k_{td}\mu_0)\mu_1^1 + k_{fp}\mu_0(v_2^0 + v_2^1) \\ & + k_p[M]\mu_0^1 \end{aligned} \quad (3.27)$$

$$\begin{aligned} \frac{d\mu_2^1}{dt} = & -(k_{fs}[S] + k_{fm}[M] + k_{fp}v_1)\mu_2^1 - (k_{tc}\mu_0 + k_{td}\mu_0)\mu_2^1 + k_{fp}\mu_0(v_3^0 + v_3^1) \\ & + k_p[M](2\mu_1^1 + \mu_0^1) \end{aligned} \quad (3.28)$$

#### Moment rates for $i^{\text{th}}$ generation live polymer chains:

$$\frac{d\mu_0^i}{dt} = -(k_{fs}[S] + k_{fm}[M] + k_{fp}v_1)\mu_0^i - (k_{tc}\mu_0 + k_{td}\mu_0)\mu_0^i + k_{fp}\mu_0 v_1^i \quad (3.29)$$

$$\frac{d\mu_1^i}{dt} = -(k_{fs}[S] + k_{fm}[M] + k_{fp}v_1)\mu_1^i - (k_{tc}\mu_0 + k_{td}\mu_0)\mu_1^i + k_{fp}\mu_0 v_2^i + k_p[M]\mu_0^i \quad (3.30)$$

$$\frac{d\mu_2^i}{dt} = -(k_{fs}[S] + k_{fm}[M] + k_{fp}v_1)\mu_2^i - (k_{tc}\mu_0 + k_{td}\mu_0)\mu_2^i + k_{fp}\mu_0v_3^i + k_p[M](2\mu_1^i + \mu_0^i) \quad (3.31)$$

**Moment rates for linear dead polymer chains:**

$$\frac{dv_0^0}{dt} = (k_{fs}[S] + k_{fm}[M] + k_{fp}v_1 + k_{td}\mu_0)\mu_0^0 - k_{fp}\mu_0v_1^0 + \frac{k_{tc}}{2}(\mu_0^0)^2 \quad (3.32)$$

$$\frac{dv_1^0}{dt} = (k_{fs}[S] + k_{fm}[M] + k_{fp}v_1 + k_{td}\mu_0)\mu_1^0 - k_{fp}\mu_0v_2^0 + k_{tc}\mu_0^0\mu_1^0 \quad (3.33)$$

$$\frac{dv_2^0}{dt} = (k_{fs}[S] + k_{fm}[M] + k_{fp}v_1 + k_{td}\mu_0)\mu_2^0 - k_{fp}\mu_0v_3^0 + k_{tc}(\mu_0^0\mu_2^0 + (\mu_0^0)^2) \quad (3.34)$$

**Moment rates for first generation dead polymer chains:**

$$\frac{dv_0^1}{dt} = (k_{fs}[S] + k_{fm}[M] + k_{fp}v_1 + k_{td}\mu_0)\mu_0^1 - k_{fp}\mu_0v_1^1 + k_{tc}\mu_0^1\mu_0^0 \quad (3.35)$$

$$\frac{dv_1^1}{dt} = (k_{fs}[S] + k_{fm}[M] + k_{fp}v_1 + k_{td}\mu_0)\mu_1^1 - k_{fp}\mu_0v_2^1 + k_{tc}(\mu_0^1\mu_1^0 + \mu_1^1\mu_0^0) \quad (3.36)$$

$$\frac{dv_2^1}{dt} = (k_{fs}[S] + k_{fm}[M] + k_{fp}v_1 + k_{td}\mu_0)\mu_2^1 - k_{fp}\mu_0v_3^1 + k_{tc}(\mu_0^1\mu_2^0 + 2\mu_1^1\mu_1^0 + \mu_2^1\mu_0^0) \quad (3.37)$$

**Moment rates for  $i^{\text{th}}$  generation dead polymer chains:**

$$\frac{dv_0^i}{dt} = (k_{fs}[S] + k_{fm}[M] + k_{fp}v_1 + k_{td}\mu_0)\mu_0^i - k_{fp}\mu_0v_1^i + \frac{k_{tc}}{2}(\mu_0^{i-1})^2 + k_{tc}[\mu_0^i \sum_{j=0}^{i-1} \mu_0^j] \quad (3.38)$$

$$\frac{dv_1^i}{dt} = (k_{fs}[S] + k_{fm}[M] + k_{fp}v_1 + k_{td}\mu_0)\mu_1^i - k_{fp}\mu_0v_2^i + k_{tc}(\mu_0^{i-1}\mu_1^{i-1}) + k_{tc}[\mu_0^i \sum_{j=0}^{i-1} \mu_1^j + \mu_1^i \sum_{j=0}^{i-1} \mu_0^j] \quad (3.39)$$

$$\frac{dv_2^i}{dt} = (k_{fs}[S] + k_{fm}[M] + k_{fp}v_1 + k_{td}\mu_0)\mu_2^i - k_{fp}\mu_0v_3^i + k_{tc}(\mu_0^{i-1}\mu_2^{i-1} + (\mu_1^{i-1})^2) + k_{tc}[\mu_0^i \sum_{j=0}^{i-1} \mu_2^j + 2\mu_1^i \sum_{j=0}^{i-1} \mu_1^j + \mu_2^i \sum_{j=0}^{i-1} \mu_0^j] \quad (3.40)$$

The values of the kinetic parameters and initial concentrations used to construct the MWD are given in Table 3.3.

Table 3.3: Kinetic parameters and initial concentrations used for simulations [95]

Kinetic parameters	Value
$k_{fm}$	$9.07 \times 10^{-2}$ L/(mol.sec))
$k_{fp}$	0.5 L/(mol.sec))
$k_d$	$1.18 \times 10^{-6}$ sec <sup>-1</sup>
$k_p$	500 L/(mol.sec))
$k_{tc}$	$5.97 \times 10^6$ L/(mol.sec))
$k_{td}$	0
$f$	1
Initial concentrations	Value
$M_0$	8.43 mol/L
$I_0$	0.001 mol/L
$S_0$	0 mol/L

To construct MWD, each set of moments for an individual generation (i.e. 0<sup>th</sup>, 1<sup>st</sup>, 2<sup>nd</sup>) is used. MWD of each class of polymer chains is calculated using a two-parameter model following Schultz-Flory distribution (Equation 3.39). Finally, all the distributions are added based on their contribution to yield the overall MWD.

$$w_i(r) = \frac{y_i (ry_i)^{z_i} e^{-ry_i}}{\Gamma(z_i + 1)}; i = 0, 1, 2, \dots \text{etc.}$$

$$z_i = \frac{DP_{n,i}}{DP_{w,i} - DP_{n,i}}; y_i = \frac{z_i + 1}{DP_{w,i}} \quad (3.41)$$

The above mentioned equations have been solved by Runge-Kutta (RK) [96] type explicit numerical integration routine. FORTRAN code using RK technique to solve the above set equations is provided in Appendix A. Fig. 3.1 depicts the construction of MWD by the numerical fractionation method. The contributions of individual generations are shown under the overall MWD curve. The appearance of artificial shoulders at higher molecular weight is due to the accumulation of various chains with different number of branches in the

first generation. More number of polymers comes under the first generation without being transferred to the higher generation. But, it requires very less computational effort. However, in some cases it is not possible to provide the correct MWD description (rise to artificial shoulders at higher molecular weight.). This method is based on the assumption that the transition from one generation to the next generation occurs only by a geometric growth (say, termination by combination reaction). If chain transfer to polymer and reaction with terminal double bonds are important, the assumptions are not sufficient.

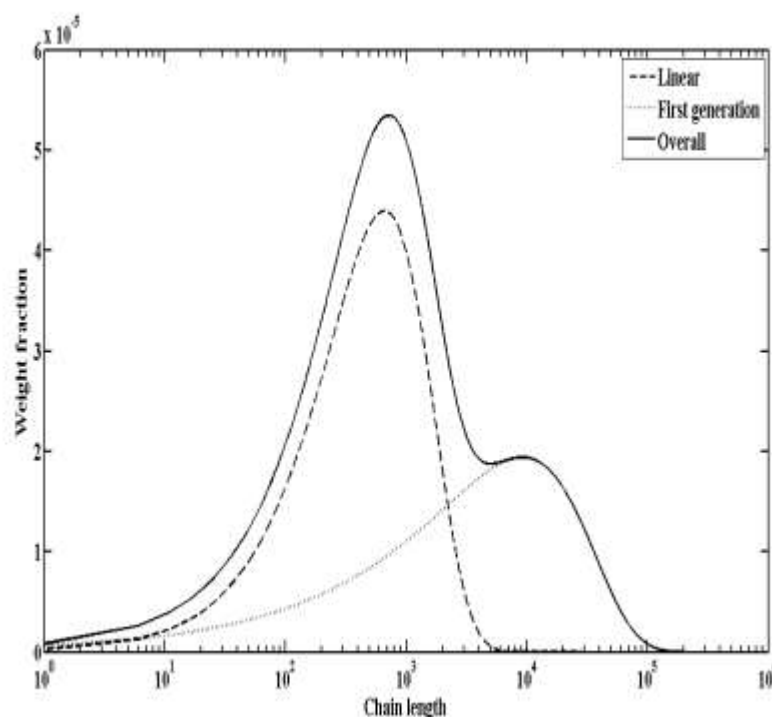
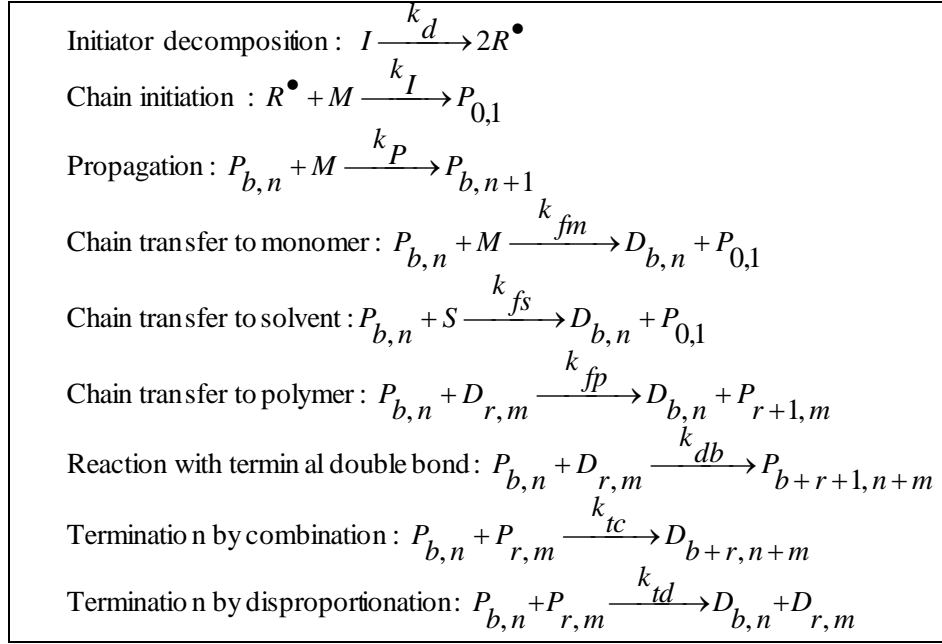


Figure 3.1: Chain length distributions at 65% monomer conversion

### 3.3.2 Partition according to the number of branches

The general free radical mechanism considered in this section is given in Table 3.4 [38]. In this method, the total polymer population is fractionated according to the number of classes, each class representing a polymer chain of similar long chain branching (LCB) content ( i.e. linear, LCB=1, LCB=2, etc.) [18].

Table 3.4: Free radical kinetic mechanism



Where  $P_{b,n}$  and  $D_{b,n}$  represent the live and dead polymers of chain length  $n$  and number of branches  $b$ . According to this method, dynamic moment balance equations are derived for each class of polymer chains including overall polymer chains. Following the kinetic mechanism given in Table 3.4, one can calculate the net rates of formation for live and dead polymer chains of each class prior to the moment balance. The following population balance equations result (Equation 3.42 to 3.45) out of this exercise:

**Net rate of formation of linear live and dead polymer chains of length  $n$ :**

$$\frac{dP_{0,n}}{dt} = 2fk_d[I]\delta(n-1) + \left[ k_{fm}[M] + k_{fs}[S] \right] \mu_0 \delta(n-1) + k_p [P_{0,n-1} - P_{0,n}][M] - (k_{fm}[M] + k_{fs}[S])P_{0,n} - k_{fp}P_{0,n}\nu_1 - k_{tc}P_{0,n}\mu_0 - k_{td}P_{0,n}\mu_0 - k_{db}P_{0,n}\nu_0 \quad (3.42)$$

$$\frac{dD_{0,n}}{dt} = (k_{fm}[M] + k_{fs}[S])P_{0,n} + k_{td}P_{0,n}\mu_0 + \frac{1}{2}k_{tc} \sum_{y=1}^{n-1} P_{0,y}^0 P_{0,n-y}^0 + k_{fp}P_{0,n}\mu_1 - k_{fp}nD_{0,n}\mu_0 - k_{db}D_{0,n}\mu_0 \quad (3.43)$$

**Net rate of formation of “i” class live and dead polymer chains of length  $n$ :**

$$\frac{dP_{i,n}}{dt} = k_p [P_{0,n-1} - P_{0,n}][M] - (k_{fm}[M] + k_{fs}[S])P_{i,n} - k_{fp}P_{i,n}\nu_1 + k_{fp}\mu_0 \left( \sum_{n=2}^{\infty} nD_n^{i-1} \right) - k_{tc}P_{i,n}\mu_0 - k_{td}P_{i,n}\mu_0 - k_{db}P_{i,n}\nu_0 + k_{db} \sum_{j=0}^{i-1} \sum_{y=1}^{n-1} P_{j,n-y} P_{i-j-1,y} \quad (3.44)$$

$$\frac{dD_{i,n}}{dt} = (k_{fm}[M] + k_{fs}[S])P_{i,n} + k_{td}P_{i,n}\mu_0 + \frac{1}{2}k_{tc} \sum_{j=0}^i \sum_{y=1}^{n-1} P_{j,y} P_{i-j,n-y} + k_{fp}P_{i,n} \sum_{j=0}^{N_c} \sum_{n=2}^{\infty} nD_{j,n} - k_{fp}nD_{i,n}\mu_0 - k_{db}D_{i,n}\mu_0 \quad (3.45)$$



After applying the moment based modeling for live and dead polymer chains of each class, the following equations will result.

**Moment rates for linear live polymer chains:**

$$\frac{d\mu_{0,0}}{dt} = 2fk_d[I] + (k_{tc} + k_{td})\mu_0\mu_{0,0} + (k_{fm}[M] + k_{fs}[S])\mu_0 + k_{fp}v_1\mu_{0,0} \quad (3.46)$$

$$\begin{aligned} \frac{d\mu_{1,0}}{dt} = & 2fk_d[I] + k_p[M]\mu_{0,0} + (k_{fm}[M] + k_{fs}[S])\mu_0 - [(k_{fm}[M] + k_{fs}[S]) \\ & + (k_{tc} + k_{td})\mu_0 + k_{fp}v_1 + k_{db}v_0]\mu_{1,0} \end{aligned} \quad (3.47)$$

$$\begin{aligned} \frac{d\mu_{2,0}}{dt} = & 2fk_d[I] + 2k_p[M]\mu_{1,0} + (k_{fm}[M] + k_{fs}[S])\mu_0 - [(k_{fm}[M] + k_{fs}[S]) \\ & + (k_{tc} + k_{td})\mu_0 + k_{fp}v_1 + k_{db}v_0]\mu_{2,0} \end{aligned} \quad (3.48)$$

**Moment rates for live polymer chains of “i<sup>th</sup>” class branched chains:**

$$\begin{aligned} \frac{d\mu_{0,i}}{dt} = & -[(k_{tc} + k_{td})\mu_0 + (k_{fm}[M] + k_{fs}[S]) + k_{fp}v_1 + k_{db}v_0]\mu_{0,i} + k_{fp}v_{1,i-1}\mu_0 + \\ & k_{db}\sum_{j=0}^{i-1}\mu_{0,j}v_{0,i-j-1} \end{aligned} \quad (3.49)$$

$$\begin{aligned} \frac{d\mu_{1,i}}{dt} = & k_p[M]\mu_{0,i} - [(k_{fm}[M] + k_{fs}[S]) + (k_{tc} + k_{td})\mu_0 + k_{fp}v_1 + k_{db}v_0]\mu_{1,i} + \\ & k_{fp}v_{2,i}\mu_0 + k_{db}\sum_{j=0}^{i-1}(\mu_{0,j}v_{1,i-j-1} + \mu_{1,j}v_{0,i-j-1}) \end{aligned} \quad (3.50)$$

$$\begin{aligned} \frac{d\mu_{2,i}}{dt} = & 2k_p[M]\mu_{1,i} - [(k_{fm}[M] + k_{fs}[S]) + (k_{tc} + k_{td})\mu_0 + k_{fp}v_1 + k_{db}v_0]\mu_{2,i} \\ & + k_{fp}v_{3,i-1}\mu_0 + k_{db}\sum_{j=0}^{i-1}(\mu_{0,j}v_{2,i-j-1} + 2\mu_{1,j}v_{1,i-j-1} + \mu_{2,j}v_{0,i-j-1}) \end{aligned} \quad (3.51)$$

**Moment rates for linear dead polymer chains:**

$$\begin{aligned} \frac{dv_{0,0}}{dt} = & (k_{fm}[M] + k_{fs}[S] + k_{td}\mu_0 + k_{fp}v_1)\mu_{0,0} + (\frac{1}{2}k_{tc})(\mu_{0,0})^2 - k_{fp}\mu_0v_{1,0} \\ & - k_{db}\mu_0v_{0,0} \end{aligned} \quad (3.52)$$

$$\begin{aligned} \frac{dv_{1,0}}{dt} = & (k_{fm}[M] + k_{fs}[S] + k_{td}\mu_0 + k_{fp}v_1)\mu_{1,0} + k_{tc}\mu_{0,0}\mu_{1,0} - k_{fp}\mu_0v_{2,0} \\ & - k_{db}\mu_0v_{1,0} \end{aligned} \quad (3.53)$$

$$\begin{aligned} \frac{dv_{2,0}}{dt} = & (k_{fm}[M] + k_{fs}[S] + k_{td}\lambda_0 + k_{fp}\mu_1)\mu_{2,0} + k_{tc}[\mu_{0,0}\mu_{2,0} + (\mu_{1,0})^2] - k_{fp}\mu_0v_{3,0} \\ & - k_{db}\mu_0v_{2,0} \end{aligned} \quad (3.54)$$

**Moment rates for “i” class branched dead polymer chains:**

$$\frac{dv_{0,i}}{dt} = (k_{fm}[M] + k_{fs}[S] + k_{td}\mu_0 + k_{fp}v_1)\mu_{0,i} + k_{tc}\sum_{j=0}^i \frac{1}{2}\mu_{0,j}\mu_{0,i-j} - k_{fp}\mu_0 v_{1,i} - k_{db}\mu_0 v_{0,i} \quad (3.55)$$

$$\frac{dv_{1,i}}{dt} = (k_{fm}[M] + k_{fs}[S] + k_{td}\mu_0 + k_{fp}v_1)\mu_{1,i} + k_{tc}\sum_{j=0}^i \mu_{0,j}\mu_{1,i-j} - k_{fp}\mu_0 v_{2,i} - k_{db}\mu_0 v_{1,i} \quad (3.56)$$

$$\frac{dv_{2,i}}{dt} = (k_{fm}[M] + k_{fs}[S] + k_{td}\mu_0 + k_{fp}v_1)\mu_{2,i} + -k_{fp}\mu_0 v_{3,i} - k_{db}\mu_0 v_{2,i} + k_{tc}\sum_{j=0}^i \left( \frac{1}{2}\mu_{0,j}\mu_{2,i-j} + \mu_{1,j}\mu_{1,i-j} + \frac{1}{2}\mu_{2,j}\mu_{0,i-j} \right) \quad (3.57)$$

Total number of classes should be chosen properly for the complete construction of molecular weight distribution (MWD). This means that the sum of the first moments of all classes should be approximately equal to the overall first moment of the polymer [18]. In this technique [18], the class number does not change by the “propagation”, “chain transfer to monomer” and “termination by disproportionation” reaction mechanisms. Class number is increased by the “chain transfer to polymer”, “reaction with terminal double bond” and “termination by combination” reaction mechanisms. Kinetic constants used in the present study are shown in Table 3.5 [38]. The model equations describing the various molar species rates can be solved by LIMEX DAE [41] variable time step solver. Using the calculated moments of each class of the polymer, a two parameter Wesslau distribution [18] has been used to calculate weight chain length distribution (Equation 3.56). The overall molecular weight distribution is the weighted sum of all class distributions in the population. The program which is integrated with LIMEX solver has been provided in appendix B. Fig. 3.2 represents the MWD-LCB at different chain lengths for (number of average degree of branching)  $B_n = 0.9$  and temperature of  $80^\circ\text{C}$ . Here, the molecular weight distributions of PVAc are plotted for different long chain branches (i.e. LCB = 0, 1, 2, 3, 4, 5, 6). It can be seen from this plot that the linear polymer (i.e. LCB = 0) dominates at the starting of polymerization followed by LCB = 1, 2 etc. This figure shows the information of LCB distribution for different chain lengths and the inset figure represents the overall MWD.

$$W_i(n) = (2\pi\sigma_i^2)^{-1/2} \exp\left[-\frac{(\ln n - \ln n_{mi})^2}{2\sigma_i^2}\right]$$

$$n_{mi} = (v_{2,i}/v_{1,i})^{1/2}, \exp(\sigma_i^2) = v_{0,i}v_{2,i}/(v_{1,i})^2$$

$$W_{total}(n) = \sum_{i=0}^{Nc} (W_i(n)v_{1,i})/v_1 \quad (3.58)$$

Table 3.5 Kinetic parameters and initial concentrations used for simulations [38]

Kinetic parameters	Value
$k_{fm}$	$4.957 \times 10^8 \exp(-10480/RT)$ (L/mol.min)
$k_{fp}$	$5.177 \times 10^8 \exp(-11440/RT)$ (L/mol.min)
$k_d$	$2.7 \times 10^{16} \exp(-30000/RT)$ (1/min)
$k_p$	$4.2 \times 10^9 \exp(-6300/RT)$ (L/mol.min)
$k_{tc}$	$1.62 \times 10^{12} \exp(-2800/RT)$ ( L/mol.min)
$k_{td}$	0
$f$	0.5
Initial concentrations	Value
$M_0$	12 mol/L
$I_0$	0.0001 mol/L
$S_0$	0 mol/L

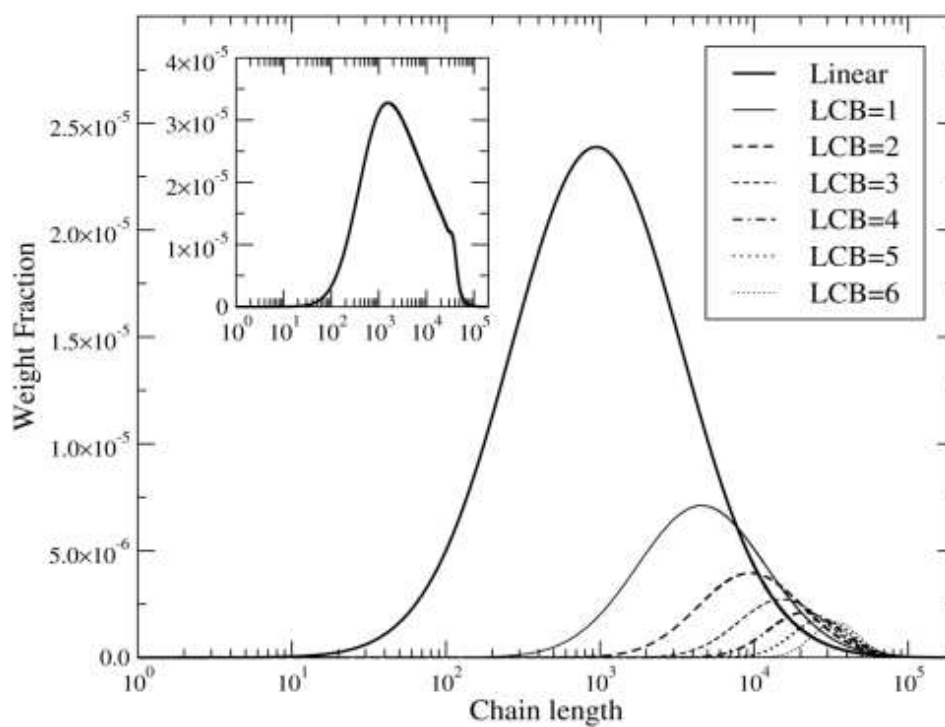


Figure 3.2: Molecular weight distribution at 80°C for  $B_n = 0.9$  for different long chain branching

### 3.3.3 Fixed Pivot Technique

In this method, a 2-dimensional sectional grid was used [38] to solve the above population balance equations (Equations 3.40 to 3.43). This technique [39] was applied for calculating the polymer chain populations in a free radical polymerization reactor [38]. By using this method, the original infinitely large numbers of population balance equations were reduced to finite number of ODEs. This method has the capability to calculate the polymer concentration directly. Following the development of Kumar and Rama Krishna [39], Meimaroglou *et al.*, [38] utilized this technique to calculate molecular weight distributions by discretizing the total polymer chain length and long chain branches per chain (LCB) into 2-dimensional finite elements.

Let  $N_{n+1}$  and  $N_{b+1}$  are the number of discrete points in total chain length domain and long chain branching domain. The symbols  $u_n(i)$  ( $i=1,2,\dots, N_{n+1}$ ) and  $u_b(j)$  ( $j=1,2,\dots, N_{b+1}$ ) indicate the discrete values of chain length and long chain branches. Let us assume  $P(j,i,t)$  and  $D(j,i,t)$  be the molar concentrations of live and dead polymers in the center of 2-D element, which are defined by 4 discrete neighbor points ( $(u_n(i), u_b(j))$ ,  $(u_n(i), u_b(j+1))$ ,  $(u_n(i+1), u_b(j))$ ,  $(u_n(i+1), u_b(j+1))$ ). And the corresponding discrete values for total chain length and long chain branches are  $n(i)$  and  $b(j)$ . If new polymer chains are formed within 2-D domain ( $(n(i), b(j))$ ,  $(n(i), b(j+1))$ ,  $(n(i+1), b(j))$ ,  $(n(i+1), b(j+1))$ ); Fig. 3.3), their concentrations are assigned to the 4 neighboring grid points. From this technique, the following continuous rate equations for active and dead polymers can be obtained.

$$\begin{aligned}
 r_p(1,i,t) = & 2fk_d[I]\delta(i-1) + k_{fs}\left[S\left(\sum_{l=1}^{N_{e,b}}\sum_{k=1}^{N_{e,n}}P(l,k,t)\right)\right]\delta(i-1) + \\
 & k_{fm}\left[M\left(\sum_{l=1}^{N_{e,b}}\sum_{k=1}^{N_{e,n}}P(l,k,t)\right)\right]\delta(i-1) + k_p[M]\sum_{k=1}^iA(i,k)P(1,i,t) \\
 & - k_p[M]P(1,i,t) - k_{fs}[S]P(1,i,t) - k_{fm}[M]P(1,i,t) - \\
 & k_{fp}P(1,i,t)\left(\sum_{l=1}^{N_{e,b}}\sum_{k=1}^{N_{e,n}}n(k)D(l,k,t)\right) - k_{db}P(1,i,t)\left(\sum_{l=1}^{N_{e,b}}\sum_{k=1}^{N_{e,n}}D(l,k,t)\right) \\
 & - k_{td}P(1,i,t)\left(\sum_{l=1}^{N_{e,b}}\sum_{k=1}^{N_{e,n}}P(l,k,t)\right) - k_{tc}P(1,i,t)\left(\sum_{l=1}^{N_{e,b}}\sum_{k=1}^{N_{e,n}}P(l,k,t)\right)
 \end{aligned} \tag{3.59}$$

$$\begin{aligned}
r_p(j, i, t) = & k_p [M] \sum_{k=1}^i A(i, k) P(j, k, t) - k_p [M] P(j, i, t) - k_{fs} [S] P(j, i, t) \\
& - k_{fm} [M] P(j, i, t) - k_{fp} P(j, i, t) \left( \sum_{l=1}^{N_{e,b}} \sum_{k=1}^{N_{e,n}} n(k) D(l, k, t) \right) + \\
& k_{fp} n(i) \left( \sum_{l=1}^{N_{e,b}} \sum_{k=1}^{N_{e,n}} P(l, k, t) \right) \left( \sum_{l=1}^j C(j, l) D(l, i, t) \right) - \\
& k_{db} P(j, i, t) \left( \sum_{l=1}^{N_{e,b}} \sum_{k=1}^{N_{e,n}} D(l, k, t) \right) - k_{td} P(j, i, t) \left( \sum_{l=1}^{N_{e,b}} \sum_{k=1}^{N_{e,n}} P(l, k, t) \right) - \\
& k_{db} \sum_{l=1}^j \sum_{q=1}^j \sum_{k=1}^i \sum_{m=1}^i B(i, k, m) T(j, l, q) P(l, k, t) D(q, m, t) \\
& - k_{tc} P(j, i, t) \left( \sum_{l=1}^{N_{e,b}} \sum_{k=1}^{N_{e,n}} P(l, k, t) \right)
\end{aligned} \tag{3.60}$$

$$\begin{aligned}
r_D(1, i, t) = & k_{fs} [S] P(1, i, t) + k_{fp} P(1, i, t) \left( \sum_{l=1}^{N_{e,b}} \sum_{k=1}^{N_{e,n}} n(k) D(l, k, t) \right) + \\
& k_{fm} [M] P(1, i, t) + k_{td} P(1, i, t) \left( \sum_{l=1}^{N_{e,b}} \sum_{k=1}^{N_{e,n}} P(l, k, t) \right) + \\
& k_{tc} \sum_{k=1}^i \sum_{m=k}^i B(i, k, m) P(1, k, t) P(1, m, t) - \\
& k_{fp} n(i) D(1, i, t) \left( \sum_{l=1}^{N_{e,b}} \sum_{k=1}^{N_{e,n}} P(l, k, t) \right) - k_{db} D(1, i, t) \left( \sum_{l=1}^{N_{e,b}} \sum_{k=1}^{N_{e,n}} P(l, k, t) \right)
\end{aligned} \tag{3.61}$$

$$\begin{aligned}
r_D(j, i, t) = & k_{fs} [S] P(j, i, t) + k_{fp} P(j, i, t) \left( \sum_{l=1}^{N_{e,b}} \sum_{k=1}^{N_{e,n}} n(k) D(l, k, t) \right) + \\
& k_{fm} [M] P(j, i, t) + k_{td} P(j, i, t) \left( \sum_{l=1}^{N_{e,b}} \sum_{k=1}^{N_{e,n}} P(l, k, t) \right) - \\
& k_{fp} n(i) D(j, i, t) \left( \sum_{l=1}^{N_{e,b}} \sum_{k=1}^{N_{e,n}} P(l, k, t) \right) - k_{db} D(j, i, t) \left( \sum_{l=1}^{N_{e,b}} \sum_{k=1}^{N_{e,n}} P(l, k, t) \right) - \\
& k_{tc} \sum_{l=1}^j \sum_{q=1}^j \sum_{k=1}^i \sum_{m=1}^i B(i, k, m) O(j, l, q) P(l, k, t) P(q, m, t)
\end{aligned} \tag{3.62}$$

The matrices  $A(i, k)$ ,  $B(i, k, m)$ ,  $C(j, l)$ ,  $T(j, l, q)$  and  $O(j, l, q)$  can be calculated by the following equations:

$$A(i, k) = \begin{cases} \frac{n(i+1) - n}{n(i+1) - n(i)} n(i) \leq n \leq n(i+1) \\ \frac{n - n(i-1)}{n(i) - n(i-1)} n(i-1) \leq n \leq n(i) \\ n = n(k) + 1 \end{cases}$$

$$B(i,k,m) = \begin{cases} \frac{n(i+1)-n}{n(i+1)-n(i)} n(i) \leq n \leq n(i+1) \\ \frac{n-n(i-1)}{n(i)-n(i-1)} n(i-1) \leq n \leq n(i) \\ n = n(k) + n(m) \end{cases}$$

$$C(j,l) = \begin{cases} \frac{b(j+1)-b}{b(j+1)-b(j)} b(j) \leq b \leq b(j+1) \\ \frac{b-b(j-1)}{b(j)-b(j-1)} b(j-1) \leq b \leq b(j) \\ b = b(l) + 1 \end{cases}$$

$$T(j,l,q) = \begin{cases} \frac{b(j+1)-b}{b(j+1)-b(j)} b(j) \leq b \leq b(j+1) \\ \frac{b-b(j-1)}{b(j)-b(j-1)} b(j-1) \leq b \leq b(j) \\ b = b(l) + b(q) + 1 \end{cases}$$

$$O(j,l,q) = \begin{cases} \frac{b(j+1)-b}{b(j+1)-b(j)} b(j) \leq b \leq b(j+1) \\ \frac{b-b(j-1)}{b(j)-b(j-1)} b(j-1) \leq b \leq b(j) \\ b = b(l) + b(q) \end{cases}$$

After calculating the live and dead polymer chains at the grid points, weight chain length distribution for a specific branching (i.e.  $b(j)$ ) can be calculated by the following expression:

$$W(j,i,t) = \frac{n(i)D(j,i,t)}{(u_n(i+1) - u_n(i))}; i = 1, 2, \dots, N_n \quad (3.63)$$

Overall molecular weight distribution can be calculated by sum of all distributions that corresponds to the grid points in the long chain branching domain (Equation 3.64).

$$W_t(i,t) = \frac{\sum_{l=1}^{N_b} [n(i)D(l,i,t)/(u_n(i+1) - u_n(i))]}{\sum_{l=1}^{N_b} \sum_{k=1}^{N_n} n(k)D(l,k,t)} \quad (3.64)$$

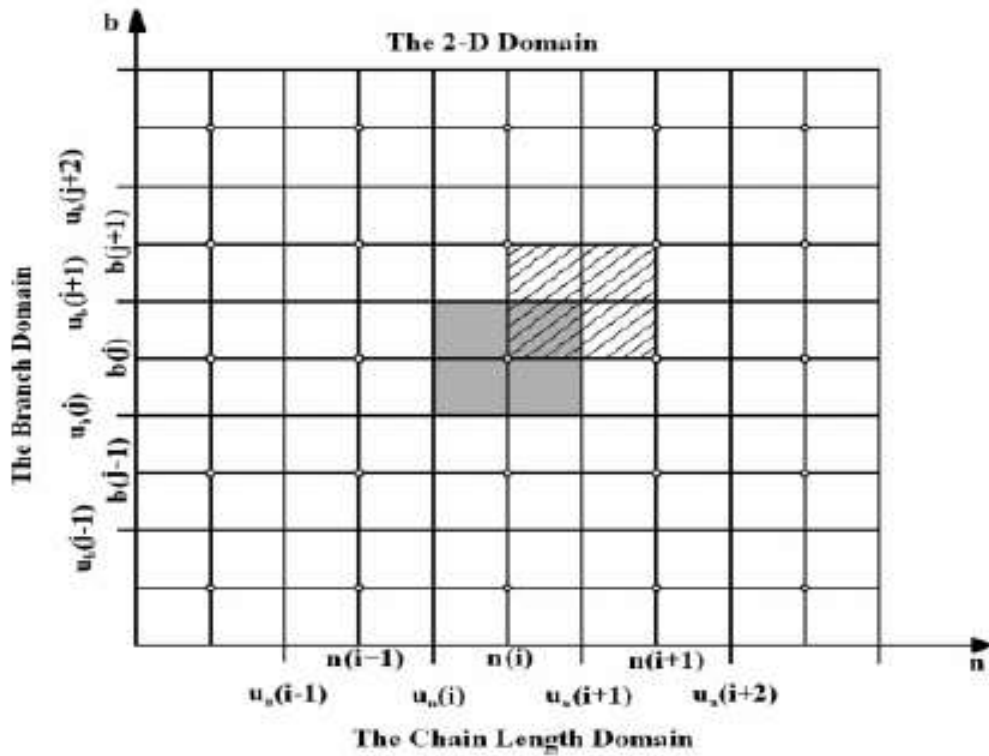


Figure 3.3: 2-D sectional grid used in Fixed pivot method [38]

### 3.4 Solver

LIMEX is an extrapolation integrator for solving linearly-implicit differential-algebraic systems of the form

$$B(t,y) * y'(t) = f(t,y)$$

where  $B$  is a  $(n \times n)$ -matrix whose rank is less than or equal to  $n$  and  $y$  is the real array of size  $n$ . This value of  $y$  must be set at the starting point. On exit,  $y$  contains the solution at the final point. (The discretization of LIMEX is based on the elementary linearly implicit Euler discretization

$$(B(t,y(k)) - h J) (y(k+1) - y(k)) = hf(t(k+1),y(k))$$

Where  $h$  is the initial step size guess and  $J$  is the (approximate) Jacobian of the residual

$$\left( \frac{d}{dy} (f - By^1) \right)_{t=t(0)}$$

Combined with extrapolation, this one step method permits an adaptive control of step size. The efficiency of LIMEX mainly depends on the performance of the evaluation of the Jacobian and in particular on the solution of the linear systems. Throughout the solver a

local error control is implemented, which requires that the local error of a component  $y(i)$  is less than  $rTol * abs ( y(i) ) + aTol(i)$  ( $rTol$ =relative error tolerance,  $aTol$ =absolute error tolerance). This approach enables to specify more or less sensitive components of the solution vector. The code which is integrated with LIMEX solver has been provided in appendix B. In that,  $n$  and  $nz$  are the total number of equations and total number of odes, respectively. Since all equations are odes,  $n$  and  $nz$  are equal. For more information, the solver is provided in the web page <http://www.zib.de>.



## Chapter 4

# Multi-Objective Optimization of Bulk Vinyl Acetate Polymerization with Branching

This chapter describes the kinetic scheme adopted and the related modeling procedure to calculate molecular properties of the polymer. Further, the simulation results of multi-objective optimization and its rationale behind the formulation of the problem is provided.

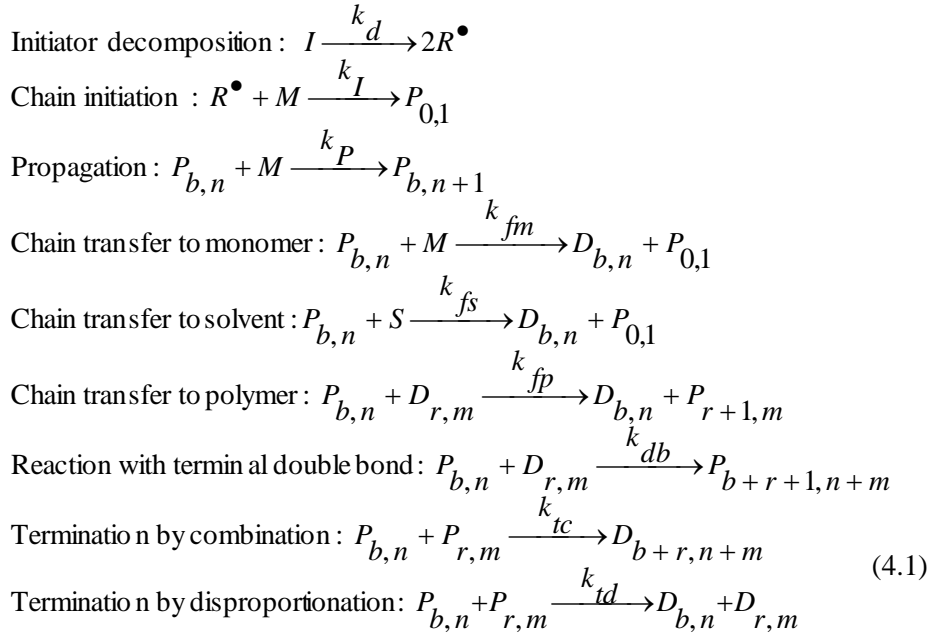
### 4.1 Introduction

In the present effort, bulk free radical polymerization of vinyl acetate, which is a highly branched polymer, is considered. The model is validated with the batch experiment for bulk vinyl acetate polymerization conducted by Thomas [1]. While using numerical fractionation technique in this study for calculating MWD, the entire polymer population has been fractionated based on the number of branches. For each class, moment based modeling is applied for live and dead polymer chains to reduce the number of equations. From this technique, average polymer properties such as number average molecular weight ( $M_n$ ), weight average molecular weight ( $M_w$ ), number average degree of branching ( $B_n$ ) etc. are calculated. Finally, MWD is calculated for each class (i.e. having same long chain branching (LCB)) by Wesslau distribution [18] using the above mentioned numerical technique (i.e. partition according to number of branches) [18] and the overall MWD is calculated as the weighed sum of MWDs of individual class. Here, the class number is increased by chain transfer to polymer reaction and reaction with terminal double bond as it increases long chain branching (LCB). In chain transfer to polymer reaction, internal radical is formed from dead polymer chain by hydrogen abstraction [37]. Monomer units present in the reactor attack the internal radical leading to formation of LCB. It is important to note

that at higher monomer conversion, gel formation occurs and viscosity of the polymer increases. At this point, termination rate becomes slower and therefore rate determining. As the long chain branching and monomer conversion increase, number of classes should also be large to construct the complete MWD. There is a chance of forming gel at higher monomer conversion where there is a sudden rise in molecular weight, i.e. gel point. An empirical relation has been deduced between monomer conversion and temperature to predict the gel point. With such prediction in place, the final goal here is to find out the optimal process conditions to get the desired combination of various conflicting objectives avoiding the gel effect. Addition amounts of monomer and initiator in batch mode are to be decided by the optimization routine (decision variables). Simultaneous minimization of total polymerization time ( $t_p$ ), maximization of weight-average molecular weight ( $M_w$ ) and number average degree of branching ( $B_n$ ) are taken as objective functions (conflicting to one another). Pareto optimal (PO) or trade-off solutions for batch polymerization of vinyl acetate are obtained by real coded non-dominated sorting genetic algorithm II (NSGA II) [19], a well-established multi-objective optimization (MOO) technique. The rest of the chapter is organized as follows. Section 4.2 describes the kinetic scheme adopted and the related modeling procedure to provide a link between the molecular architecture and polymer properties. The rationale behind the formulation of the optimization problem is provided in section 4.3. Results of the optimization problem are presented in section 4.4 followed by the concluding remarks in section 4.5.

## 4.2 Model

Thomas [1] used 2, 2 azobisisobutyronitrile (AIBN) as initiator with two different concentrations (i.e.  $5 \times 10^{-5}$  mol/lit and  $1 \times 10^{-4}$  mol/lit) at two different temperatures (i.e.  $60^\circ\text{C}$  and  $80^\circ\text{C}$ ) for the bulk polymerization of vinyl acetate. The general free radical polymerization kinetic model [38, 97] for PVAc considered in this chapter is given below.



where  $P_{b,n}$  and  $D_{b,n}$  represent live and dead polymer chains of length “n” and “b” long chain branches, respectively. The rate of formation of live and dead polymer chains from the above kinetic mechanism is derived and is given in chapter 3 (section 3.3.2). This results in a large number of equations. To reduce the total number of equations, method of moments has been applied for live and dead polymer chains of each class (i.e. linear, single branch, two branches etc.) and they are defined by

$$\mu_{x,i} = \sum_{n=1}^{\infty} n^x P_{i,n} \tag{4.2}$$

$$\nu_{x,i} = \sum_{n=1}^{\infty} n^x D_{i,n} \tag{4.3}$$

Where, x and n represent moment number and chain length, respectively, and i represents the class number (i = 0, 1, 2, 3 etc.). The resultant ordinary differential equations initial value problem (ODE-IVPs) is integrated by LIMEX DAE [41] variable time step solver. Polymer properties such as  $M_n$  and  $M_w$  are calculated from moments and are given by

$$M_n = (\nu_1/\nu_0)MW \tag{4.4}$$

$$M_w = (\nu_2/\nu_1)MW \tag{4.5}$$

In this technique [18], the class number does not change by the “propagation”, “chain transfer to monomer” and “termination by disproportionation” reaction mechanisms (see Equation 4.1). Class number is increased by the “chain transfer to polymer”, “reaction with

terminal double bond” and “termination by combination” reaction mechanisms (see equation 4.1). Kinetic constants used in the present study are shown in Table 4.1.

Table 4.1: Kinetic constants used in the present study [38]

$k_p$	$4.2 \times 10^9 \exp(-6300/RT)(L/mol.min)$
$k_{tc}$	$1.62 \times 10^{12} \exp(-2800/RT)(L/mol.min)$
$k_{td}$	0
$k_{fm}$	$4.957 \times 10^8 \exp(-10480/RT) (L/mol.min)$
$k_{fp}$	$5.177 \times 10^8 \exp(-11440/RT) (L/mol.min)$
$k_{db}$	0.66 $K_p$
$k_d$	$2.7 \times 10^{16} \exp(-30000/RT) (1/min)$

### 4.3 Optimization problem formulation

In the optimization formulation, monomer addition ( $u_1$ ) and initiator addition ( $u_2$ ) at zero<sup>th</sup> time and temperature ( $T$ ) are taken as decision variables, which are to be decided by the optimization routine. Improvement in certain properties of the polymer such as weight average molecular weight ( $M_w$ ) and number average degree of branching ( $B_n$ ) comes from the deterioration of other properties. For example, to get a polymer of high  $M_w$  and  $B_n$ , one has to compromise either polymerization time and polydispersity index (PDI). Minimization of total polymerization time, maximization of weight average molecular weight and maximization of number average degree of branching are taken as objective functions (case 1: Table 4.2). Analysis of the above stated model reveals that live radical species in polymer population are responsible for branching in polymer via chain transfer mechanism. Maximization of concentration of live polymer and the effect of monomer and initiator addition on them can be the other study of importance (case 2: Table 4.3). In this case also, the decision variables are temperature, monomer and initiator addition amounts ( $u_1$  and  $u_2$ ) as presented earlier. Once temperature, monomer and initiator additions are decided by optimizer, monomer conversion at gel (autoacceleration) point is calculated by the empirical relation between monomer conversion and temperature (Equation 4.6). This autoacceleration leading to a sharp rise in the degree of polymerization [37], beyond which process is difficult to control. Gel point conversion ( $Conv_{Gel}$ ) is dynamic in nature.

$$Conv_{Gel} = 1.47 \times 10^{-3} \times T + 0.32 \quad (4.6)$$

This equation is obtained from Fig. 4.1 of conversion vs.  $M_w$  at two temperatures. By taking the point at which  $M_w$  rises suddenly for two cases at two different temperatures, one may get the temperature dependency of gel point conversion by linear fitting. Based on the conversion value obtained at the gel point, the simulation is allowed to proceed up to 3% lesser than that conversion value to avoid gel effect at a particular temperature e.g. if the conversion value obtained at the gel point is 80% for a particular temperature, the simulation of the model is allowed to run up to 77% of the monomer conversion. All decision variables ( $T$ ,  $u_1$  and  $u_2$ ) are bound so that they lie between their lower and upper bounds (denoted by the superscripts, min and max). The limiting values for the various constraints such as  $M_w$ , PDI are decided by the experimental study to avoid any extrapolation error arising from the model predictions [1]. The above model is integrated with NSGA II to perform multi-objective optimization. NSGA II is a nature-inspired evolutionary method for handling multi-objective optimization problems. As compared to classical techniques handling multi-objective optimization problems which generate single PO solution in single optimization run, NSGA II is established as a robust multi-objective optimization technique that can find a set of well-spread PO solutions in single simulation run [19].

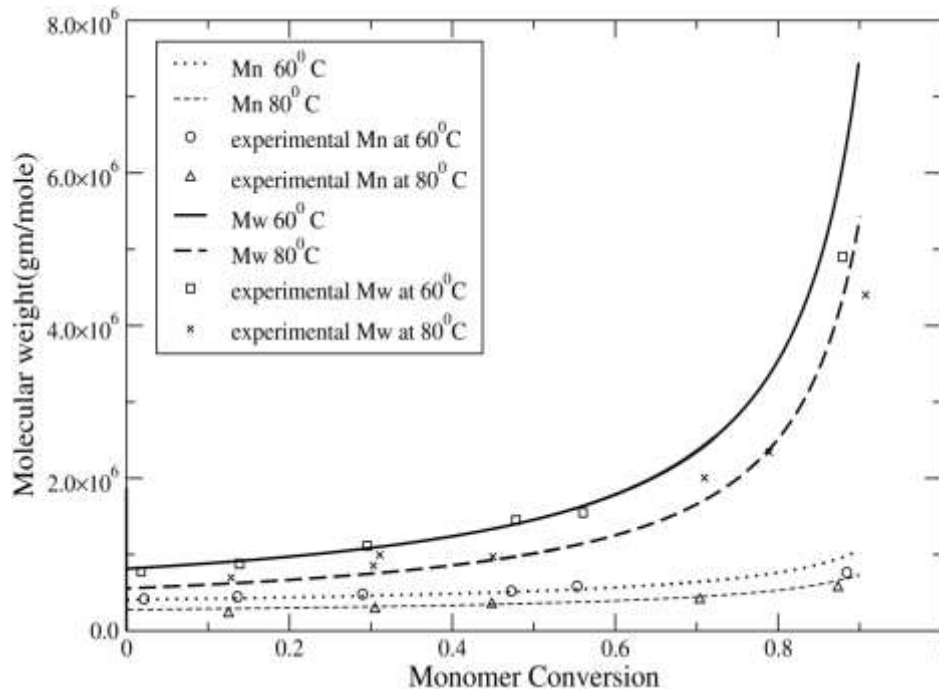


Figure 4.1: Comparison of molecular weight between the experimental values and the model prediction.

In NSGA II, the decision variables are represented by chromosomes. As there are three decision variables in this case, a chromosome consists of three real values of decision variables (each decision variable called as gene). There are  $N$  such chromosomes (called population) present in each iteration (called generation) of NSGA II. In course of optimization, this population of candidate solutions is initially being created, classified, selected, preferred and modified from one generation to other before finally converging to the PO solutions. To start with, each chromosome in a population of size  $N$  is randomly generated which means three real valued genes (i.e.  $u_1, u_2, T$ ) are randomly created within their given bounds (expressed by superscript max and min). Once the values are created, objective functions and constraints are evaluated for the entire population from the model. For different values of  $u_1, u_2$  and  $T$ , the model returns different sets of values of  $M_w, B_n$ . If they satisfy all the constraints, the solution is chosen as feasible, otherwise infeasible. From this parent population, a children population size of  $N$  is created by simulated binary crossover (SBX) and polynomial mutation operators [19]. Probability of mutation and crossover (i.e.  $p_m = 0.1, p_c = 0.9$ ) are used in this study. As this is elitist approach, parent and children population are merged together which results into a total population size of  $2N$ . From this merged population,  $N$  solutions are forwarded to the next generation based on non-dominated sorting and crowded tournament selection operation [19]. While comparing two solutions (say, solution 1 and solution 2), if solution 1 is better than solution 2 in terms of all objective functions, solution 1 is said to dominate solution 2. Similarly, another case could be solution 2 dominating solution 1. If none of them dominates, they are called non-dominated solutions. To obtain such fronts, each of the solutions is compared with all other solutions in the population. The solutions which are not dominated by any other solutions are classified as non-dominated solutions of rank 1. After deleting these solutions, the entire population is again sorted based on non-dominance and the solutions found are named as non-dominated solutions of rank 2. In this manner, the feasible solutions of the entire population are sorted first. If this process creates some  $m$  fronts, the infeasible points are targeted next for ranking and they are numbered  $m+1$  onwards based on ascending degree of overall constraint violation. Since only  $N$  slots are available for accommodation, not all solutions can be accommodated and for this, the crowded tournament selection has been used. Binary tournament selection picks up two candidate solutions randomly and the one having better ranking is selected. Since infeasible solutions get an inferior rank, feasible solutions are always preferred to infeasible solutions. Infeasible solutions can be repaired by the genetic operators to convert to feasible solutions in the next generation. If both of them are happened to be from the same front and feasible, the one having higher crowding

distance is selected. Crowding distance is a metric which provides some idea of the solution being crowded by neighboring solutions. Higher the crowding distance, the solution is less crowded by neighbors and vice versa. The newly obtained population with  $N$  candidate solutions is used to generate a new children population in the next generation and this procedure continues with predefined number of generations ( $N_{\text{genmax}}$ ) before the final PO solutions (rank 1 solutions in generation number  $N_{\text{genmax}}$ ) are emerged. Values of NSGA II parameters used in this case are:  $N_{\text{genmax}} = 40$ ,  $N$  (population size) = 70, distribution index for real coded crossover = 0.01, distribution index for real coded mutation = 0.01. The algorithm mentioned in Table 4.4 represents the NSGA II optimization routine in the present study. Since three objective functions are involved, a small population size may not lead to a well spread Pareto. However, a large population size is also not recommended since that leads to more number of function evaluations. So, a population size has 70 has been chosen. Changes in population size, crossover probability and mutation probability do not lead to any significant change in PO solutions.

Table 4.2: Batch multi-objective optimization problem formulation: Case 1

$  \begin{aligned}  & \textit{Maximize} \quad M_w \\  & \textit{Maximize} \quad B_n \\  & \textit{Minimize} \quad t_{poly} \\  & M_w \geq M_w^{\min} \\  & PDI \leq PDI^{\max}  \end{aligned}  $
--

The values of  $u_1^{\min}$ ,  $u_1^{\max}$  and temperature (decision variables) are:

$$u_1^{\min} = 10.0; \quad u_1^{\max} = 14.0;$$

$$u_2^{\min} = 3.0E - 05; \quad u_2^{\max} = 1.5E - 04;$$

$$T^{\min} = 333K; \quad T^{\max} = 353K;$$

Table 4.3: Batch multi-objective optimization problem formulation: Case 2

$$\begin{array}{l} \textit{Maximize} \quad \lambda_0 \\ \textit{Maximize} \quad B_n \\ \textit{Minimize} \quad t_{poly} \\ M_w \geq M_w^{\min} \\ PDI \leq PDI^{\max} \end{array}$$

The values of  $u_i^{\min}$ ,  $u_i^{\max}$  and temperature (decision variables) are:

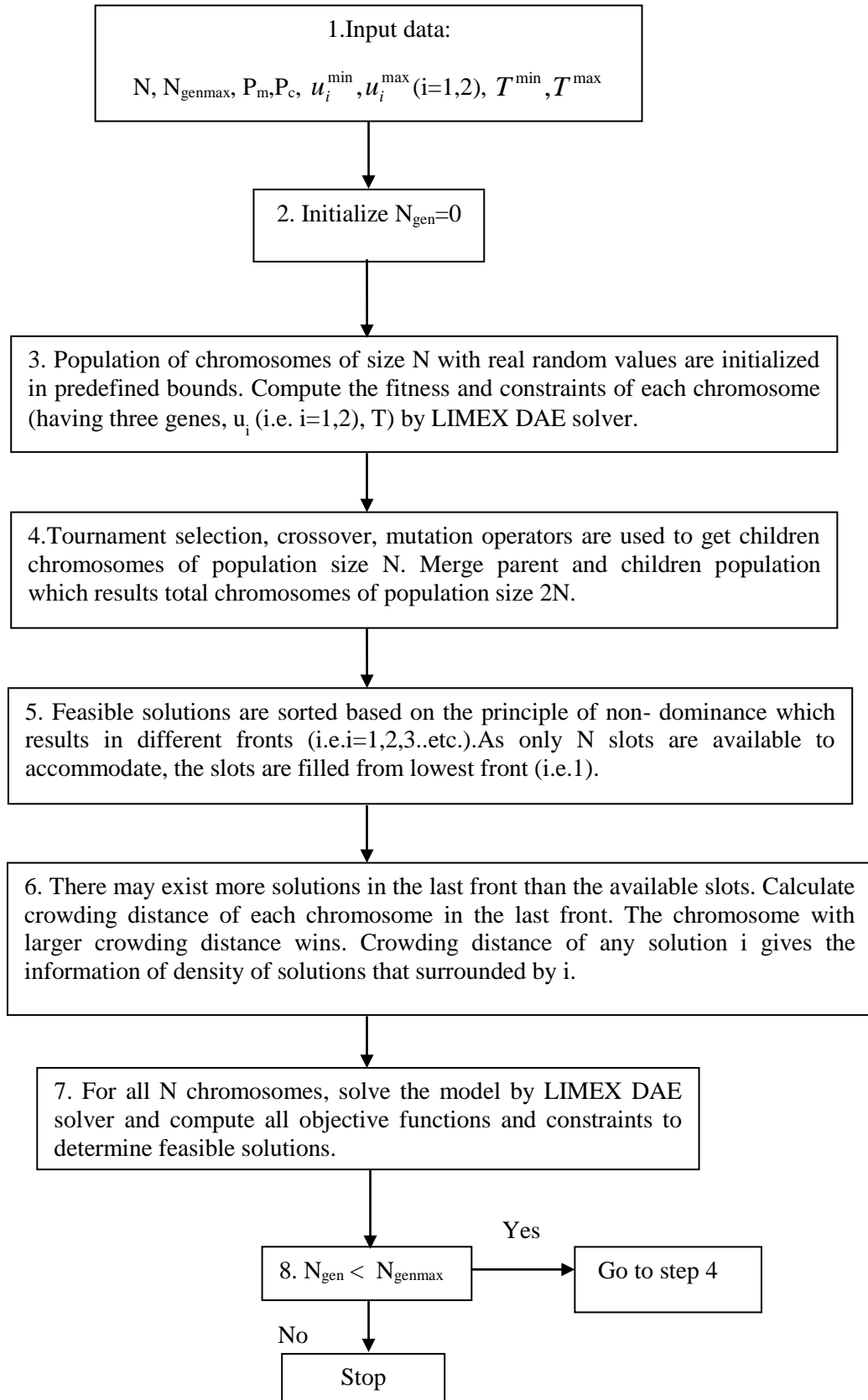
$$u_1^{\min} = 10.0; \quad u_1^{\max} = 14.0;$$

$$u_2^{\min} = 3.0E-05; \quad u_2^{\max} = 1.5E-04;$$

$$T^{\min} = 333K; \quad T^{\max} = 353K;$$



Table 4.4: NSGAI algorithm adopted in the present optimization study [19]



## 4.4 Results and discussion

### 4.4.1 Model validation

Polymer properties such as  $M_n$ ,  $M_w$ ,  $B_n$  are validated [106] with the experimental results of bulk polymerization of vinyl acetate [1] at two different temperatures (60°C and 80°C) and two different initiator concentrations (0.00005 mol/L and 0.0001 mol/L) using the numerical fractionation method [18] (i.e. from linear to different levels of LCB = 0, 1, 2, 3 etc.). Total number of classes has to be chosen properly for the complete construction of molecular weight distribution (MWD). This means that the sum of the first moments of all classes should be approximately equal to the overall first moment of the polymer [18]. Fig. 4.1 shows the experimental validation of  $M_n$  and  $M_w$  with the model used in this study. At higher monomer conversion, the rate of termination becomes slower due to increase in viscosity. From Fig. 4.1, it is also evident that at higher temperature, molecular weight of the polymer is less. The probable reason is the faster termination of live radicals at 80°C (due to higher termination rate) and this results in the formation of small polymers thus the molecular weight remains comparatively lower. The faster termination at 80°C is due to the lower average life time of live radical as compared at 60°C. Fig. 4.2 depicts that  $B_n$  increases with monomer conversion due to the prominent role of chain transfer to polymer and terminal double bond reactions as more live radicals are participating in these reactions. Since both these figures show the very importance of live radicals in the reaction medium, Fig. 4.3 shows the profile of live radical concentration with respect to number average degree of branching ( $B_n$ ) (for two different temperatures). Since the onset polymerization, live polymer concentration increases rapidly due to faster initiator decomposition, and this is more at 80°C compared to 60°C (faster initiator decomposition at higher temperature). Afterwards, live polymer concentration decreases with increase of  $B_n$  due to faster termination of live polymer to dead polymer. It is evident from here that  $B_n$  increases more rapidly at 60°C than at 80°C. This is due to early termination at 80°C than at 60°C, which leads to the formation of polymers with less LCB at higher temperature. As the monomer conversion increases, increase in  $B_n$  became more at 80°C compared to 60°C. This may account for the fact that the lower termination rate is the natural outcome of the process, as and when large number of high molecular weight polymer molecules accumulates in the reactor at 60°C.

Fig. 4.4 represents the MWD-LCB at different chain lengths for  $B_n = 0.9$  and temperature of 80°C. Here, the molecular weight distributions of PVAc are plotted for different long

chain branches (i.e. LCB = 0, 1, 2, 3, 4, 5, 6). It can be seen from this plot that the linear polymer (i.e. LCB = 0) dominates at the starting of polymerization followed by LCB = 1, 2 etc. This figure shows the information of LCB distribution for different chain lengths and the inset figure represents the overall MWD. The small shoulder (inset figure) in overall MWD curve indicates the signature of long chain branching. Overall MWD is calculated from the weighed sum of individual MWDs (i.e. LCB = 0, 1, 2, 3, 4, 5, 6).

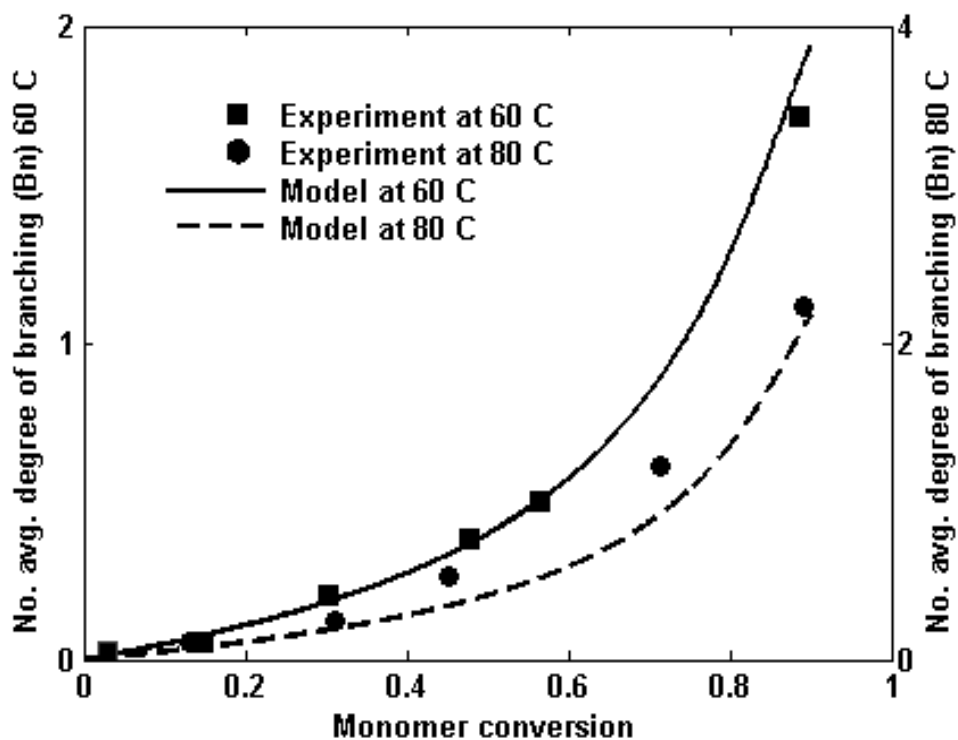


Figure 4.2: Comparison of number average degree of branching between the experimental value and the model prediction.

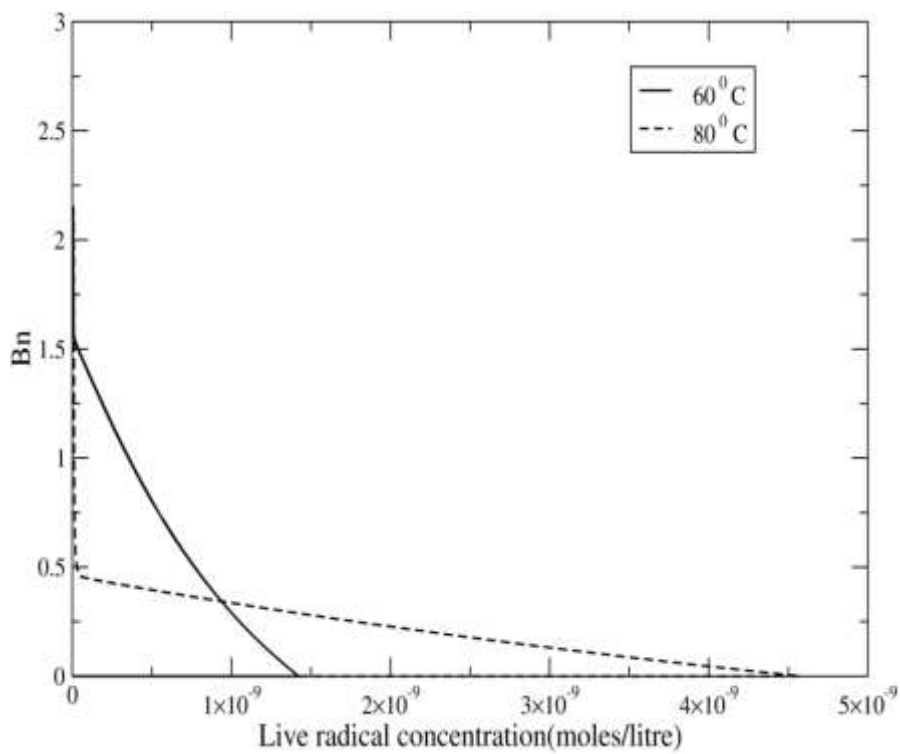


Figure 4.3: Live radical concentrations vs. number average degree of branching at different temperatures.

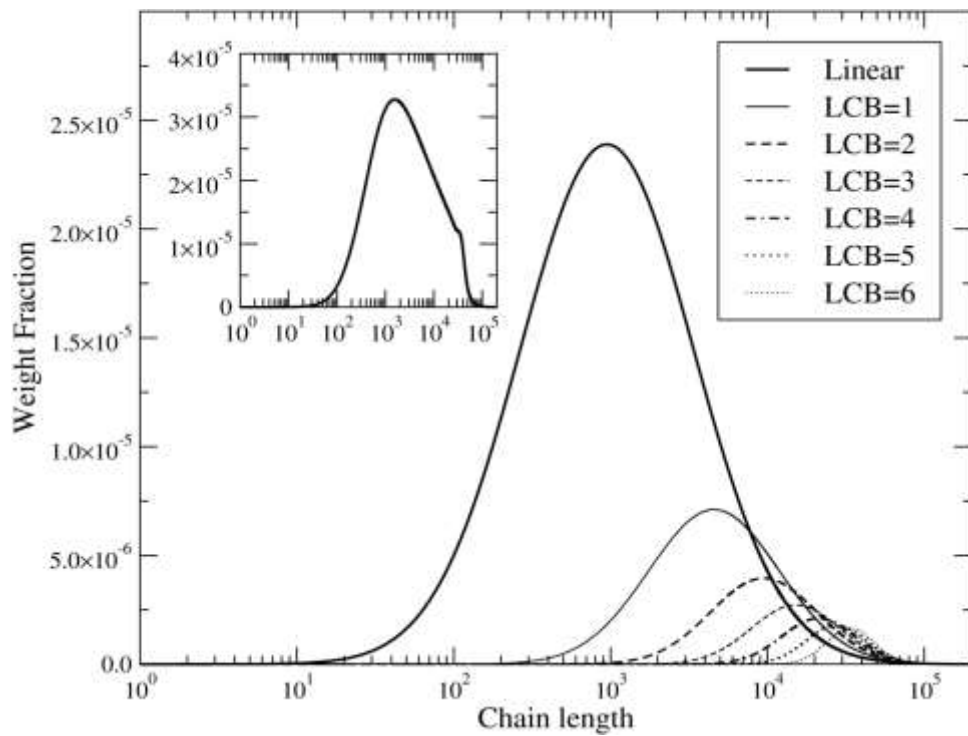


Figure 4.4: Molecular weight distribution at 80°C for  $B_n = 0.9$  for different long chain branching

#### 4.4.2 Optimization

After getting some information about the general trends of the PVAc polymerization in Figs. 4.1 to 4.4, the next level of investigation leads to optimizing the process performance, which has been formulated in previous section. The main purpose of these optimization studies is to find the optimal process conditions to maximize long chain branching before the gel point is reached because long chain branched polymers exhibit enhanced processing properties compared to the linear polymers with same molecular weight. Multi-objective Pareto solutions for the first optimization case (case 1) are obtained among three conflicting objectives and shown in Fig. 4.5. As pointed out earlier, multi-objective optimization problems have more than one solution and it is difficult to distinguish among them. These solutions are known as non-dominated solutions and all of them are equally important solution. The conflict among these solutions is clear as improvement in certain objective comes at the cost of other objective. For example, if the operator chooses the operating conditions for more  $M_w$  and  $B_n$ , she/he sacrifices in terms of more processing time. These solutions are generally a wide range of alternatives to a process engineer and each point in the Pareto is associated with a particular operating condition. Based on different requirements (requirement can be defined by a set of values of  $M_n$ , time and  $B_n$ ), the reactor can be run with different optimized process operating conditions. Solutions for performance objectives in Fig. 4.5 and the corresponding process conditions on various objectives are represented in Fig. 4.6(a) to 4.6(c). These figures can act as truth table to a process engineer. This kind of process analysis, which is achieved here by multi-objective optimization study of the polymerization process, is generally achieved in a shop-floor by collecting data from the process over a very long time and thereby gaining experience to operate it. We can explain this kind of trends in the similar lines of batch simulation study. Low temperature gives a polymer of high  $M_w$  (Fig. 4.1 and Fig. 4.6) due to slow termination of live radical species. All points are scattered in Figs. 4.6a to c, which is due to large variation in initial initiator concentrations (Fig. 4.6b). But, at high temperature, the rate of branching increases (Fig. 4.6c) after certain conversion possibly due to increase in chain transfer to polymer and terminal double bond mechanisms, which grew faster with temperature. Thus to find a polymer of more  $B_n$  with more  $M_w$ , the optimization routine prefers the entire temperature range as lower temperature prefers higher  $M_w$  and higher temperatures choose higher  $B_n$ . It can be noticed from Fig. 4.2 that  $B_n$  increases rapidly after a certain conversion even with a low temperature case. So, low temperature can also result higher  $B_n$  provided the conversion is on the higher side. As a choice, low temperature is thus a safer choice as long as conversion is high. This trend has a limit as gel point conversion has to be avoided at any

cost and for that reason, such operation poses a process control challenge. Needless to say that at higher conversion, measurement as well as control of the process is difficult because of the higher viscosity of the reaction medium.

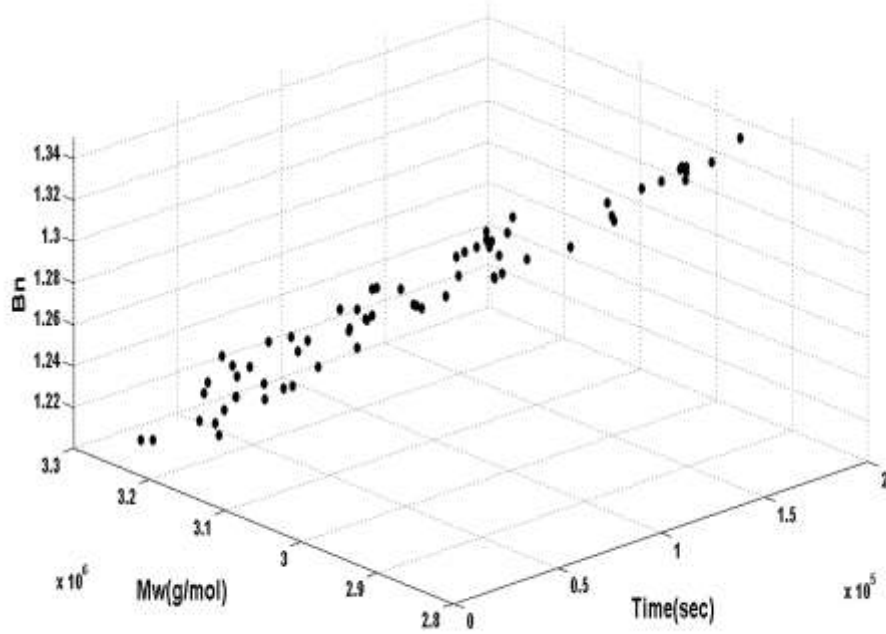


Figure 4.5: Multi-objective PO solutions for case 1

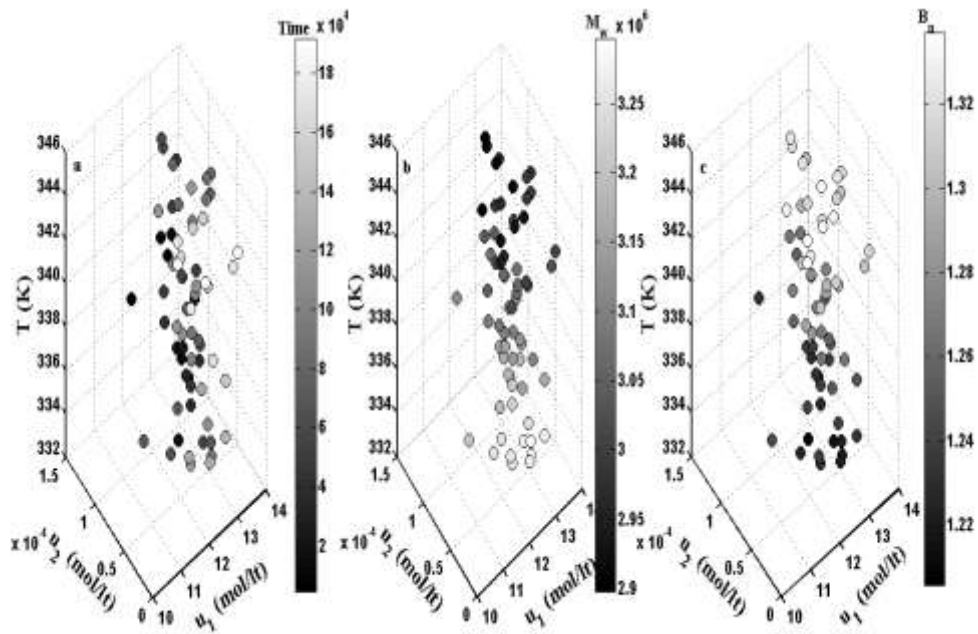


Figure 4.6: Variation of decision variables w.r.t. objective functions for case 1

Optimization exercise brings out the process conflicts to understand the process better and thus sharpening the further definition for more in-depth studies. It can be observed throughout this study that polymer molecular weight and long chain branching are related to the live polymer concentration. So, to find a polymer of higher branching, concentration of live polymer needs to be increased. The second multi-objective optimization study (case 2) has, therefore, been performed to see the impact of the process conditions on live polymer and polymer properties. PO solutions for this case are shown in Fig. 4.7 and the corresponding effect of decision variables (addition of monomer, initiator and temperature) on those objective functions are shown from Figs. 4.8a to c. As the live radical concentration is maximized, most of the points with faster processing time are moved to higher initiator concentration region to allow formation of more radicals and high temperature to achieve more  $B_n$  value. But for this situation, polymerization time is also more (Fig. 4.8a) to achieve polymer of higher molecular weight. At higher temperature range, optimizer has chosen more initial initiator concentration. This is due to the increase in conversion at higher initiator concentration. However, the molecular weight is reported to be less due to higher live radical concentration because of smaller polymer formation. Another subtle thing to be noticed that the PO solutions of the second optimization problem are less scattered compared to those of the first problem. This proves that the second optimization definition is more precise and solution for the first one has helped a lot to define more focused objective. In other polymer systems also, similar learning can be found in literature i.e. the overall process objectives help in defining more precise formulation, thus giving more information about the system [58].

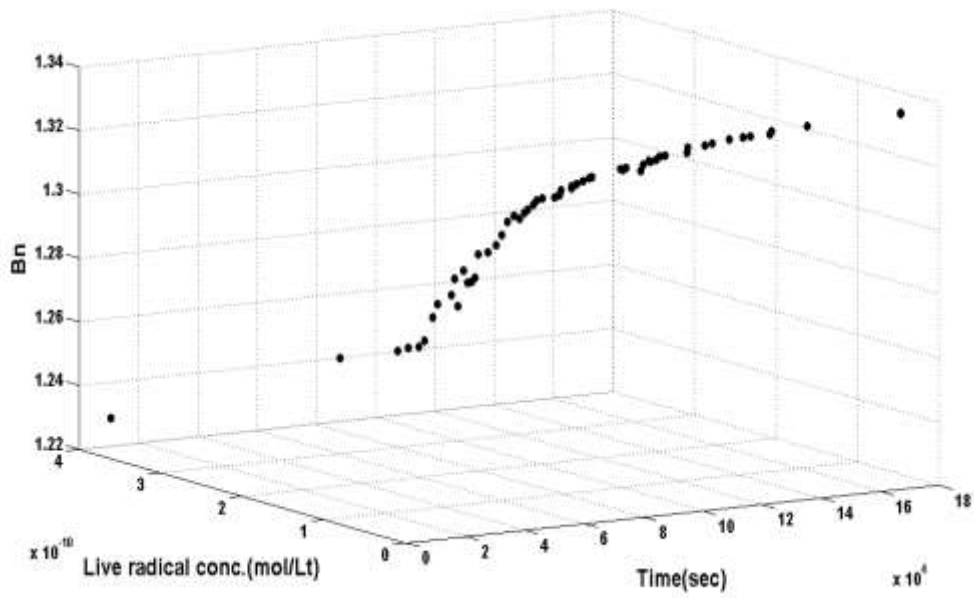


Figure 4.7: Multi-objective PO solutions for case 2.

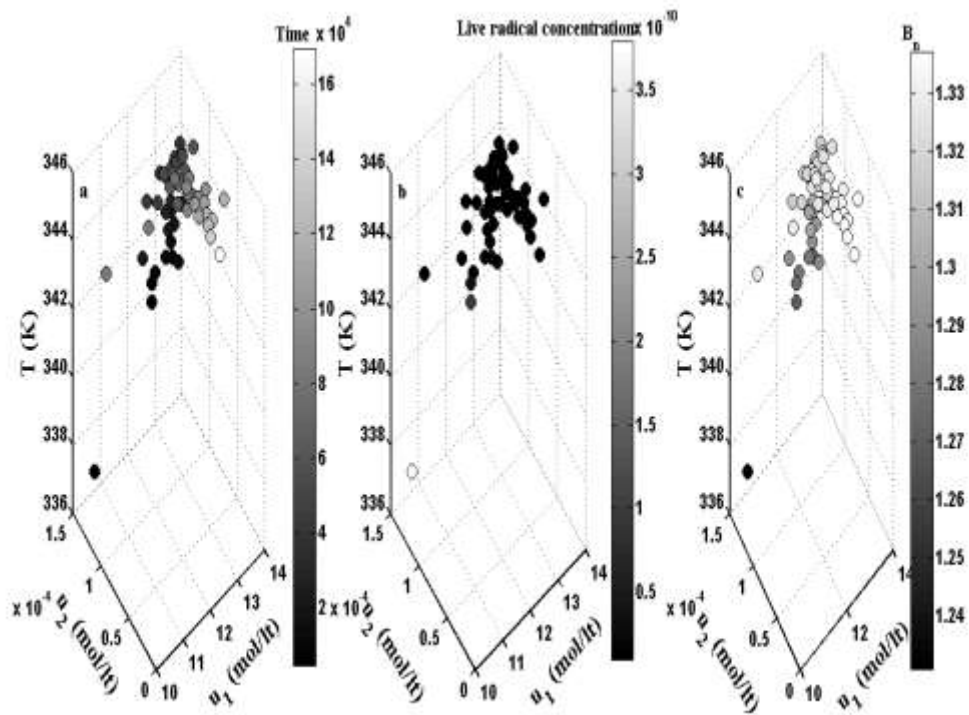


Figure 4.8: Variation of decision variables w.r.t. objective functions for case 2.



It is also evident that from Figs. 4.6a-c and Figs. 4.8a-c, monomer concentration does not show much effect on polymerization time and polymer molecular properties on bulk free radical polymerization. In both cases (case 1 and case 2), the amount of initial initiator concentration and temperature are playing prominent role in deciding polymer molecular properties. Moreover, all parameter values and variable ranges have been tightly maintained within the limits of experimental conditions [1] so that the optimization results remain realistic. Moment based modeling with further complications like branching for bulk polymerization for PVAc finally reveals many optimum operating conditions and some conflicting situations through a detailed simulation study.

#### **4.5 Conclusion**

NSGA II has been utilized to find optimal process conditions for batch vinyl acetate polymerization process. Polymer properties such as overall  $M_n$ ,  $M_w$  and  $B_n$ , are calculated by fractionation of polymers according to number of branches and validated with experimental data available in open literature. Maximization of weight average molecular weight and number average degree of branching have been attained along with simultaneous minimization of processing time without violating the relevant process constraints. Monomer addition, initiator addition and reaction temperature are taken as decision variables within prescribed experimental bounds. Initiator addition is found to be completely dependent on temperature and processing time. For the first optimization study, optimizer has provided wide range of initiator and temperature values to maximize branching and molecular weight. So, an operator can get many optimal choices to operate the reactor at different point in time based on the optimality criteria set. The second optimization case results in another variety of solutions at relatively higher temperature range with higher live radical concentration. In short, looking at varying scenario faced by today's process operator, batch vinyl acetate polymerization process has been revisited with additional capability of controlling the degree of branching and optimum sets of operating conditions have been identified with a trade-off between conflicting process objectives for a range of temperatures.

# Chapter 5

## Modeling of propylene polymerization with long chain branching

The objective of this chapter is to develop a kinetic model of the long chain branched polypropylene system to replicate the experimental data available in literature which is probably the first step to build a model before it can be scaled up for pilot study and thereafter for industrial practices.

### 5.1 Introduction

In this work, we have chosen the example of LCB PP (isotactic back bones and atactic side chains) with binary catalyst system  $(2\text{-ArN}=\text{C}(\text{Me})_2\text{C}_5\text{H}_3\text{N})\{\text{FeCl}_2/\text{MMAO}$  (1) and *rac*- $\text{Me}_2\text{Si}(2\text{-MeBenz}[e]\text{Ind})_2\text{ZrCl}_2/\text{MMAO}$  (2)) [16] and presented a model which can validate experimental findings [16] with a newly proposed kinetic mechanism. In the chosen example, the catalyst (1) is capable of forming short chain atactic polypropylene macromonomers (having terminal double bonds) and the catalyst (2) can copolymerize propylene with macromonomers to form LCB PP. In this mechanism, both short chain atactic polypropylene macromonomer formation and copolymerization of propylene with macromonomers occur simultaneously in the same reactor to form LCB PP which has a potential to produce LCB PP with lesser fixed and operating cost. General single site coordination mechanism has been chosen for the two-catalyst system.

Modeling study has been conducted by Zhu and Li [48] with the use of binary metallocene catalyst system to obtain highly comb-branched polymers in steady state CSTR and obtained an olefin polymer of narrow molecular weight distribution with a maximum polydispersity index of 2.25. By this catalyst systems, back bone and side chains provide a theoretical polydispersity index of 2 (Schulz-Flory distribution) [48] only. However, Ye and

Zhu [16] obtained aPP macromonomers with polydispersity index to the order of 1.3 during their experiments which the above mentioned model [48] cannot explain. It has been identified that by taking the reversible chain transfer step, the molecular weight distribution becomes narrow [98] for the aPP macromonomers (with a polydispersity index nearer to 1.3) as compared to Schulz-Flory distribution. So, the idea of Hustad *et al.* [98] has been borrowed, which leads to a polydispersity index value less than 2 as opposed to Schulz-Flory distribution [48]. From the kinetic model derived from the proposed mechanism, the net formation of the live and the dead polymers has been derived next. Due to the resultant large number of equations, moment based modeling has been applied and the 0<sup>th</sup>, 1<sup>st</sup> and 2<sup>nd</sup> order moments for the live and the dead polymers have been derived. These equations are highly non-linear ODEs, which are solved here using an established open source DAE solver (LIMEX) [41]. Kinetic parameters are estimated by minimizing the sum of the square of the error between the experimental and simulated values of variety of molecular properties such as weight average molecular weight ( $M_w$ ), polydispersity index (PDI) of isotactic polypropylene and atactic polypropylene as well as grafting density (number aPP side chains per 1000 isotactic backbone monomer units) by real coded genetic algorithm (RCGA) [19]. The rationale behind the choice of this evolutionary algorithm is its established capability of finding global optimum as compared to the classical optimization techniques. To construct molecular weight distribution (MWD) of polymer species, Teymour and Campbell [35] have developed “Numerical Fractionation” method. In this method, polymer is divided into linear and branched chains. Branched polymer chains are again divided into number of generations according to the geometric growth. Finally the molecular weight distribution of the LCB PP has been calculated by the fractionation of total polymer population into a series of classes, each class representing the same long chain branching content [49]. In this method, total polymer population is classified into different classes based on the same number of long chain branches (i.e. LCB=0, LCB=1, LCB=2 etc.).

## 5.2 Model

Experimental runs [16] were conducted at 25°C and 1 atm. propylene pressure in 200 ml of toluene solvent. There are very few articles in the open literature about the kinetics of long chain branched polypropylene [45, 48, 99]. None of them are validated against experimental data. The newly proposed kinetic scheme for the two-catalyst system considered in the present effort is shown in Table 5.1. This kinetic scheme consists of

catalyst activation, initiation, propagation, chain transfer reactions and catalyst deactivation, in which,  $C_1$  and  $C_2$  represent the active sites of the catalyst (1) and (2), respectively. Monomer concentration in toluene has been calculated by Redlich-Kwong-Soave equation of state for vapor–liquid phases in equilibrium [100-101].  $P_n$  and  $D_n^-$  represent the live and the unsaturated dead polymers (macromonomers) for atactic polypropylene of chain length  $n$ , whereas,  $Q_{n,i}$  and  $R_{n,i}$  represent the live and the dead polymer chains of LCB PP having  $n$  numbers of chain length and  $i$  numbers of long chain branches (isotactic backbone and atactic side chains). The main chain transfer mechanism for 1/MMAO is  $\beta$ -hydride elimination [102] which produces vinyl terminated macromonomers and re-initiation occurs with the activated hydride catalyst complex. Reversible chain transfer mechanism has been considered to achieve polymer with narrow molecular distribution instead of Schulz-Flory distribution (polydispersity index = 2.0), which is more common for single site catalysts [48]. While for the II/MMAO, chain transfer to MMAO was dominant to avoid the formation of dendrimers [48]. Second order deactivation has been considered for this which may be due to bimolecular deactivation [103-104]. This catalyst (2) has the capability of producing backbone (main chain) chains and at the same time it can connect the macromonomers as side chains to produce LCB PP. From this kinetic mechanism, one can derive the rate of formation of the live and the dead polymers to describe the molecular properties of the polymer. Then, method of moments has been applied to reduce to a system of lower number of differential equations. Apart from the moment equations, net formation of vacant active sites and chain transfer agent consumption rate etc. are derived as shown in Table 5.2. This is based on the statistical representation of molecular weights (e.g.  $M_n$  and  $M_w$ ) of the polymer in terms of the moments of the live, the dead polymers (as shown in Equation 5.1) and the moments of the aPP live and the aPP dead polymers (as shown in Equation 5.2). Number average molecular weight ( $M_n$ ), weight average molecular weight ( $M_w$ ) and PDI are represented by Equation 5.3 and grafting density is represented by Equation 5.4.

$$\mu_x = \sum_{n=1}^{\infty} n^x Q_n \quad v_x = \sum_{n=1}^{\infty} n^x R_n \quad (5.1)$$

$$\lambda_x = \sum_{n=1}^{\infty} n^x P_n \quad \mu_x^- = \sum_{n=1}^{\infty} n^x D_n^- \quad (5.2)$$

$$M_n = \left( \frac{v_1}{v_0} \right) MW \quad M_w = \left( \frac{v_2}{v_1} \right) MW \quad PDI = \left( \frac{M_w}{M_n} \right) \quad (5.3)$$

$$GD = 1000 \left( \frac{\text{Long chain branching formation rate}}{\text{Propagation rate}} \right) \quad (5.4)$$

Table 5.1: Kinetic Scheme for the two catalyst systems

Catalyst 1	Catalyst 2
<ul style="list-style-type: none"> <li>• Initiation</li> </ul> $C_1 + M \xrightarrow{k_{i1}} P_1$	<ul style="list-style-type: none"> <li>• Catalyst activation</li> </ul> $cat_2 + cocat \xrightarrow{k_{a2}} C_2$
<ul style="list-style-type: none"> <li>• Propagation</li> </ul> $P_n + M \xrightarrow{k_{p1}} P_{n+1}$	<ul style="list-style-type: none"> <li>• Initiation</li> </ul> $C_2 + M \xrightarrow{k_{i2}} Q_{1,0}$
<ul style="list-style-type: none"> <li>• <math>\beta</math>-H elimination</li> </ul> $P_n \xrightarrow{k_{\beta}} D_n^- + C_1^H$	<ul style="list-style-type: none"> <li>• Propagation</li> </ul> $Q_{n,i} + M \xrightarrow{k_{p2}} Q_{n+1,i}$
<ul style="list-style-type: none"> <li>• Reversible chain transfer to metal</li> </ul> $D_n^- + C_1^H \xrightarrow{k_{\beta r}} P_n$	<ul style="list-style-type: none"> <li>• long chain branching</li> </ul> $Q_{n,i} + D_{m,0}^- \xrightarrow{\alpha k_{lcb}} Q_{n+m,i+1}$
<ul style="list-style-type: none"> <li>• Reinitiation</li> </ul> $C_1^H + M \xrightarrow{k_{ri1}} P_1$	<ul style="list-style-type: none"> <li>• Chain transfer to cocatalyst</li> </ul> $Q_{n,i} + cocat \xrightarrow{k_{al}} R_{n,i} + C_2^{Me}$
	<ul style="list-style-type: none"> <li>• Reinitiation</li> </ul> $C_2^{Me} + M \xrightarrow{k_{ra1}} Q_{1,0}$
	<ul style="list-style-type: none"> <li>• Bimolecular deactivation</li> </ul> $2Q_{n,i} \xrightarrow{k_{d2}} 2R_{n,i} + 2C_d$

Table 5.2: Moment rates of live and dead polymer chains for the 2 catalyst systems

Catalyst 1:

$$\begin{aligned} \frac{d\lambda_0}{dt} &= k_{i1}C_1M + k_{ri1}C_1^H M - k_\beta\lambda_0 + k_{\beta r}\mu_0^{\bar{\bar{}}}C_1^H \\ \frac{d\lambda_1}{dt} &= k_{i1}C_1M + k_{ri1}C_1^H M + k_{p1}M\lambda_0 - k_\beta\lambda_1 + k_{\beta r}\mu_1^{\bar{\bar{}}}C_1^H \\ \frac{d\lambda_2}{dt} &= k_{i1}C_1M + k_{ri1}C_1^H M + k_{p1}M(2\lambda_1 + \lambda_0) - k_\beta\lambda_2 + k_{\beta r}\mu_2^{\bar{\bar{}}}C_1^H \\ \frac{d\mu_0^{\bar{\bar{}}}}{dt} &= k_\beta\lambda_0 - k_{\beta r}\mu_0^{\bar{\bar{}}}C_1^H - \alpha k_{lcb}\mu_0^{\bar{\bar{}}}\mu_0 \\ \frac{d\mu_1^{\bar{\bar{}}}}{dt} &= k_\beta\lambda_1 - k_{\beta r}\mu_1^{\bar{\bar{}}}C_1^H - \alpha k_{lcb}\mu_1^{\bar{\bar{}}}\mu_0 \\ \frac{d\mu_2^{\bar{\bar{}}}}{dt} &= k_\beta\lambda_2 - k_{\beta r}\mu_2^{\bar{\bar{}}}C_1^H - \alpha k_{lcb}\mu_2^{\bar{\bar{}}}\mu_0 \\ \frac{dC_1}{dt} &= -k_{i1}C_1M \\ \frac{dC_1^H}{dt} &= k_\beta\lambda_0 - k_{\beta r}C_1^H\mu_0^{\bar{\bar{}}} - k_{ri1}C_1^H M \end{aligned}$$

Catalyst 2:

$$\begin{aligned} \frac{d\mu_0}{dt} &= k_{i2}C_2M + k_{ral}C_2^{Me}M - (k_{al}[\text{cocat}] + k_{d2}\mu_0)\mu_0 \\ \frac{d\mu_1}{dt} &= k_{i2}C_2M + k_{ral}C_2^{Me}M + (k_{p2}M + \alpha k_{lcb}\mu_1^{\bar{\bar{}}})\mu_0 \\ &\quad - (k_{al}[\text{cocat}] + k_{d2}\mu_0)\mu_1 \\ \frac{d\mu_2}{dt} &= k_{i2}C_2M + k_{ral}C_2^{Me}M + k_{p2}M(2\mu_1 + \mu_0) \\ &\quad - (k_{al}[\text{cocat}] + k_{d2}\mu_0)\mu_2 + \alpha k_{lcb}(2\mu_1\mu_1^{\bar{\bar{}}} + \mu_0\mu_2^{\bar{\bar{}}}) \\ \frac{dv_0}{dt} &= (k_{d2}\mu_0 + k_{al}[\text{cocat}])\mu_0 \\ \frac{dv_1}{dt} &= (k_{d2}\mu_0 + k_{al}[\text{cocat}])\mu_1 \\ \frac{dv_2}{dt} &= (k_{d2}\mu_0 + k_{al}[\text{cocat}])\mu_2 \\ \frac{d[\text{cat}_2]}{dt} &= -k_{a2}[\text{cat}_2][\text{cocat}] \\ \frac{d[\text{cocat}]}{dt} &= -k_{a2}[\text{cat}_2][\text{cocat}] - k_{al}\mu_0[\text{cocat}] \\ \frac{dC_2}{dt} &= k_{a2}[\text{cat}_2][\text{cocat}] - k_{i2}C_2M \\ \frac{dC_2^{Me}}{dt} &= k_{al}\mu_0[\text{cocat}] - k_{ral}C_2^{Me}M \end{aligned}$$

Atactic polypropylene units with terminal double bond (i.e. vinyl terminated macromonomers), which are produced by the catalyst (1), are incorporated as side chains with propylene in the presence of the catalyst (2) during copolymerization and this leads to the formation of the LCB PP. The extent of long chain branching completely depends on the addition methods (more specifically the time of catalyst additions) and the ratio of the concentrations of the catalysts [16]. For example, say, if these catalysts are added together and once in the beginning, the extent of long chain branching becomes zero [16]. This may be due to precipitation of iPP around the active sites or low concentration of macromonomer, which inhibits the diffusion of macromonomer [16]. On the other hand, if the time interval between their additions is more, branching density is found to be high [16]. Based on this fact, we introduced one more parameter (i.e.  $\alpha$ ), describing the above mentioned diffusion effect, into the modeling system apart from the kinetic constants which are to be found out during the parameter estimation stage. The parameter  $\alpha$  is a dimensionless parameter which depends on the catalyst addition time and the ratio of the concentrations of these catalysts. Without this parameter  $\alpha$ , grafting density predictions are much away from the experimental data.

The resultant model equations are solved by the LIMEX DAE [41] solver. Model is integrated with RCGA [19] to estimate kinetic parameters and the additional parameters  $\alpha$  and  $\eta$  (another parameter representing percentage of active sites in a catalyst defined later). These parameters are optimized by minimizing an error expression (e) derived through the comparison of experimental and simulated data as shown in Equation 5.5. Here the error expression comprises sum of the squares of the normalized error between the experimental and simulated values of weight average molecular weight ( $M_w$ ), polydispersity index (PDI) of iPP and aPP and grafting density (GD, i.e. number of aPP side chains per 1000 iPP backbone units).

$$\begin{aligned}
 e = & \sum_1^5 \left( \frac{M_{w, \text{appsim}} - M_{w, \text{appexp}}}{M_{w, \text{appexp}}} \right)^2 + \sum_1^5 \left( \frac{\text{PDI}_{\text{appsim}} - \text{PDI}_{\text{appexp}}}{\text{PDI}_{\text{appexp}}} \right)^2 + \\
 & \sum_1^5 \left( \frac{M_{w, \text{ippsim}} - M_{w, \text{ippexp}}}{M_{w, \text{ippexp}}} \right)^2 + \sum_1^5 \left( \frac{\text{PDI}_{\text{ippsim}} - \text{PDI}_{\text{ippexp}}}{\text{PDI}_{\text{ippexp}}} \right)^2 + \sum_1^3 \left( \frac{\text{GD}_{\text{sim}} - \text{GD}_{\text{exp}}}{\text{GD}_{\text{exp}}} \right)^2
 \end{aligned}
 \tag{5.5}$$

Here each of the first four components in the above error function (e) are summed for five data sets (experimental runs) and the last component is summed for three data sets (GD given for three experimental runs).

For most of the classical optimization techniques, based on the initial guess, the solution may stick to a local minimum present in the near vicinity of the valley where the initial solution is provided. Rather than a single point, RCGA works with a number of solutions (called chromosomes) and to start with, these solutions are generated randomly within the bounds provided for the optimizing parameters. So, the initial number, say  $N$ , of candidate solutions form the initial population where each chromosome is composed of all the optimizing parameters, called decision variables (i.e., kinetic parameters,  $\alpha$  and  $\eta$ ). In a population, the fitness function ( $1/(1+\text{error})$ ) for each chromosome is computed by solving the model equations for the different sets of parameter values for different chromosomes. By using the tournament selection operator, a mating pool is created. The entire population is divided into two classes of solutions i.e. feasible (solutions which obey constraints) and infeasible solutions (solutions which violate constraints). Two solutions are randomly picked and feasible solutions are preferred over the infeasible solutions. Among feasible solutions, the one with better fitness function is preferred whereas solution with less constraint violation is preferred among infeasible solutions. New chromosomes for the next generation are generated by using crossover and mutation operator on the mating pool candidates [19]. This procedure is repeated till the maximum number of generations, say  $N_{\max}$  is reached.

The parameter  $\alpha$  depends on various other parameters such as the time gap between the two catalyst additions, ratio of catalyst 1 to catalyst 2 initial concentrations and copolymerization time. Based on the different  $\alpha$  values predicted by the optimizer for different experimental conditions, an empirical relation has been developed for  $\alpha$ , which is a function of time gap between the two catalyst additions,  $\text{cat}_1/\text{cat}_2$  ratio and copolymerization time (time starting after the second catalyst is added till completion of polymerization) and is shown in Equation 5.6. From this, it is evident that if two catalysts are added at a time, the value of  $\alpha$  is zero signifying the scenario where no aPP macromonomers attack iPP as evident in the experimental findings. If the time gap between the catalyst additions and the ratio of concentrations of catalyst 1 and catalyst 2 are more, more macromonomers will be grafted to iPP backbone [16] which is due to accumulation of more macromonomers in the



reactor before the addition of the catalyst (2). It is worthwhile, to mention, that the major significance of  $\alpha$  is to correct the kinetics for the fact that all macromonomers will not be available to attack the iPP backbone because of diffusional limitations. This value is not dependent on concentration of iPP. In kinetics,  $\alpha.k_{lcb}$  represents the effective long chain branching rate constant.

$$\alpha = \left(4.75 \times 10^{-9} \times t_1\right)^{0.837} \left(\frac{\text{cat}_1}{\text{cat}_2}\right)^{1.37} (32.319 \times t_1 + 15.6752 \times t_2) \quad (5.6)$$

Here  $t_1$  is catalyst (2) addition time and  $t_2$  is copolymerization time and  $\text{cat}_1$  and  $\text{cat}_2$  represent catalyst 1 and catalyst 2 concentrations.

Following the effort of Pladis and Kiparissides [18], molecular weight long chain branching distribution (MW-LCBD) for the binary catalyst system is calculated by the fractionation of the total polymer based on the same long chain branching content (i.e. linear, 1 LCB, 2 LCB etc.). According to this method, one can derive dynamic balance equations for the live and the dead polymers of each class. The net rate of formation of the linear as well as the branched isotactic polypropylene chains of the live and the dead chains is represented in Table 5.3 where, the first subscript represents the chain length and the second subscript represents branching. Method of moments has been applied again to each class to reduce the large number of equations to the tractable set of equations as represented in Table 5.4. Molecular weight distribution (MWD) of each class, calculated by Schultz-Flory two parameter model [49], is shown in Equation 5.7. Overall molecular weight distribution is calculated by the weighed sum of distributions for all such classes.

Table 5.3: Net formation of linear, branched live and dead polymer chains

$$\begin{aligned} \frac{dQ_{n,0}}{dt} &= k_{i2}C_2M + k_{ral}C_2^{Me}M + k_{p2}MQ_{n-1,0} \\ &\quad - (k_{p2}M + k_{lcb}\alpha\mu_0 + k_{al}[\text{cocat}] + k_{d2}\mu_0)Q_{n,0} \\ \frac{dQ_{n,m}}{dt} &= k_{p2}MQ_{n-1,m} + \alpha k_{lcb} \sum_{s=2}^{r-2} Q_{s,m-1}D_{n-s,0} \\ &\quad - (k_{p2}M + \alpha k_{lcb}\mu_0 + k_{al}[\text{cocat}] + k_{d2}\mu_0)Q_{n,m} \\ \frac{dR_{n,m}}{dt} &= (k_{al}[\text{cocat}] + k_{d2}\mu_0)Q_{n,m} \end{aligned}$$

Table 5.4: Moment rate equations for linear, branched live and dead polymer chains

Linear live and dead chains:

$$\begin{aligned}\frac{d\mu_{0,0}}{dt} &= k_{i2}C_2M + k_{ral}C_2^{Me}M - (k_{al}[\text{cocat}] + k_{d2}\mu_0 + \alpha k_{lcb}\mu_0^-)\mu_{0,0} \\ \frac{d\mu_{1,0}}{dt} &= (k_{i2}C_2 + k_{ral}C_2^{Me} + k_{p2}\lambda_{0,0})M - (k_{al}[\text{cocat}] + k_{d2}\mu_0 + \alpha k_{lcb}\mu_0^-)\mu_{1,0} \\ \frac{d\mu_{2,0}}{dt} &= (k_{i2}C_2 + k_{ral}C_2^{Me})M + k_{p2}M(2\lambda_{1,0} + \lambda_{0,0}) - \\ &\quad (k_{al}[\text{cocat}] + k_{d2}\mu_0 + \alpha k_{lcb}\mu_0^-)\mu_{2,0} \\ \frac{dv_{0,0}}{dt} &= (k_{al}[\text{cocat}] + k_{d2}\mu_0)\mu_{0,0} \\ \frac{dv_{1,0}}{dt} &= (k_{al}[\text{cocat}] + k_{d2}\mu_0)\mu_{1,0} \\ \frac{dv_{2,0}}{dt} &= (k_{al}[\text{cocat}] + k_{d2}\mu_0)\mu_{2,0}\end{aligned}$$

Branched live and dead polymer chains:

$$\begin{aligned}\frac{d\mu_{0,m}}{dt} &= \alpha k_{lcb}\lambda_{0,m-1}\mu_0^- - (k_{al}[\text{cocat}] + k_{d2}\mu_0 + \alpha k_{lcb}\mu_0^-)\mu_{0,m} \\ \frac{d\mu_{1,m}}{dt} &= k_{p2}\mu_{0,m}M + \alpha k_{lcb}(\mu_{1,m-1}\mu_0^- + \mu_{0,m-1}\mu_1^-) - (k_{al}[\text{cocat}] + k_{d2}\mu_0 + \alpha k_{lcb}\mu_0^-)\mu_{1,m} \\ \frac{d\mu_{2,m}}{dt} &= k_{p2}M(2\mu_{1,m} + \mu_{0,m}) + \alpha k_{lcb}(\mu_{2,m-1}\mu_0^- + 2\mu_{1,m-1}\mu_1^- + \mu_{0,m-1}\mu_2^-) \\ &\quad - (k_{al}[\text{cocat}] + k_{d2}\mu_0 + \alpha k_{lcb}\mu_0^-)\mu_{2,m} \\ \frac{dv_{0,m}}{dt} &= (k_{al}[\text{cocat}] + k_{d2}\mu_0)\mu_{0,m} \\ \frac{dv_{1,m}}{dt} &= (k_{al}[\text{cocat}] + k_{d2}\mu_0)\mu_{1,m} \\ \frac{dv_{2,m}}{dt} &= (k_{al}[\text{cocat}] + k_{d2}\mu_0)\mu_{2,m}\end{aligned}$$

$$w_m(r) = \frac{y_m(ry_m)^{z_m} e^{-ry_m}}{\Gamma(z_m + 1)}; m = 0, 1, 2 \dots \text{et.}$$

$$z_m = \frac{DP_{n,m}}{DP_{w,m} - DP_{n,m}}; y_m = \frac{z_m + 1}{DP_{w,m}} \quad (5.7)$$

Here  $w_{m(r)}$  denotes the  $m^{\text{th}}$  class weight fraction of the polymer with a degree of polymerization of  $r$ ,  $DP_{n,m}$  and  $DP_{w,m}$  represent the number average and weight average degree of polymerization, respectively. As the number of classes are increasing, PDI of each class ( $\frac{DP_{w,m}}{DP_{n,m}}$ , i.e.  $< 2$ ) of the polymer decreases [49].

### 5.3 Results and discussion

Polymer properties such as  $M_w$ , PDI of aPP macromonomers and iPP copolymers along with grafting density of aPP macromonomers to the back bone of iPP polymer are validated with the experimental results [16]. The kinetic scheme proposed in this paper (Table 5.1) is based on the following assumptions: (i) Two-catalyst system acts as single center catalyst individually; (ii) Deactivation of the catalyst (2) results from bimolecular deactivation [103]. Deactivation of catalyst (1) is neglected as this does not show much impact on the model predictions. Generally, sensitivity of model can be reduced by considering the less number of parameters. If more number of parameters is involved in the model, uncertainty of the model increases. With less number of parameters, model will become more robust. Catalyst (1) system propagates via 2,1 insertion mechanism which produces 1-propenyl ended macromonomers followed by  $\beta$ -H elimination [102]. Two types of saturated end groups have been identified [16]: n-butyl and 3-methyl-n-butyl groups. Termination mechanism by  $\beta$ -H elimination leads to the iron-hydride formation and n-butyl end group is generated by the 1,2 insertion of propylene monomer to the iron hydride followed by 2,1 insertion of propylene monomer [102]. Small and Brookhart [102] explained the formation of 3-methyl-n-butyl group which is formed by 2,1 insertion of propylene monomer into an iron isobutyl species (formed by activating the iron complex with MMAO, the cocatalyst). The polymers produced by this catalyst system exhibit narrow molecular weight distribution with a PDI value around 1.3. By the single site catalyst system, polymer can be produced with a theoretical PDI value of 2 [98]. To obtain a polymer with very narrow molecular weight distribution (as observed in the experimental findings) instead of Schulz-Flory distribution, the step of chain transfer to the metal should be made reversible to get the Poisson distribution [98]. As the catalyst (1) system produces macromonomers (polymers with terminal unsaturation), the chain transfer mechanism might be occurring by transfer to metal or monomer. By increasing Al/Fe ratio, percentage of catalyst active sites also increases, i.e.  $C_1 = \eta \text{cat}_1$ , where,  $\text{cat}_1$  is the moles of catalyst introduced,  $C_1$  is the moles of catalyst sites activated and  $\eta$  is the efficiency factor varies from 0 to 1 [99]. The

estimation of parameter  $\eta$  has been included in the parameter estimation exercise (Equation 5.1). Experimental and model predictions of aPP macromonomers are represented in Table 5.5. In this table, first 4 experimental runs had Al/Fe ratio of 1000, while 5<sup>th</sup> run had Al/Fe ratio of 3000. So, for the first four runs, optimization routine returns  $\eta = 18.97\%$ , while for the last case, the optimization routine returns  $\eta = 88.8\%$ . As the parameters are determined by parameter estimation exercise, the effort was to obtain parameters that lead to minimum error between the model prediction and experimental results. In the Table 5.5, all PDI values are obtained in the range of 1.3 to 1.4 by considering fast reversible chain transfer mechanism, which is in line with experimental results [16].

Table 5.5: Experimental and predicted  $M_w$ , PDI of aPP macromonomers

RunNo.	aPP Experiment		aPP Predicted		% error	
	$M_w$ (kg/mol)	PDI	$M_w$ (kg/mol)	PDI	$M_w$	PDI
1	3.6	1.3	4.4	1.4	-22.2	-7.7
2	3.6	1.4	3.2	1.34	13.3	4.3
3	3.3	1.3	4.5	1.4	-36.4	-7.7
4	3.1	1.3	2.5	1.34	19.4	-3.1
5	3.0	1.3	2.6	1.33	13.3	-2.3
6	3.4	1.3	2.5	1.34	26.4	-3.1

Catalyst (2) system (2/MMAO) copolymerizes aPP macromonomers with the propylene monomer. It generates backbone chains and connects the side chains at the same time to obtain the comb branched polymers. This catalyst should favor termination reactions other than  $\beta$ -hydride elimination to avoid the formation of dendrimers [48]. So, we considered chain transfer to MMAO and bimolecular deactivation of live polymer chains [103] in the proposed mechanism. Estimated kinetic parameters for the kinetic scheme are shown in Table 5.6. Based on the best knowledge of the author, there are no data available in the literature for the rate constants of the LCB PP system, which is validating with the experimental data. As the concentration of cocatalyst increases, polymer chain length decreases due to chain transfer to cocatalyst. Here the cocatalyst (MMAO) concentration is present in much higher amount than the catalyst (Zr) concentration. Hence the term " $k_{al} \times [\text{MMAO}]$ " may be assumed as constant during the polymerization. For the first 4 runs, the value of this constant is higher than the last run, since cocatalyst concentration is less for the last run as compared to the first four runs. Due to this, the predicted weight average molecular weight of the last run is higher than the first four runs (we call this case as case1;

Table 5.7). In case 1, effect of bimolecular deactivation on Al/Zr ratio has not been considered. So, the present model (case 1) can predict the influence of MMAO concentration in the chain transfer reactions. As Al/Zr (cocatalyst/catalyst) ratio increases, more chain length polymers will be produced due to weaker bimolecular deactivation. This builds a rationale of considering the effect of cocatalyst/catalyst ratio on the deactivation constant. In the modeling of PP system, Ochoteco *et al.* [103] considered the effect of MAO concentration on deactivation assuming that the deactivation constant is a function of MAO concentration which decreases with the increase in MAO concentration. In case 1 study, dependence of bimolecular deactivation on Al/Zr ratio is not considered and molecular weights are under estimated for the first 2 runs even though this ratio is high compared to other runs. So, in another case (we call this case as case 2), the effect of bimolecular deactivation constant on Al/Zr ratio is considered [103]. Two such ratios are there (i.e. Al/Zr = 5000, 7500) and the deactivation constant is estimated considering the effect of these two ratios on it and is represented in Table 5.8. It can be noticed from Table 5.8 that as Al/Zr ratio increases, there is a decrease in bimolecular deactivation leading to the production of polymers with more chain length. Experimental and model comparison of molecular weights and polydispersity index of iPP by considering the effect of Al/Zr ratio on bimolecular deactivation is depicted in Table 5.7. For the first 2 runs where the Al/Zr ratio is 7500, higher chain length polymers are obtained due to weaker bimolecular deactivation of live polymer chains as compared to the other 3 runs. Predictions for grafting density values (number of aPP side chains per 1000 iPP backbone monomer units) for different runs are shown in Table 5.9. Model predicted values for the first three runs seem to have in good agreement with the experimental values. Grafting density values for the last two runs are predicted from the model (experimental data not available) and these values are compared with the melting points [16] of the iPP copolymer since the experimental values are not available for them. As the long chain branching density increases, melting point of the copolymer decreases [16] because of higher participation of aPP in the overall polymer architecture. Higher melting point of the 4<sup>th</sup> run compared to the 3<sup>rd</sup> run indicates lower branching density. Similarly, higher melting point of the 5<sup>th</sup> run indicates fewer amounts of aPP macromonomers being grafted into the iPP back bone. Grafting density of aPP macromonomers to the iPP copolymer depends on the second catalyst addition time, the catalyst 1/catalyst 2 (i.e. Fe/Zr) molar ratio and the copolymerization time. By comparing the 1<sup>st</sup> run with the 2<sup>nd</sup> run, where the catalyst ratio is maintained same and the time interval between the two catalyst additions is only changed, the effect of time interval on the grafting density of aPP macromonomers in the copolymer can be identified. If more time is

allowed before the catalyst (2) addition, more amounts of aPP macromonomers are available to be copolymerized with the iPP. This is due to the accumulation of more amounts of aPP macromonomers in the reactor before the catalyst (2) addition [16]. Similarly, by comparing the 4<sup>th</sup> and the 5<sup>th</sup> runs, for a constant catalyst (2) addition time, the effect of catalyst ratio on grafting density can be identified (grafting density is more due to high catalyst 1/catalyst 2 ratio). Validation results of 6<sup>th</sup> run has been provided, which is not included in the parameter estimation exercise. The value of aPP Mw will not show much impact on the copolymer molecular weight (due to very low molecular weight of aPP Mw as compared to the iPP Mw) and grafting density. Fig. 5.1 depicts such variability i.e. the variation of grafting density and  $\alpha$  with the time gap between the two catalyst additions for different catalyst ratios for a copolymerization time of 90 minutes.

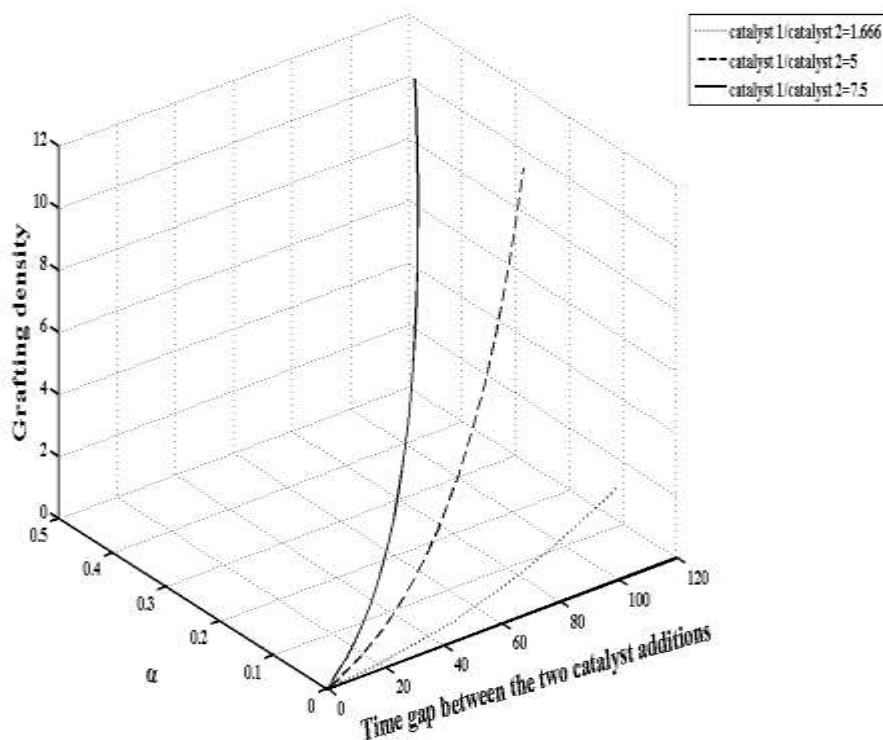


Figure 5.1: Effect of time gap between the two catalyst additions, Fe/Zr ratio on  $\alpha$  and grafting density

Table 5.6: Kinetic rate constants for first and second catalyst systems

$k_{i1}$	$4.7789 \times 10^3$ (L/(mol.min))
$k_{p1}$	$1.0659 \times 10^6$ (L/(mol.min))
$k_{\beta}$	$8.9738 \times 10^7$ (1/min)
$k_{\beta r}$	$8.3145 \times 10^6$ (L/(mol.min))
$k_{ri1}$	1.4799 (L/(mol.min))
$k_{a2}$	$8.8243 \times 10^2$ (L/(mol.min))
$k_{i2}$	$6.5754 \times 10^3$ (L/(mol.min))
$k_{p2}$	$9.4277 \times 10^7$ (L/(mol.min))
$k_{lcb}$	$8.3375 \times 10^8$ (L/(mol.min))
$k_{al}$	$8.5325 \times 10^4$ (L/(mol.min))
$k_{ral}$	$13.9312 \times 10^4$ (L/(mol.min))
$k_{d2}$	$22.7379 \times 10^{10}$ (L/(mol.min))

Table 5.7: Experimental and predicted  $M_w$ , PDI of iPP copolymer for case 1 and case 2

Run No.	iPP Experiment		iPP Predicted (case 1)		iPP Predicted (case 2)		% error	
	$M_w$ (kg/mol)	PDI	$M_w$ (kg/mol)	PDI	$M_w$ (kg/mol)	PDI	$M_w$	PDI
1	631.8	2.7	563.3	2.3	632	2.2	-0.03	18.5
2	564.7	2.5	474.9	2.29	544	2.2	3.66	12
3	447.3	2.3	535.3	2.33	485	2.4	-8.42	-4.34
4	395.2	2.4	422.6	2.3	378	2.4	4.35	0
5	514.4	2.3	620	2.3	554	2.4	-7.69	-4.34
6	548.8	2.5	682	2.1	595	2.1	-8.41	16

Table 5.8: Bimolecular deactivation constant w.r.t. Al/Zr ratio

Al/Zr	$k_{d2}$ (L/(mol.min))
7500	$12.6322 \times 10^{10}$
5000	$56.8449 \times 10^{10}$

Table 5.9: Various experimental runs along with the comparison of experimental [16] grafting density with the model predictions

Run Number	Zr:Fe:Al	Zr ( $\mu\text{M}$ )	Grafting Density		Melting Point	% error
			Experimental	Simulated		Grafting density
1	2:15:15000	10	8.4	8.2	144.4	2.38
2	2:15:15000	10	1.7	1.7	148.6	0
3	3:15:15000	15	8.6	7.5	145.6	12.79
4	3:15:15000	15		0.31	149.7	
5	3:5:15000	10		0.008	153.5	
6	1:15:15000	5	0	0	155.1	

Calculation of molecular weight long chain branching distribution is very important because it has a large impact on rheological and mechanical properties of the polymer. Fig. 5.2 depicts the molecular weight distributions of branched iPP copolymer calculated by fractionation of polymers based on number of branches [49]. This is for the 2<sup>nd</sup> experimental run and corresponds to the grafting density value of 1.7 (of aPP macromonomers). In this figure, weight chain length distributions of linear and branched polymers are shown. The computational time requirement for the numerical fractionation method depends on the total number of classes required for the construction of MWD. Number of classes increases with the extent of branching also. Total number of classes required for this case was found to be around 20. Total number of classes has to be chosen properly for the construction of MWD. This has been established for a particular number of classes for which the sum of the first moments of all classes is approximately equal to the overall first moment of the iPP copolymer. Variation of weight average degree of polymerization and polydispersity index of each class of polymer chains, corresponding to Fig. 5.2, is represented in Fig. 5.3. It can be noticed from Fig. 5.3 that the weight average chain length increases linearly as the number of classes increases. On the other hand, polydispersity index decreases and reaches around the value of 1.1 as the number of long chain branches increases. However, polydispersity index of linear polymer chains obtained a theoretical value of 2 [98].



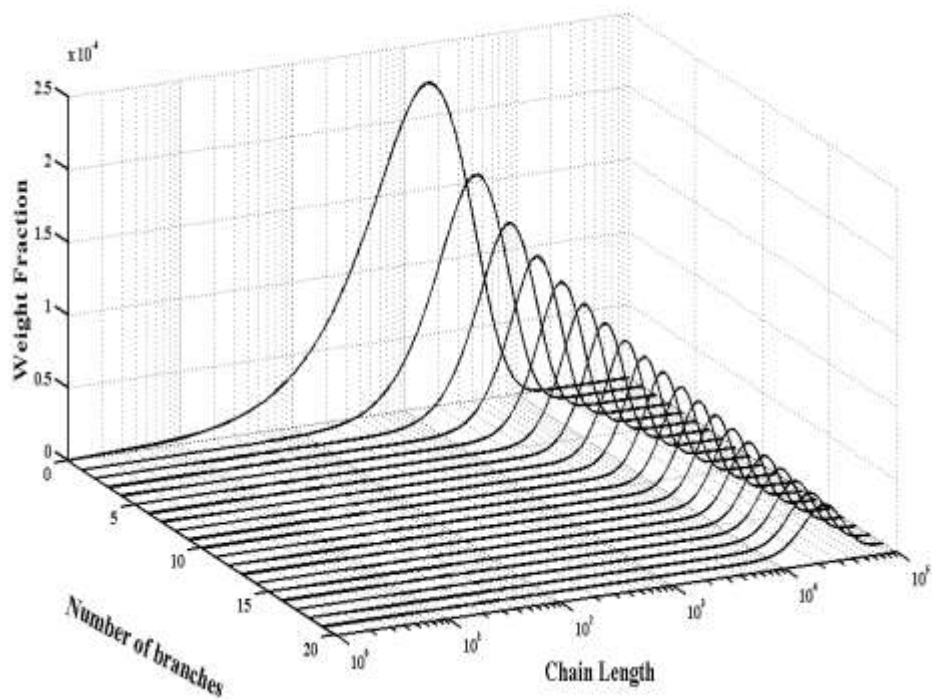


Figure 5.2: Molecular weight distributions for the 2<sup>nd</sup> run

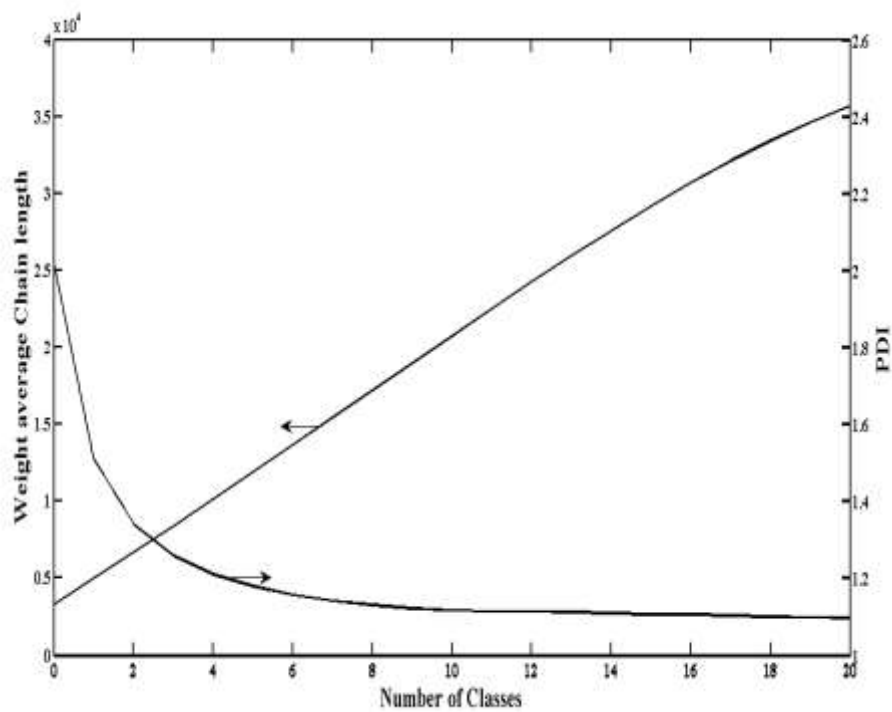


Figure 5.3: Variation of weight average degree of polymerization and polydispersity index with respect to class number

The sensitivity study of the kinetic parameters has been carried out for run 1 to see the effect of long chain branching density and weight average molecular weight of the iPP copolymer. The effect of  $\alpha.k_{lcb}$  on aPP macromonomer grafting density and molecular weight of the copolymer is shown in Fig. 5.4. It can be evident that the rate of macromonomer insertion increases as the  $\alpha.k_{lcb}$  increases. This in turn means an increase in the value of  $\alpha.k_{lcb} / k_{p2}$  and long chain branching density and thereby the number of classes required for the construction of MWD. However, there is a small increase in molecular weight of the copolymer which is due to the fact that the molecular weight of attacking macromonomers is very less as compared to the molecular weight of isotactic backbone units. If  $k_{p2}$  (propagation rate constant) is increased, the ratio of macromonomer insertion rate to propagation rate decreases, which results decrease in the grafting density as well. However, there is a linear increase in molecular weight of the copolymer which is depicted in Fig. 5.5. This is due to the high propagation rate of propylene monomer to the back bone of iPP polymer. Cocatalyst (MMAO) concentration plays an important role on the molecular weight of the iPP copolymer. Fig. 5.6 illustrates the effect of  $k_{al}$  on the molecular weight and the long chain branching content. Molecular weight of the polymer is decreased due to the high chain transfer rate to cocatalyst. However, grafting density of aPP macromonomers is almost constant. This may be due to the fact that the rate of macromonomer insertion and the rate of propagation are not affected by the cocatalyst. However, higher molecular weight polymers can be produced with the decrease of bimolecular deactivation (Fig. 5.7). Sensitivity analysis reveals that grafting density is strongly influenced by the long chain branching reaction (i.e. reaction with macromonomer) and copolymer propagation reaction. Similarly, iPP  $M_w$  strongly depends on propagation reaction, chain transfer reaction and bimolecular deactivation reaction.

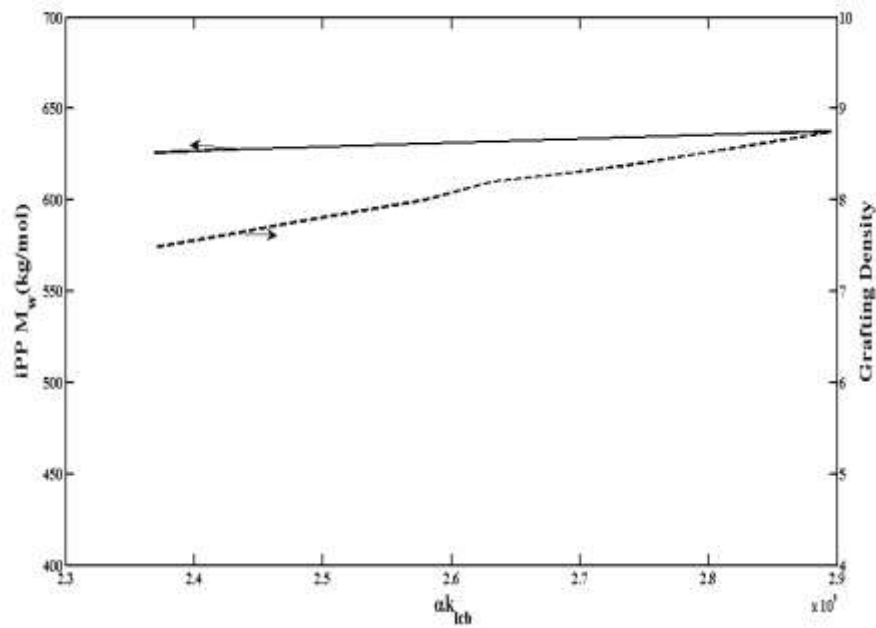


Figure 5.4: Effect of  $\alpha k_{lcb}$  on  $M_w$  and grafting density

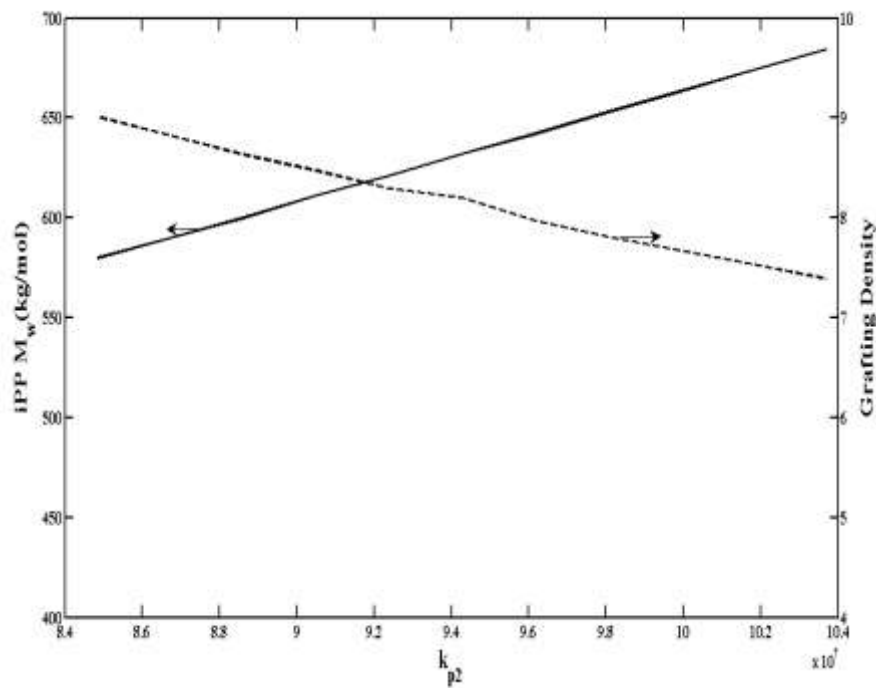


Figure 5.5: Effect of  $k_p$  on  $M_w$  and grafting density

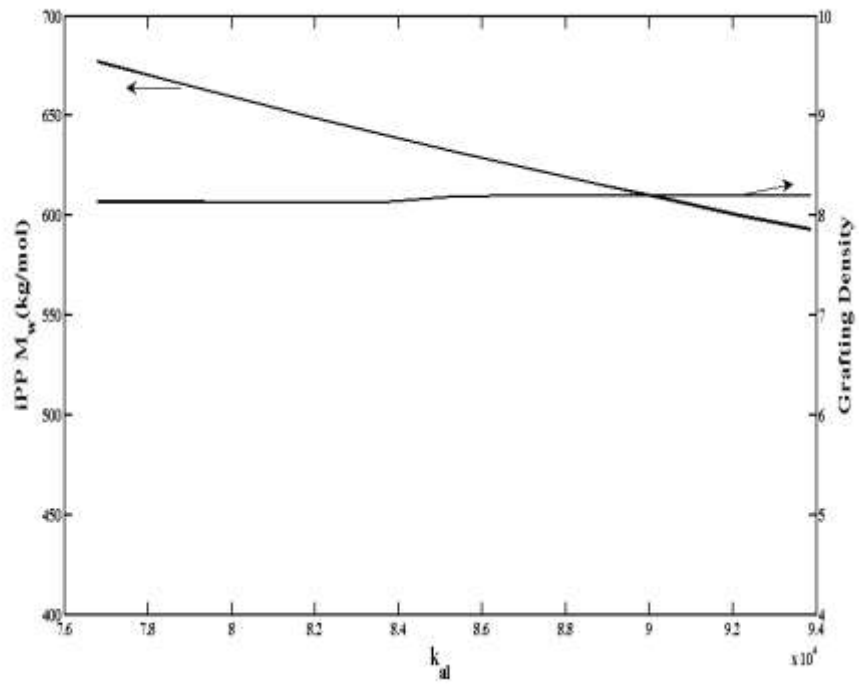


Figure 5.6: Effect of  $k_{d1}$  on  $M_w$  and grafting density

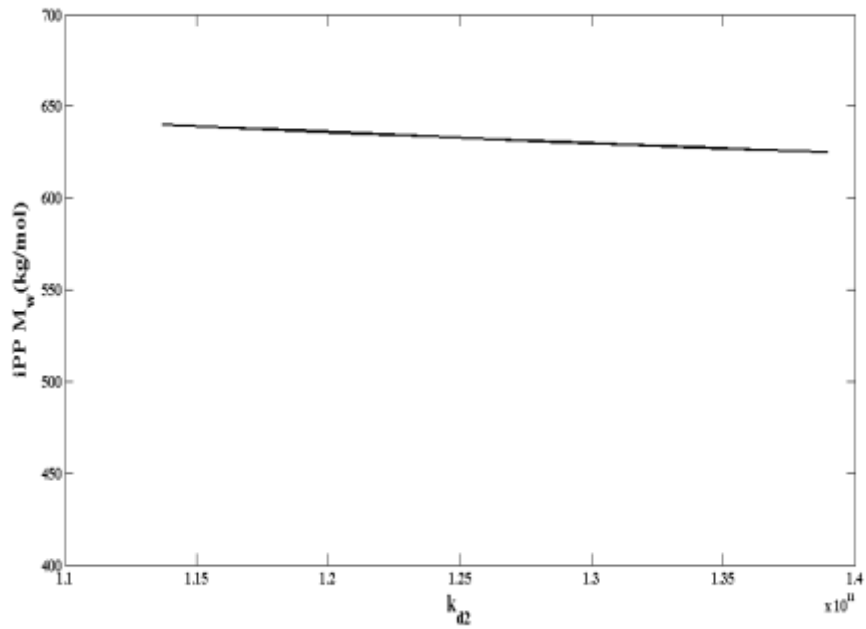


Figure 5.7: Effect of  $k_{d2}$  on  $M_w$

## 5.4 Conclusion

A mathematical model with a newly proposed chemical mechanism for a LCB PP (isotactic back bones and atactic side chains) system with twin catalysts has been presented in this work which can validate the available experimental results [16]. The proposed model can predict the molecular properties such as molecular weight, PDI and grafting density by the tandem action of the two catalyst system with different Al/Zr ratio, cocatalyst concentration and Fe/Zr ratio. Following important points are revealed out of this modeling exercise: (i) Molecular weight of the iPP copolymer is found to depend on the cocatalyst concentration (due to chain transfer reaction) and the cocatalyst/catalyst ratio (due to the bimolecular deactivation). (ii) Grafting density depends on the catalyst (2) addition time, Fe/Zr ratio and copolymerization time. (iii) If more time is allowed before the catalyst (2) addition, long chain branching content is increased in the copolymer due to accumulation of more amounts of aPP macromonomers in the reactor. (iv) By increasing the Fe/Zr ratio, more aPP macromonomers are grafted to the back bone of iPP because of the higher macromonomer concentration in the reactor. Sensitivity analysis reveals that grafting density is strongly influenced by the long chain branching reaction (i.e. reaction with macromonomer) and copolymer propagation reaction. Similarly, iPP  $M_w$  strongly depends on propagation reaction, chain transfer reaction and bimolecular deactivation reaction. The model captured the iPP  $M_w$ , PDI, grafting density and aPP PDI well except deviations in aPP  $M_w$  as compared to the experimental data. In literature,  $M_w$  value of 280.5 kg/mol and PDI of 2.22 has been reported with the binary catalyst system [48]. The model agrees well quantitatively with the PDI value and similar order of magnitude with  $M_w$  value.

## Chapter 6

# Multi-objective Optimization of Long Chain Branched Propylene Polymerization

This chapter deals with the multi-objective optimization of long chain branched polypropylene system, which discusses the simulation results of multi-objective optimization to produce a polymer of high molecular weight and grafting density (number of macromonomers per 1000 backbone monomer units) in less polymerization time.

### 6.1 Introduction

In this chapter, an example of LCBPP that is produced by a binary catalyst system has been considered. The experimental details of this binary catalyst system can be found from the work of Ye and Zhu [16]. The aim here is to develop a model with a mechanism which can validate the given experimental data [16] and then use the model to optimize and control the degree of branching of the polymer. Single site coordination mechanism has been considered to model this system. The detailed kinetic model has been given in chapter 5. In the optimization exercise, the validated model is extended to find the optimal values of addition of catalysts and cocatalyst, second catalyst addition time that minimizes the total polymerization time while maximizing the iPP copolymer  $M_w$  and grafting density, simultaneously. Multi-objective optimization techniques are excellent candidates to find out optimal solutions that are conflicting in nature. It is known that polymer with higher molecular weight can be obtained in higher polymerization time; on the contrary, the objective is to attain polymers with higher molecular weight in less time - here lies the conflict. Moreover, to maintain the competitive advantage, it is more apparent that enterprises need to produce products in such operating conditions that solve multiple conflicting operating objectives simultaneously than attaining only one goal. Multi-

objective optimization works are, therefore, gaining popularity to solve optimization problems in the polymerization domain over the last few decades. Since, the three objectives mentioned above are conflicting in nature, there is a need to find out the optimal process conditions to get the desired combination of these conflicting objectives. To cater this, a multi-objective optimization study has been performed using well established non-dominated sorting genetic algorithm II (NSGA II) [19] to find the PO solutions. PO (Pareto optimal) solutions are the set of solutions given by multi-objective optimization problem (MOOP) which are non-dominating in nature. This study can be extremely beneficial for operating branched polypropylene reactors that can lead to the desired results with optimal operating conditions.

## 6.2 Problem Formulation and Optimization Procedure

Addition amounts for the two catalysts ( $u_1$  and  $u_2$ ) and cocatalyst (MMAO) ( $u_3$ ), time of addition for the second catalyst ( $u_4$ ) and the total polymerization ( $t_p$ ) (70 min. to 180 min.) are considered as decision variables for the optimization problem. These decision variables are to be decided by the optimization routine while attaining simultaneous minimization of total polymerization time, maximization of  $M_w$  and maximization of GD. As these objectives are conflicting in nature, solving the multi-objective optimization problem helps in obtaining the PO or trade off solutions among various conflicting objectives. The above mentioned problem formulation with relevant constraints is shown in Table 6.1. The constraint bounds in the optimization problem formulation have been chosen completely based on the experimental values [16] to avoid extrapolation errors of the model. For example, aPP PDI experimental values are 1.3 and 1.4 respectively. The constraint limit for this has been chosen less than or equal to 1.45. In this, case 1 represents the multi objective optimization formulation based on the decision variable values of experimental run no. 1 whereas, case 2 is based on the entire experimental range. This case 2 multi-objective optimization study has been extended based on the process performance improvement in the case 1. To find a polymer in less processing time, one may get less  $M_w$  and GD. A multi-objective optimization study for LCBPP is, therefore, performed here to obtain trade off solutions in the above-mentioned conflicting scenario. To reduce the extrapolation errors, the bounds on the decision variables are fixed at the  $\pm 10\%$  of the experimental values [16] and additional constraints are posed (Table 6.1). All decision variables [16] are forced to lie within the lower and upper bounds to obtain a realistic final solution. Multi objective optimization (MOOP) has been performed by integrating the validated model with a well-established multi optimization routine, real coded non-dominated sorting genetic algorithm

(NSGA II) [19]. The rationale behind selecting NSGA II over other multi-objective evolutionary algorithms is the success of NSGA II on various complicated practical problems in the past.

Table 6.1: Multi-objective optimization problem formulation

<p><i>Maximize</i> <math>M_w</math></p> <p><i>Maximize</i> <math>GD</math></p> <p><i>Minimize</i> <math>t_p</math></p> <p><math>500000 \leq M_w \leq 700000</math></p> <p><math>4500 \leq \frac{cocat}{cat_2} \leq 8000</math></p> <p><math>M_{w,app} \geq 2500</math></p> <p><math>PDI_{app} \leq 1.45</math></p> <p><math>GD \geq 7</math></p> <p>Bounds on decision variables:</p> <p>Case 1:</p> <p><math>u_1^{\min} = 67.5E - 06 \text{ mol/L}; u_1^{\max} = 82.5E - 06 \text{ mol/L}</math></p> <p><math>u_2^{\min} = 9E - 06 \text{ mol/L}; u_2^{\max} = 11E - 06 \text{ mol/L}</math></p> <p><math>u_3^{\min} = 0.0675 \text{ mol/L}; u_3^{\max} = 0.0825 \text{ mol/L}</math></p> <p><math>u_4^{\min} = 0.2t_p \text{ min}; u_4^{\max} = 0.8t_p \text{ min}</math></p> <p><math>t_p^{\min} = 70 \text{ min}; t_p^{\max} = 180 \text{ min}</math></p> <p>Case 2:</p> <p><math>u_1^{\min} = 14E - 06 \text{ mol/L}; u_1^{\max} = 82.5E - 06 \text{ mol/L}</math></p> <p><math>u_2^{\min} = 9E - 06 \text{ mol/L}; u_2^{\max} = 16.5E - 06 \text{ mol/L}</math></p> <p><math>u_3^{\min} = 0.045 \text{ mol/L}; u_3^{\max} = 0.0825 \text{ mol/L}</math></p> <p><math>u_4^{\min} = 0.2t_p \text{ min}; u_4^{\max} = 0.8t_p \text{ min}</math></p> <p><math>t_p^{\min} = 70 \text{ min}; t_p^{\max} = 180 \text{ min}</math></p>
--



### 6.3 Results and discussion

All experimental runs [16] were conducted at 1 atm. propylene pressure and 25°C in 200 ml toluene solvent and various molecular properties such as  $M_w$ , PDI (of aPP, iPP- copolymer) and grafting density were determined. Propylene concentration in toluene is calculated by Soave-Redlich-Kwong (SRK) equation of state for vapor–liquid phases in equilibrium [100-101]. Kinetic parameters, those are estimated by the parameter estimation exercise as explained earlier, are presented in chapter 5. Once the parameters are estimated, the model is ready for use in optimization of process operating conditions within the experimental range. As the first catalyst produces only macromonomers,  $\beta$ -hydride elimination mechanism has been considered as the chain transfer step [102]. Percentage of catalyst active sites for the first catalyst system (1/MMAO) is calculated by  $C_1 = \eta \text{Cat}_1$ , [99] where  $\text{Cat}_1$  represents the number of moles of catalyst introduced,  $C_1$  is the moles of catalyst active sites and  $\eta$  is the efficiency factor.  $\eta$  depends on the cocat/cat<sub>1</sub> (Al/Fe) ratio e.g. as the ratio increases, number of moles activated catalyst sites also increases. For the second catalyst system (2/MMAO), the mechanism of chain transfer to cocatalyst and bimolecular deactivation of live polymers have been considered [99]. Compared to the second catalyst concentration, the cocatalyst (MMAO) is found to be present in much higher amount [16]. So, the term “ $k_{al} \times [\text{MMAO}]$ ” is considered to be constant [99] during the polymerization. Polymer chain length increases with the decrease in cocatalyst concentration, which is due to lower chain transfer to cocatalyst. The effect of cocatalyst (MAO) on bimolecular deactivation has been considered in literature [103]. Decrease in bimolecular deactivation has been observed with increase in cocatalyst/catalyst ratio [103]. In the present effort, the effect of MMAO/Zr (cocat/cat<sub>2</sub>) ratio on bimolecular deactivation has been taken into account. This rate constant is estimated by considering the related experimental values (i.e. cocat/cat<sub>2</sub>=5000, 7500) and shown in chapter 5. With the decrease in this value, bimolecular deactivation increases that leads to produce polymers of lower chain length. In the present work, the adopted model has been validated with the experimental [16] findings and the result is represented in Table 6.2. Model predictions for polymer properties for all experimental runs are found to corroborate experimental data reasonably well. Higher molecular weight polymers are obtained for the first two runs, which are due to lower bimolecular deactivation as compared to the last three runs (Table 6.2). While comparing between the 3<sup>rd</sup> and 5<sup>th</sup> runs (of same cocat/cat<sub>2</sub>=5000), 5<sup>th</sup> run has provided higher chain length polymers. This is due to high chain transfer to cocatalyst in case of 3<sup>rd</sup> run as compared to the 5<sup>th</sup> run. Grafting density predictions are also shown in Table 6.2. As

explained earlier, this value completely depends on the time gap between the two catalyst additions, two catalyst ratios and copolymerization time. For run1, grafting density value is more as compared to the value in run 2, which is due to more time gap between two catalyst additions, while same  $cat_1/cat_2$  ratio has been maintained. Similarly, by comparing 3<sup>rd</sup> and 4<sup>th</sup> run of (having similar catalyst concentrations), 4<sup>th</sup> run has lower long chain branching density. This is due to less macromonomers present in the reactor because of less time gap between two catalyst additions. However, no experimental data for grafting density are available for the 4<sup>th</sup> and 5<sup>th</sup> runs. These values are predicted from the model. Lower branching density of 4<sup>th</sup> run as compared to the 3<sup>rd</sup> run indicates higher melting point [16], which is in line with experimental observations. By comparing the 4<sup>th</sup> and 5<sup>th</sup> runs of having the same time gap between the two catalyst additions and copolymerization time with varying  $cat_1/cat_2$  ratio, 4<sup>th</sup> run shows more grafting density value compared to the 5<sup>th</sup> run (Table 6.2) due to more  $cat_1/cat_2$  ratio. In the same table, validation results of 6<sup>th</sup> run has been provided, which is not included in the parameter estimation exercise.

Table 6.2: Comparison of model predicted values with experimental [16] data.

Run No.	$cat_1$ ( $\mu$ M)	$cat_2$ ( $\mu$ M)	Al (M)	Second catalyst addition time (min)	aPP Experiment		aPP Predicted	
					$M_w \times 10^{-3}$ (gm/mol)	PDI	$M_w \times 10^{-3}$ (gm/mol)	PDI
1	75	10	0.075	90	3.6	1.3	4.4	1.4
2	75	10	0.075	30	3.6	1.4	3.2	1.34
3	75	15	0.075	120	3.3	1.3	4.5	1.4
4	75	15	0.075	30	3.1	1.3	2.5	1.34
5	16.67	10	0.05	30	3.0	1.3	2.6	1.33
6	75	5	0.075	0	3.4	1.3	2.5	1.34

Run No.	iPP Experiment [16]		iPP Predicted	
	$M_w \times 10^{-3}$ (gm/mol)	PDI	$M_w \times 10^{-3}$ (gm/mol)	PDI
1	631.8	2.7	632	2.2
2	564.7	2.5	544	2.2
3	447.3	2.3	485	2.4
4	395.2	2.4	378	2.4
5	514.4	2.3	554	2.4
6	548.8	2.5	595	2.1

Run No.	GD		Melting Point [16]
	Experiment	Predicted	
1	8.4	8.2	144.4
2	1.7	1.7	148.6
3	8.6	7.5	145.6
4		0.31	149.7
5		0.008	153.5
6	0	0	155.1

After the model is validated with the experimental data, it has been extended to investigate the optimal process operating conditions to attain specific objectives as described in Table 6.1. First of all, one might be curious to see whether optimization result can give any better solution than the experimental results. First a targeted optimization search is done in a narrow decision variable space to figure out the performance similar or better than run 1 (Table 6.1: case 1). Multi-objective optimization study is carried out for the run 1 experimental range (i.e. within  $\pm 10\%$  of the experimental process conditions; henceforth called as case 1). The set of Pareto optimal solutions for population of 100 is represented in Fig. 6.1. Polymerization time is arranged in ascending order in terms of an ordered chromosome number (Fig. 6.1a). Fig. 6.1b and 6.1c represent the remaining two objective functions by using the same ordered chromosome numbers as shown in Fig. 6.1a. This way of representing the objectives helps to see the embedded trade-off among objectives. These are multiple numbers of optimal solutions competing with each other. No single solution can be pointed as better than other solution in terms of overall objectives. While comparing two solutions (say, a and b), if one objective for a solution (solution a) looks better than another solution (solution b), this would definitely have some compromise in some other objective (i.e. other objective of solution a might be inferior to solution b). In that sense, all these solutions are equally important and none of them can be discarded right away. From this figure, with  $\sim 8\%$  increase in first catalyst concentration, grafting density is more as compared to the experimental run 1 in less polymerization time (see Table 6.3). That means, as the ratio of two catalysts increases ( $cat_1/cat_2$ ), grafting density also increases. This grafting density also strongly depends on second catalyst addition time. One has to allow certain span of copolymerization time to get more iPP  $M_w$ . Based on these results; certain process improvement (in terms of  $M_w$ , PDI) has been obtained. So, multi-objective optimization study has been extended to the entire range of experimental data (henceforth called as case 2) to see more variety of process performance as well as improving the same strictly within the experimental limits.

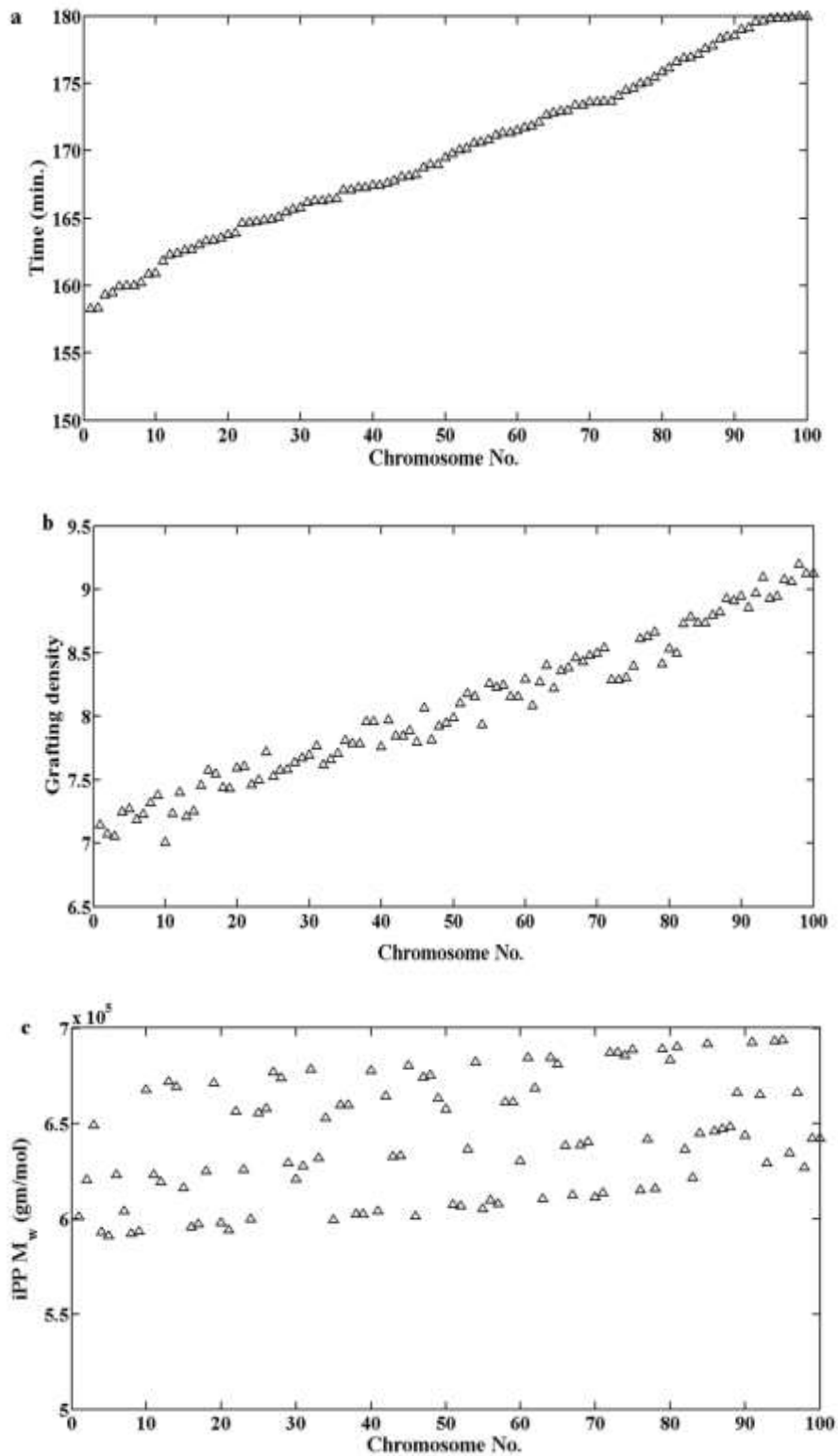


Figure 6.1: Results of three objective functions of case1 (a)  $t_p$  (in ascending order) (b) corresponding values of GD, and (c) iPP  $M_w$ .

Table 6.3: Process performance with various decision variables for case 1

Data set	Fe ( $\mu\text{M}$ )	Zr ( $\mu\text{M}$ )	cocatalyst (M)	polymerization time (min)	$M_w \times 10^{-3}$ (gm/mol)	GD
Experimental	75	10	0.075	180	631.8	8.4
MOOP	82.3	9.83	0.0751	178	648	8.92
MOOP	82.3	9.5	0.0716	178.4	666	8.9

Fig. 6.2 depicts the multi-objective PO solutions for the above mentioned three conflicting objectives for the entire range of experimental data. All decision variables are kept within the  $\pm 10\%$  experimental range to control the model extrapolation errors because the estimated kinetic parameters are valid for a certain range of operating conditions. These PO solutions are projected into the individual two dimensional planes to have better understanding of the situation. Experimental points of run 1 and run 3 (which have  $\text{GD} > 8$ ) are represented in the same plot as filled points (circled points). A significant number of PO solutions are found better than the experimental points. The corresponding decision variables (amount of first catalyst, second catalyst, cocatalyst and second catalyst addition time) have been presented in Figs. 6.3a – d in different shades. Fig 6.3a represents PO solutions with the first catalyst concentration (Fe) as decision variable. Figs. 6.3b, 6.3c, 6.3d are the same PO solutions where second catalyst concentration (Zr), cocatalyst concentration and second catalyst addition time have been taken as decision variables, respectively. We can characterize these PO solutions and can find an interesting trend among the decision variables. If we concentrate on grafting density alone, we can see higher grafting density can be achieved by maintaining operating conditions with higher values of  $\text{cat}_1/\text{cat}_2$  ratio (Fe/Zr) as well as higher second catalyst addition time. The amount of first catalyst addition (in Fig. 6.3) spans across medium to higher range, whereas other decision variables are present across the entire ranges. As told earlier, this is due to increase in the ratio of the first catalyst to second catalyst, which leads to more GD. Similarly, the time minimization occurs for higher values for  $u_1$  (first catalyst) and moderate values for  $u_2, u_3, u_4$ . Of course, one has to see for a solution considering all three objectives in mind because settling for higher grafting density and iPP  $M_w$  may lead to solutions with poor time productivity. From the PO set given in Fig. 6.3, a particular solution can be chosen based on decision maker's preference and corresponding trends among the decision variables can be found out. This kind of optimal trend can be extremely useful for an operator to run a plant without much intervention of mere qualitative perceptions.

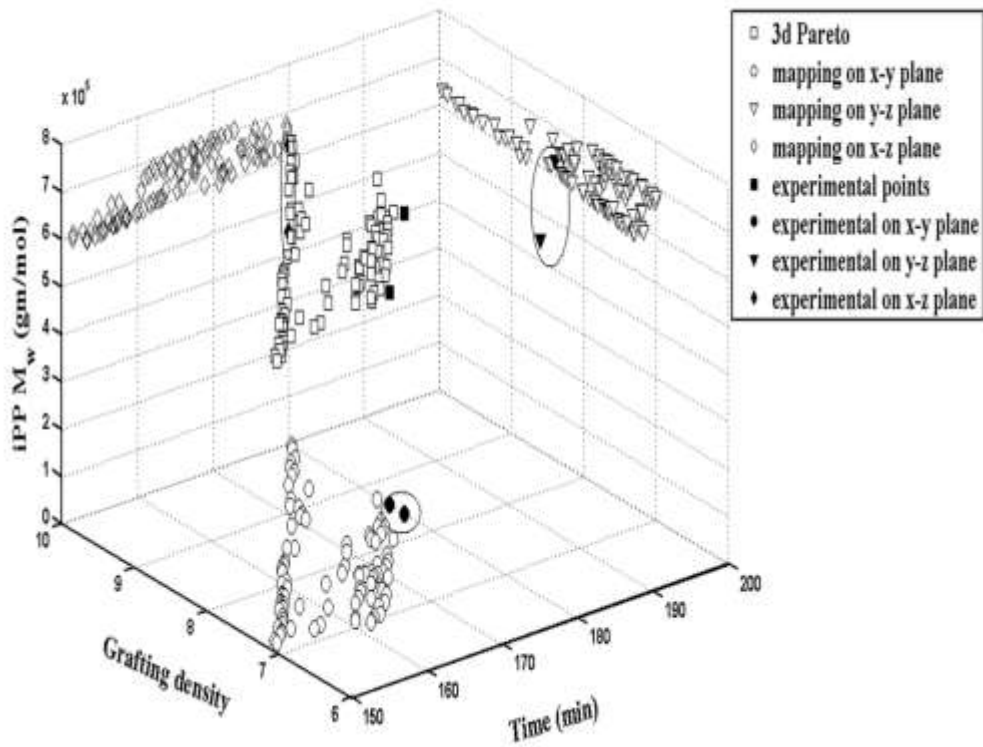


Figure 6.2: PO solutions for case 2 (x: Time (min.), y: Grafting density, z: iPP  $M_w$  (gm/mol)).

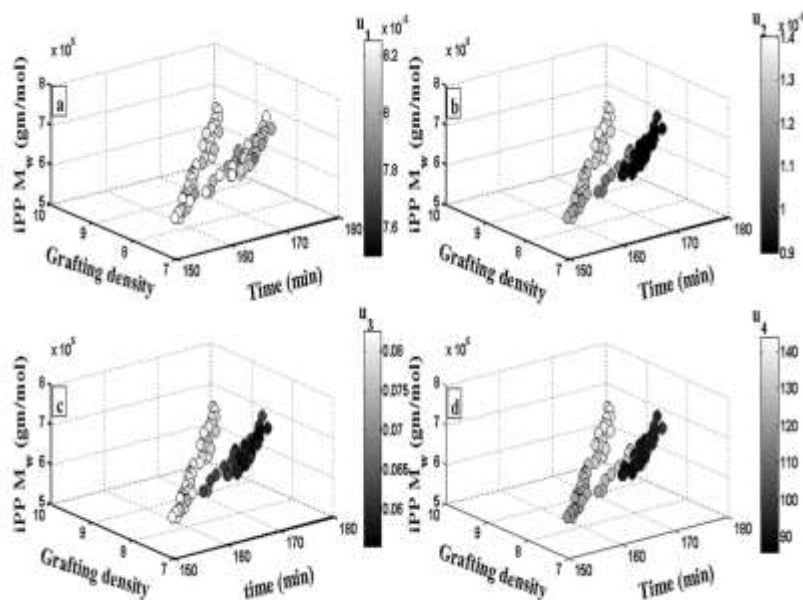


Figure 6.3a-d: PO solutions with total search space consisting of widely varying scenarios ( $u_1$ : first catalyst concentration,  $u_2$ : second catalyst concentration,  $u_3$ : cocatalyst concentration,  $u_4$ : time gap between the two catalyst additions) for case 2.

The PO solutions presented in Fig. 6.3, along with their corresponding values of ratio of catalyst 1 to catalyst 2, grafting density and second catalyst addition time are shown in Fig. 6.4 with varying copolymerization time (presented in shades). A primary look at the figure divides the points into two regions: 1: solutions with less copolymerization time and less catalysts ratio; 2: solutions with medium to high copolymerization time and high catalysts ratio. In the first region, their GD and second catalyst addition times are found to be quite varying. In the other region, the variation is found less for GD as well as for second catalyst addition time. Moreover, with lower catalyst ratio, the optimizer has chosen more time gap between the two catalyst additions to achieve more GD at a less copolymerization time. However, lesser value of iPP  $M_w$  is obtained in less copolymerization time as evident from Fig.6.5. In the same figure, the solutions which are grouped by an ellipse have almost similar copolymerization time. In case of these solutions, high  $M_w$  points appear for low cocatalyst concentration. This is happening due to low chain transfer to cocatalyst. Multi-objective optimization leads to multiple number of trade-off solutions as opposed to a single solution in case of single objective optimization. Trade-off among solutions is clear as improvement in certain objective comes at the cost of deterioration in other objectives. However, at the end of the optimization study, one has to choose only one solution as the solution of choice and this selection needs decision maker's knowledge about how to prioritize among various objectives. The formulation given in Table 6.1 could have been also presented by optimizing grafting density and polymerization time and constraining the  $M_w$  to some higher value in the commercial range instead of considering  $M_w$  in the objectives. This is because in commercial operation one would be interested to produce polymer with same quality in terms of  $M_w$ . However, the formulation presented in Table 6.1 is more beneficial when the decision maker is not sure whether there exists a Pareto solution at a particular value of  $M_w$  (say, 500 kg/mol). In these cases, it is better to see at what different values of  $M_w$  the solution exists and then decide which value of  $M_w$  (may be 490 kg/mol) to be chosen. For a clear depiction, polymerization time vs. grafting density has been plotted in Fig. 6.6 to show different polymers of almost similar molecular weight (e.g.  $M_w=670000$  gm/mol to 676000 gm/mol).

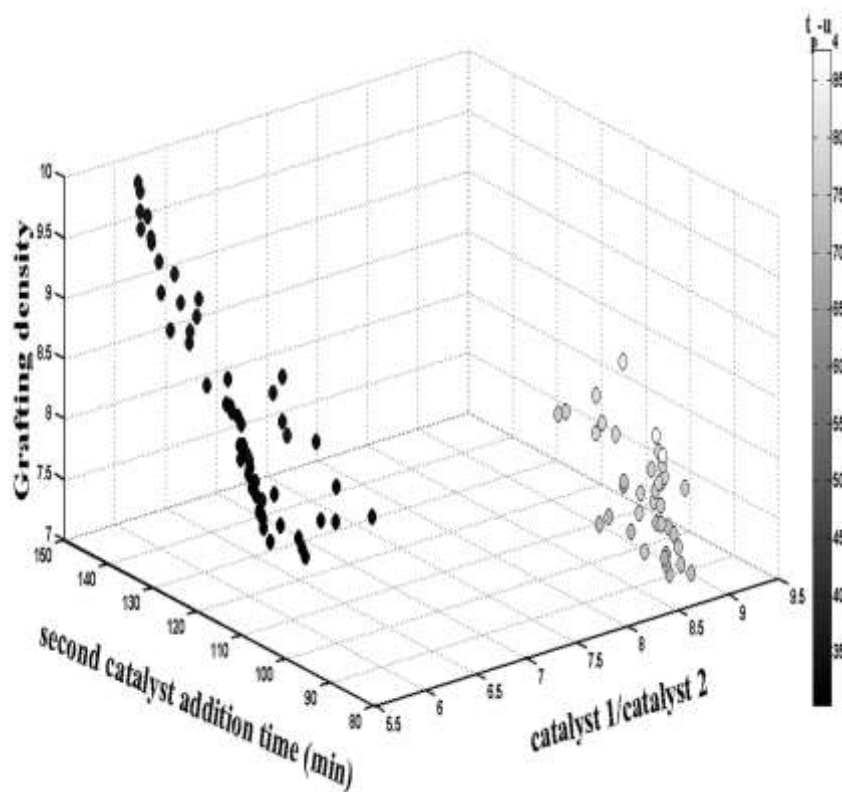


Figure 6.4: Variation of grafting density with the ratio of the two catalysts, second catalyst addition time ( $t_p-u_4$ : copolymerization time).

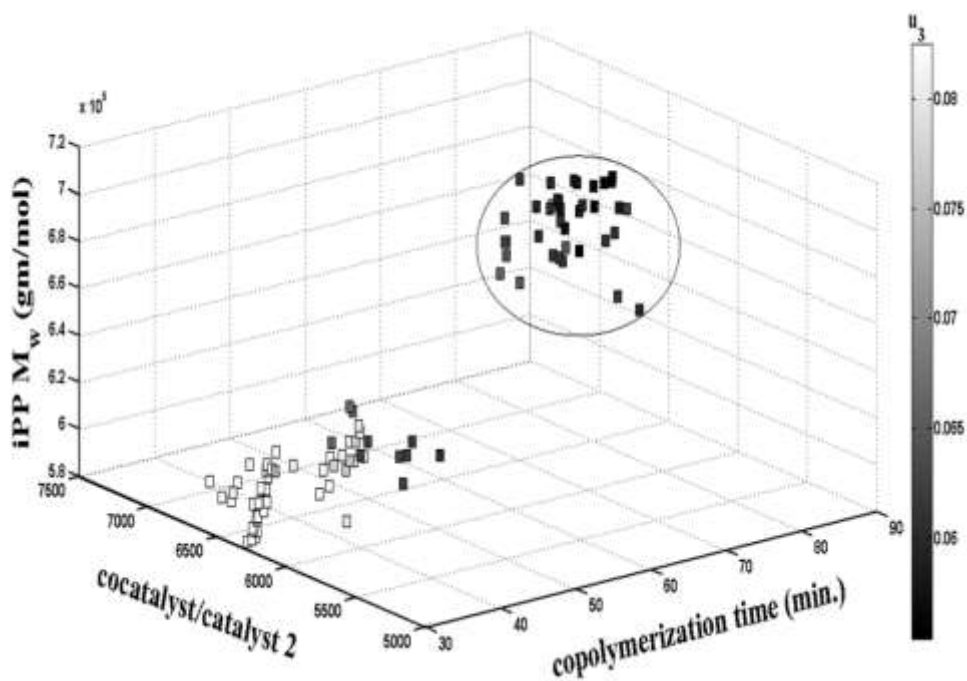


Figure 6.5: Effect of copolymerization time, cocatalyst/catalyst2 ratio on iPP molecular weight ( $u_3$ : cocatalyst concentrations, points inside the circle are high molecular weight).



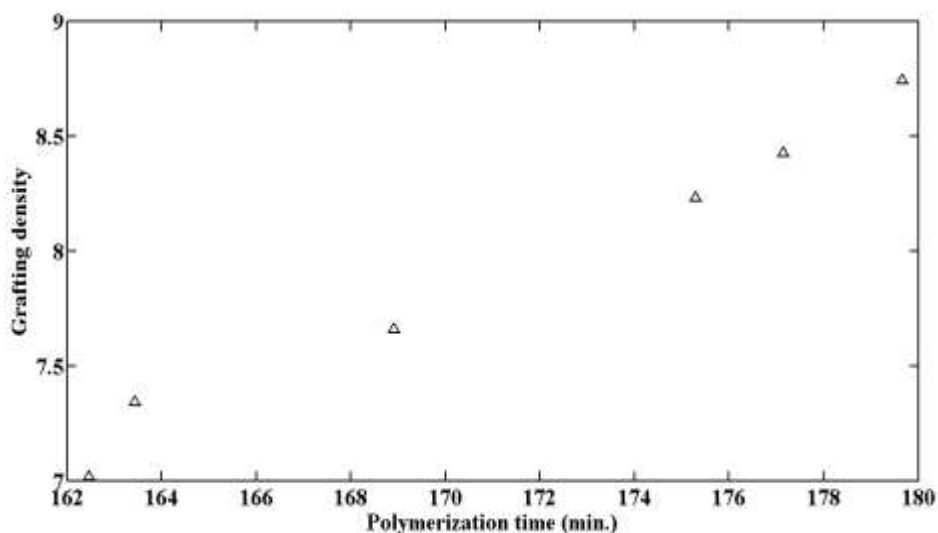


Figure 6.6: Polymerization time vs. grafting density for  $M_w=670000$  gm/mol to 676000 gm/mol.

As the molecular weight distribution (MWD) is of great interest due to its direct relationship with various polymer properties, MWD of two PO points are calculated. One of the ways to calculate the MWD for branched polymer is numerical fractionation, where the whole polymer population is classified into number of classes based on the number of branches [49] (e.g. linear polymers belong to zero<sup>th</sup> class, polymers with one LCB go to class 1 and so on.). According to this method [49], the rates of moments have been derived for each class of live and dead polymer chains and are shown in chapter 5. MWD of each class of polymer chains is calculated using a two-parameter model following Schultz-Flory distribution (Equation 6.1). Once the individual distribution is achieved, the overall MWD is calculated by the weighed sum of all individual class distributions. In this method, the number of classes should be chosen properly to construct the complete MWD. The below mentioned convergence criteria has been applied for accurate construction of MWD (Equation 6.2). MWDs for the two Pareto points of having different  $M_w$  and GD are compared and shown in the Fig. 6.7, and the corresponding MWDs of grafted side chains is represented in Fig. 6.8. From this figure, it can be concluded that grafted side chains may exhibit very narrow molecular weight distribution. It is evident from this figure that high  $M_w$  plot exhibits wider MWD and shifted towards higher chain length as compared to the curve with lower  $M_w$ .

$$w_m(r) = \frac{y_m (ry_m)^{z_m} e^{-ry_m}}{\Gamma(z_m + 1)}; m = 0, 1, 2 \dots \text{et.} \quad (6.1)$$

$$z_m = \frac{DP_{n,m}}{DP_{w,m} - DP_{n,m}}; y_m = \frac{z_m + 1}{DP_{w,m}}$$

$$\frac{(v_1 - \sum_{m=0}^N v_{1,m})}{v_1} \leq 0.02 \quad (6.2)$$

Where  $w_m(r)$  represents the weight fraction of the polymer chains of  $m^{\text{th}}$  class with a degree of polymerization of  $r$ .

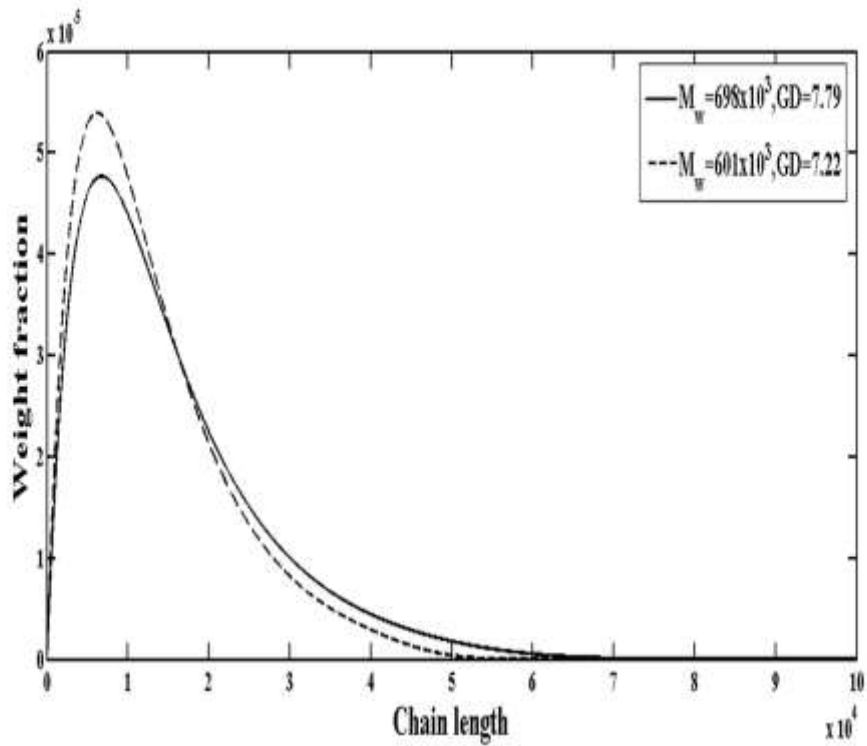


Figure 6.7: MWD comparison for two different Pareto points.

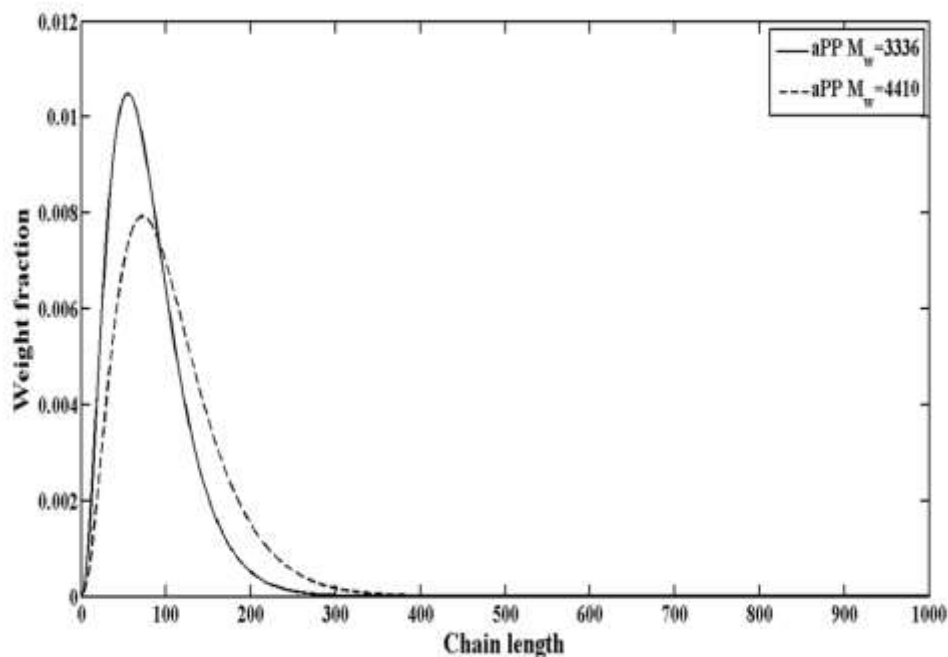


Figure 6.8: MWD comparison of grafted side chains that corresponds to Fig. 6.7.

## 6.4 Conclusion

Multi-objective optimization has been formulated for various conflicting objectives with relevant constraints using the above validated model. Maximization of iPP weight average molecular weight and grafting density have been attained along with simultaneous minimization of total polymerization time without violating the process constraints. Real coded NSGS II has been used to find the multi-objective Pareto optimal solution and corresponding operating conditions. The optimization approach provided a wide variety of solutions in the entire terrain of search for this dual catalyst system. Two catalysts and one cocatalyst concentrations, time gap between the two catalyst additions and total polymerization time are used as decision variables. One of the objective functions, viz. grafting density, strongly depends on the time gap between the two catalyst additions, ratio of the two catalysts and copolymerization time. The optimization exercise not only leads to a variety of competitive process choices but also shows improvement in process objectives as compared to the existing literature data. Solutions originating from different regions of the PO set were considered and the possible reasons for their occurrence were analyzed in detail in terms of reaction mechanisms proposed.

# Chapter 7

## Kriging Surrogate based Multi-objective Optimization of Bulk Vinyl Acetate Polymerization with Branching

In this chapter, the primary aim is to replace the computationally expensive model for a batch free radical polymerization of vinyl acetate process with a Kriging surrogate based faster model while solving a multi-objective optimization problem and observe the merits and demerits in this approach in terms of improvement in execution time and reliability of the obtained solutions.

### 7.1 Introduction

From the computationally expensive kinetic model for polyvinyl acetate (PVAc) [38, 106] molecular properties such as number average molecular weight ( $M_n$ ), weight average molecular weight ( $M_w$ ), number average degree of branching ( $B_n$ ) etc. are calculated and validated with the batch experiment conducted by Thomas [1]. At high monomer conversion, there is a possibility of formation of gel causing a sudden rise in molecular weight and thereby choking of the reactor. The target, therefore, is to find the optimal process conditions for various desired combinations of conflicting objectives (minimization of  $t_p$ , maximization of  $M_w$  and  $B_n$ ) avoiding the gel effect while honoring the constraints defined for  $M_w$  and PDI. Additions of monomer and initiator in the beginning and the temperature of the process are taken as the process conditions to be optimized (i.e. decision variables) for the above isothermal process. Gaussian process based individual Kriging models for objective functions and constraints are built first. This model building exercise starts with a relatively less number of input-output data points for training the intermediate crude surrogate model, whose accuracy is improved further by adding additional data points at locations (i.e. infilling) where the model needs improvement. This process is continued

till the desired model accuracy is achieved. Gaussian process based infill criteria such as expected improvement of the intermediate crude Kriging model is used to determine the location where the model needs further improvement. The ability to find the size of input-output data required to build a parsimonious surrogate model and the locations where the data is required are the outperforming features that the Kriging possesses over ANN. Population based real coded non-dominated sorting genetic algorithm-II (NSGA-II) [19] has been used to obtain the PO solutions among the above mentioned conflicting objectives using the Kriging based surrogate models as well as the expensive model. The final surrogate based PO solutions are compared with those obtained using the expensive first principle models and the aspects of fastness in model execution without losing the rigor of the model built are analyzed.

## 7.2 Optimization problem formulation

The kinetic recipe for the polymerization of vinyl acetate is given in chapter 4. In the present formulation, batch addition amount of monomer (M) and initiator (I), temperature to be maintained during the isothermal process of polymerization (T) are taken as decision variables. The aim here is to obtain polymer of high  $M_w$  and  $B_n$  in minimum  $t_{poly}$  (Table 7.1). Once decision variables (M, I and T) are decided by the optimization routine, conversion at gel point is calculated [106] from the empirical relation between monomer gel point conversion and temperature which is shown in Equation 7.1.

Table 7.1 Optimization problem formulation

$  \begin{aligned}  & \textit{Maximize } M_w \\  & \textit{Maximize } B_n \\  & \textit{Minimize } t_{poly} \\  & M_w \geq M_w^{\min} \\  & PDI \leq PDI^{\max} \\  & Conv \leq Conv_{Gel}(T) - 3  \end{aligned}  $
---

With decision variable bounds are:

$$10 \leq M \leq 14; \quad 0.00003 \leq I \leq 0.00015; \quad 333K \leq T \leq 353K$$

$$Conv_{Gel}(T) = 1.47 \times 10^{-3} \times T + 0.32 \quad (7.1)$$

This empirical relation is obtained from the data of monomer conversion and  $M_w$  at different temperatures [38, 97]. Identifying the gel points at different temperatures from these curves

(where the sudden rise of  $M_w$  occurs, i.e. Trommsdorff effect), the temperature dependency of conversion can be obtained by linear fitting. Depending upon the gel point conversion value obtained at a temperature, the simulation is allowed to proceed up to 3% lesser than that conversion value to avoid the gel effect (i.e. for a specified temperature, if the monomer conversion at gel point is 80%, the simulation of the model is allowed to run up to 77% of the monomer conversion). All decision variables (M, I and T) are forced to lie between their lower and upper bounds. The limiting values for the various constraints such as  $M_w$ , PDI are decided by the experimental study [1] so that the prediction through optimization results is realizable.

Since the above moment based model is computationally expensive, performing multi-objective optimization using this model becomes a prohibitive proposition. For example, when such an optimization is carried out with 70 candidate solutions for 40 generations using NSGA II, the execution time is of the order of 192 hours in an Intel(R) Xeon(R) CPU E5-2690 0 @ 2.90GHz (2 processors) 128 GB RAM machine. However, the main focus in this work is to replace the original expensive model with a surrogate model (i.e. Kriging) and carry out the same multi-objective optimization study for the desired conflicting objectives to analyze the extent of time advantage achieved by this approach within a reasonable prediction accuracy thereby making the application more amenable for using online. The choice of NSGA II as a multi-objective optimization technique is primarily based on its already established outperforming ability to find out the well spread near optimal Pareto solutions in single simulation run as compared to many classical as well as evolutionary techniques [19].

### **7.3 Kriging Model development**

In this section, a brief description of Kriging is given, which includes the formulation and implementation of the process of surrogate model building for the polymerization system. Let us consider the modeling of input – output relationship in case of one of the outputs i.e. polymerization time where the overall task is to build such models for each of the responses [ $t_{poly}$ ,  $M_w$ ,  $B_n$ , PDI] for the same input vector [M, I, T]. The proposition in Kriging assumes that the value of the response at a new point is uncertain before a sampling is performed at that point. This uncertainty can be modeled as a Gaussian random process with  $\mu$  mean and  $\sigma$  standard deviation. This means the value of the response at the point is typically  $\mu$  with a variance of  $\pm 3\sigma$ . Similarly, we can say that two such new points, where responses are

uncertain, can be weakly correlated with each other, if they are away from each other, whereas the correlations are going to be very strong when they are close to each other. This goes with the assumption that the function being modeled through the responses is continuous. One of the ways of representing such correlations statistically is

$$\Psi = \text{Corr}[t_{\text{poly}}^{(i)} - t_{\text{poly}}^{(l)}] = \exp(-[\theta_m | M^{(i)} - M^{(l)} |^2 + \theta_i | I^{(i)} - I^{(l)} |^2 + \theta_t | T^{(i)} - T^{(l)} |^2]) \quad (7.2)$$

Using the above equation, an  $n \times n$  correlation matrix ( $\Psi$ ) can be constructed for all observed  $n$  data,  $[M^{(i)}, I^{(i)}, T^{(i)}, t_{\text{poly}}^{(i)}; i = 1, 2, \dots, n]$  where  $\theta_m, \theta_i, \theta_t$  are the unknown parameters. The parameters  $\mu, \sigma^2$  and  $\theta_m, \theta_i, \theta_t$  are estimated by maximizing the log likelihood function [22, 89] generated by the above mentioned correlation coefficient  $\Psi$  (Equation 7.3 excluding constant term). This action intuitively means that the function being modeled is most consistent with the data used.

$$-\frac{n}{2} \log(\sigma^2) - \frac{1}{2} \log(|\Psi|) - \frac{(\mathbf{t}_{\text{poly}} - \mathbf{1}\mu)^T \Psi^{-1} (\mathbf{t}_{\text{poly}} - \mathbf{1}\mu)}{2\sigma^2} \quad (7.3)$$

Optimum values of  $\mu$  and  $\sigma^2$  (Equation 7.4) can be obtained by keeping the derivatives of the Equation 7.3 with respect to  $\mu$  and  $\sigma^2$  equal to zero.

$$\begin{aligned} \hat{\mu} &= \frac{\mathbf{1}^T \Psi^{-1} \mathbf{t}_{\text{poly}}}{\mathbf{1}^T \Psi^{-1} \mathbf{1}} \\ \hat{\sigma}^2 &= \frac{(\mathbf{t}_{\text{poly}} - \mathbf{1}\hat{\mu})^T \Psi^{-1} (\mathbf{t}_{\text{poly}} - \mathbf{1}\hat{\mu})}{n} \end{aligned} \quad (7.4)$$

Where  $\mathbf{t}_{\text{poly}}$  is the column vector of size  $n$  that contains values of the response at each observed point and other variables  $\hat{\mu}$  and  $\hat{\sigma}^2$  are the maximum likelihood estimates [22] of mean and variance (Equation 7.4). By substituting Equation 7.4 into 7.3, the concentrated log likelihood function can be obtained as only function of  $\Psi$  which in turn is function of the parameters  $\theta$ s

$$-\frac{n}{2} \log(\hat{\sigma}^2) - \frac{1}{2} \log(|\Psi|) \quad (7.5)$$

Since the above concentrated likelihood function now depends only on the parameters  $\theta_m, \theta_i$  and  $\theta_t$ , they can be estimated by an optimizer such as genetic algorithms while maximizing Equation 7.5 itself. This explains how to build a Kriging interpolator when  $n$  sets of data points are given.

At an unobserved new point M, I and T, Kriging prediction  $\hat{t}_{poly}$  is given by

$$\hat{t}_{poly} = \hat{\mu} + \psi^T \Psi^{-1} (t_{poly} - \hat{\mu}) \quad (7.6)$$

Where  $\psi$  is a correlation vector between observed points and a new prediction point. For an unobserved point, the mean square error ( $s^2(\mathbf{x})$ ) of the predictor calculated by standard stochastic process approach is given by

$$s^2(\mathbf{x}) = \sigma^2 \left[ 1 - \psi^T \Psi^{-1} \psi + \frac{(1 - \mathbf{1}^T \Psi^{-1} \psi)}{\mathbf{1}^T \Psi^{-1}} \right] \quad (7.7)$$

This is an approximate statistical error that the Kriging model has at any stage. This error is calculated from the curvature (second order derivative) information of the log likelihood function and using the idea of error is inversely proportional to the curvature. This means that more the curvature of log likelihood function at any point, more confident one is about the predicted value as compared to its neighboring points due to the stiff hill it forms with respect to its surrounding and this is synonymous to lesser error. This is an estimate of the statistical error that any n-point Kriging model can have at any stage whereas its mean can be given by  $\hat{t}_{poly}$ . As this expression is a function of input vector (M, I, T), the error associated with any prediction from the n-point Kriging model for any input combination can be obtained from this expression. Using this error expression, various other entities of a Gaussian statistical model such as statistical lower bound, probability of improvement with respect to a given target and expected improvement (Equation 7.8) etc. can be easily calculated. Each of these measures can be utilized while selecting the location of the (n+1)<sup>th</sup> point (i.e. infilling) for the n-point Kriging model in a region where the model is having less confidence and more error and needs information to become more accurate. This way an existing model can be made more accurate incrementally by adding more and more points into it. In the present work, the algorithm mentioned below (Table 7.2) has been used to obtain four independent Kriging models (i.e.  $t_{poly}$ ,  $M_w$ ,  $B_n$ , PDI) for the bulk free radical polymerization of PVAc. At first, 3 points are chosen from the input space using latin hypercube sampling (LHS) and a Kriging model is built using these data sets (3 sets of inputs and outputs). After that, a point has been chosen from the input space based on maximization of expected improvement  $\{E[I(\mathbf{x})]\}$  [22] (Equation 7.8:  $\Phi$  and  $\phi$  are the normal cumulative distribution function and density function) and this point is added as a new point in the database of the input-output data. This way of adding points has been shown to have



the attribute of finding global optimum [22]. After re-tuning the Kriging model, metrics such as root mean square error (RMSE) and correlation coefficient ( $R^2$ ) are used to predict 200 independently generated sample points by Latin Hypercube Sampling (LHS) [107]. This process of incremental model building while enriching the input-output database during several iterations has been stopped if the RMSE (due to its good global error estimate) [108],  $R^2$  and  $E[I(\mathbf{x})]$  values of the two consecutive intermediate models are close to a predefined tolerance limit ( $\epsilon$ ). It is worth mentioning that the validation set of 200 independently generated sample points by LHS are only used to test the maturity of the model built; they are no way used to enrich the model. In this way, Kriging can determine the size of the input-output data required as well as the location of the new point addition. Similar procedure is repeated for the remaining three responses ( $M_w$ ,  $B_n$ , PDI) to develop the corresponding Kriging models. The RMSE and  $R^2$  values for the four Kriging models are shown in Table 7.3. After developing the four independent Kriging models, the original PVAc model (expensive model) is completely replaced by these Kriging models to calculate objective functions and constraints while performing the multi-objective optimization of the problem given in Table 7.1.

$$E[I(M, I, T)] = s \left[ \left( \frac{t_{poly(min)} - \hat{t}_{poly}}{s} \right) \Phi \left( \frac{t_{poly(min)} - \hat{t}_{poly}}{s} \right) + \phi \left( \frac{t_{poly(min)} - \hat{t}_{poly}}{s} \right) \right] \quad (7.8)$$

Table 7.2 The algorithm used to develop (tune) Kriging model

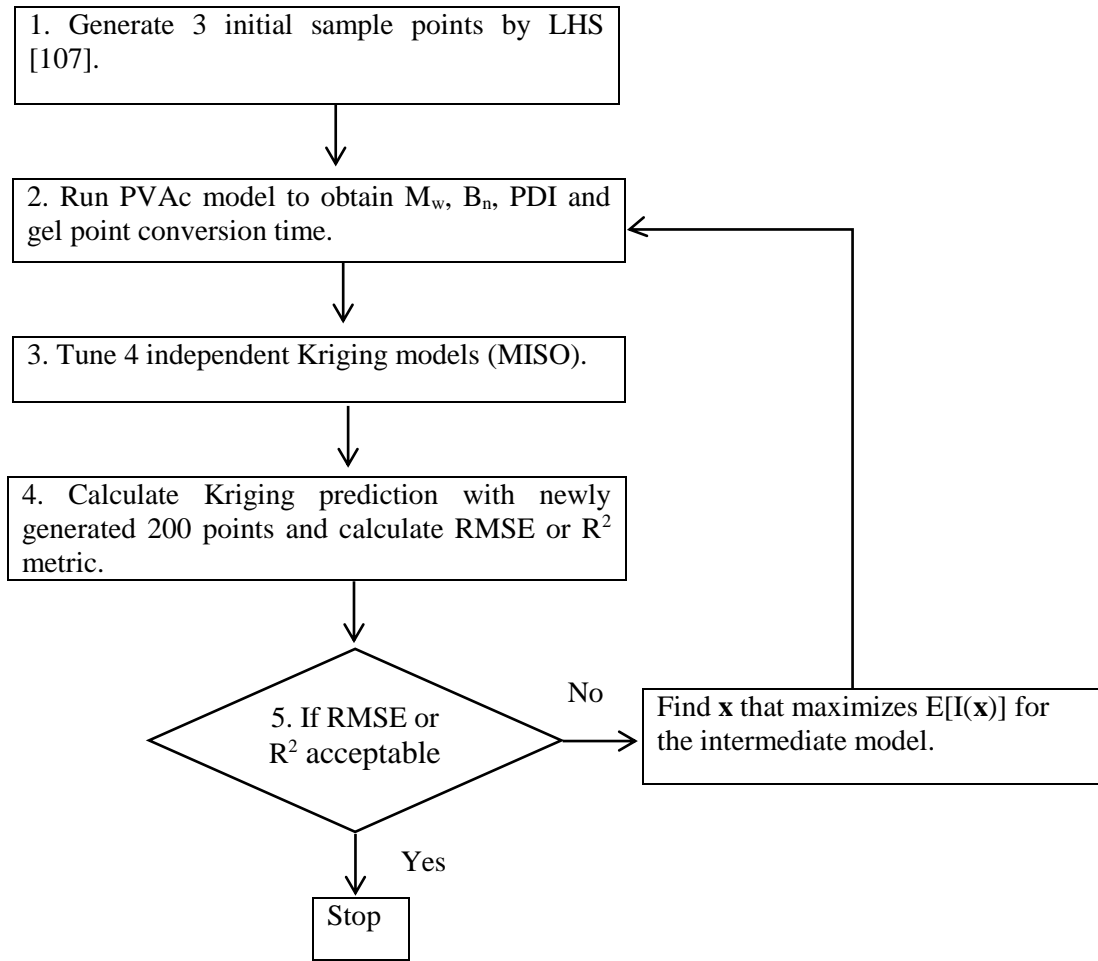


Table 7.3: RMSE and  $R^2$  comparison of four different models

Model	Number Points/ Function Calls	RMSE	$R^2$
Polymerization Time	200	0.0091	0.9987
$M_w$	9	0.0128	0.9957
$B_n$	4	0.0133	0.9953
PDI	4	0.0113	0.9882

#### 7.4 Results and discussion

Moment based modeling approach is adapted to solve the mathematical model for batch bulk free radical polymerization system. The model is validated with experimental studies of Thomas [1] in terms of experimental data available on weight average molecular weight ( $M_w$ ) and number average degree of branching ( $B_n$ ) at two different temperatures and different initiator concentrations [106]. Before building the surrogate models of the given process, a sensitivity analysis has been carried out to see the effect of inputs on various

responses. While doing this, contour plots (Fig. 7.1 to 7.4) have been generated by keeping one of the input variables at a fixed value and varying the other two inputs to show their impacts on the values of responses. From these figures, it is concluded that monomer has less impact on the objective functions. Also, initiator and temperature has more influence on polymerization time (Fig. 7.1a) as compared to  $M_w$ ,  $B_n$  and PDI (Figs. 7.2 to 7.4) on gel point conversion. The main objective in this work is to obtain the optimal process conditions for the desired combination of conflicting objectives before the gel point is reached in less computational time. For this purpose, a well-established multi-objective optimization technique real coded non dominated sorting genetic algorithm (NSGA II) [19] has been utilized. If the first principle model (i.e. PVAc model) is used to solve their objective functions, say for 40 generations with a population size of 70, the number of function calls needed is 2800 ( $70 \times 40$ ) which makes it computationally expensive due to the expensive function evaluation involved in the first principle model. This execution time is of the order of 192 hours in Intel(R) Xeon(R) CPU E5-2690 0 @ 2.90GHz (2 processors) 128 GB RAM machine. Based on several optimization runs, we come to a conclusion that the number of population mentioned above are necessary to obtain a well-spread Pareto and the generation number 40 is the point around which the PO solutions just gets saturated. Any PO solutions generated generation # 40 onwards provide no further improvement in the PO front. To reduce the computational effort, four independent Kriging models, one each for each of the responses, are developed to replace the physics driven expensive model.

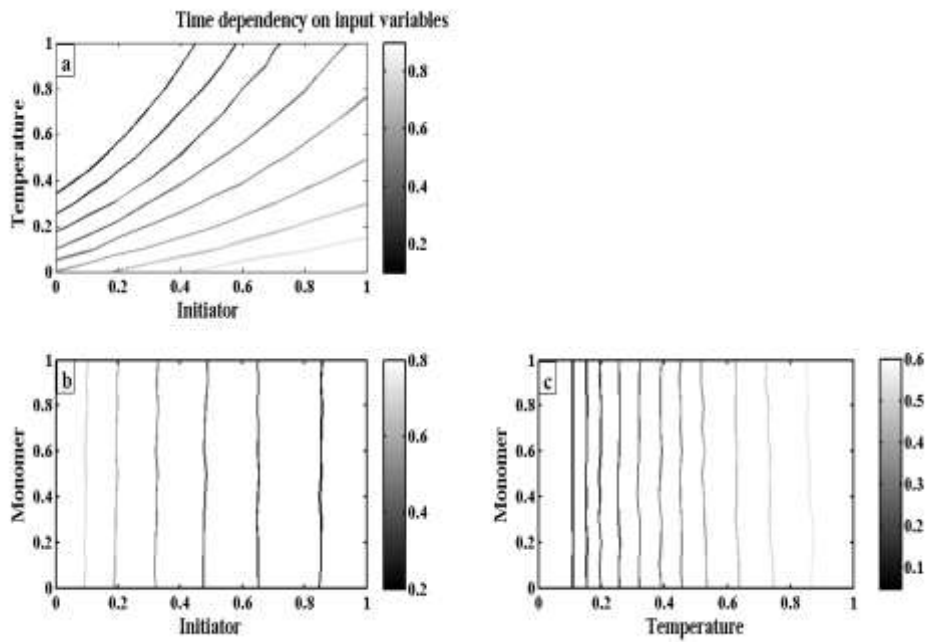


Figure 7.1: Contour of the polymerization time versus two of the three variables, while maintaining the remaining one variable at base value.

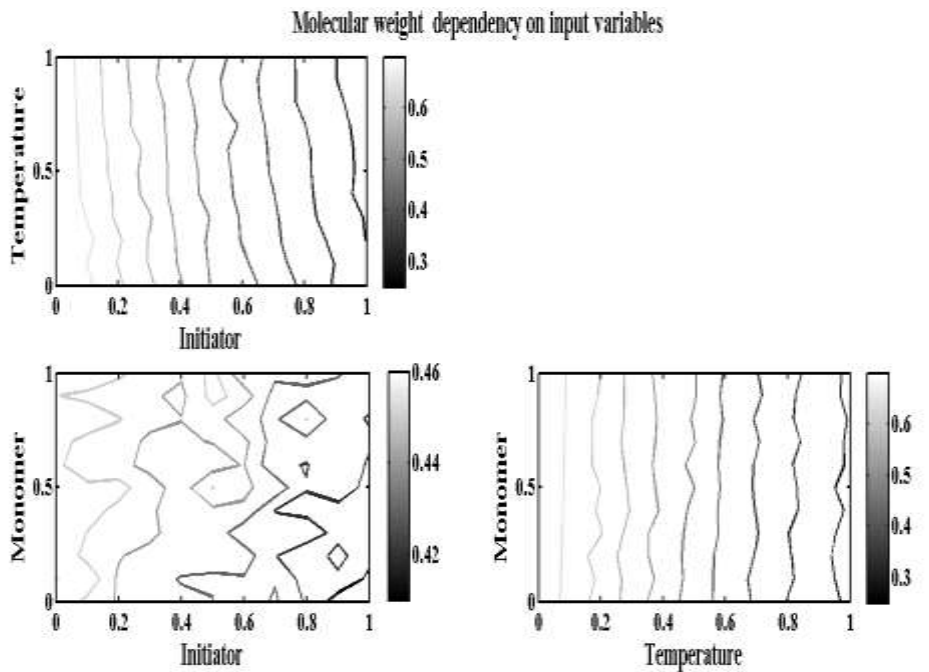


Figure 7.2: Contour of the  $M_w$  versus two of the three variables, while maintaining the remaining one variable at base value.

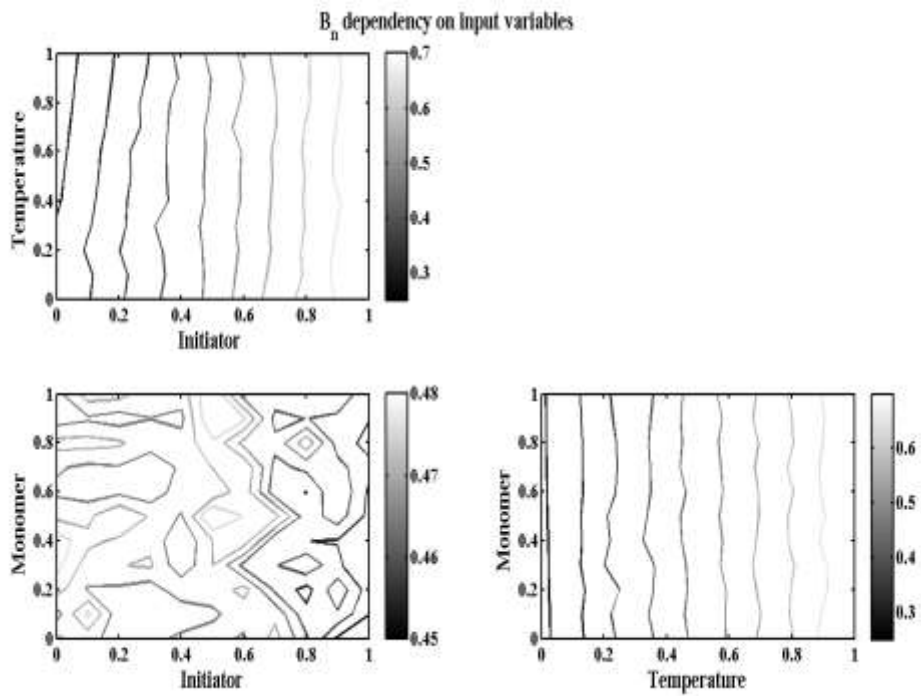


Figure 7.3: Contour of the  $B_n$  versus two of the three variables, while maintaining the remaining one variable at base value.

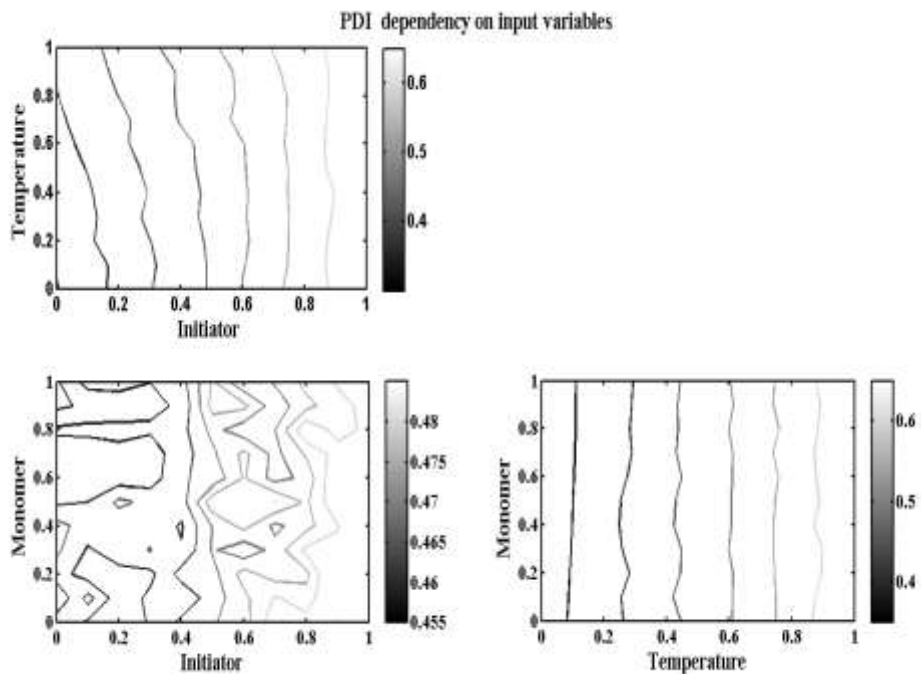


Figure 7.4: Contour of the PDI versus two of the three variables, while maintaining the remaining one variable at base value.

As mentioned earlier, the model building process has been started with 3 initial points generated by low discrepancy LHS plan [107]. The model thus developed has an error as well as expected improvement expressions (Equations 7.7 and 7.8 respectively) for any unknown point which enables a user to find a point in the input space where the model is most unreliable. A sampling made at this point probably can improve the predictability of the model most. This process of addition of sampling points (infilling) continues till a model of desired accuracy is achieved. For providing ease in understanding, input design space (Figs. 7.5a, 7.5d and 7.5g), the surface plot of total polymerization time (Figs. 7.5b, 7.5e and 7.5h) and prediction of Kriging model (Figs. 7.5c, 7.5f and 7.5i) have been shown for different intermediate stage models e.g. a 3 points starting Kriging model (Figs. 7.5a, 7.5b, 7.5c), 52 point (Figs. 7.5d, 7.5e, 7.5f) and 200 points (Figs. 7.5g, 7.5h, 7.5i) Kriging models. In the Fig. 7.5, the first subfigure is expressed in terms of [M, I, T] triplet that shows the location of the sampling points, the second subfigure is the 3 dimensional surface as well as contour plot of the response ( $t_{\text{poly}}$  in this case) in terms of two most significant inputs (T and I here as M has negligible effect on  $t_{\text{poly}}$ ) and the third subfigure is the comparative plot between the predictions of the Kriging model and the expensive physics driven model for same 200 input points from the testing set. As evident from the Fig. 7.5, Kriging model predictions have improved as more numbers of infill points are added. Validation results for 200 independent LHS points for four different Kriging models are presented in Fig. 7.6. This figure shows that the four surrogates generated are quite accurate (i.e. all points are close to the  $45^\circ$  line). While building the surrogate models, the total number of expensive function calls is found to be 417 (i.e. for  $t_{\text{poly}}$ ,  $M_w$ ,  $B_n$ , PDI, the individual expensive physics driven model has been called for 200, 9, 4, 4 times, respectively plus 200 function evaluations for creating the testing set). Here, one should note that the size of the testing set could have been reduced further to report further computational gain. As this testing set is the indication of the surrogate model built, no compromise has been made on the quality of the model.

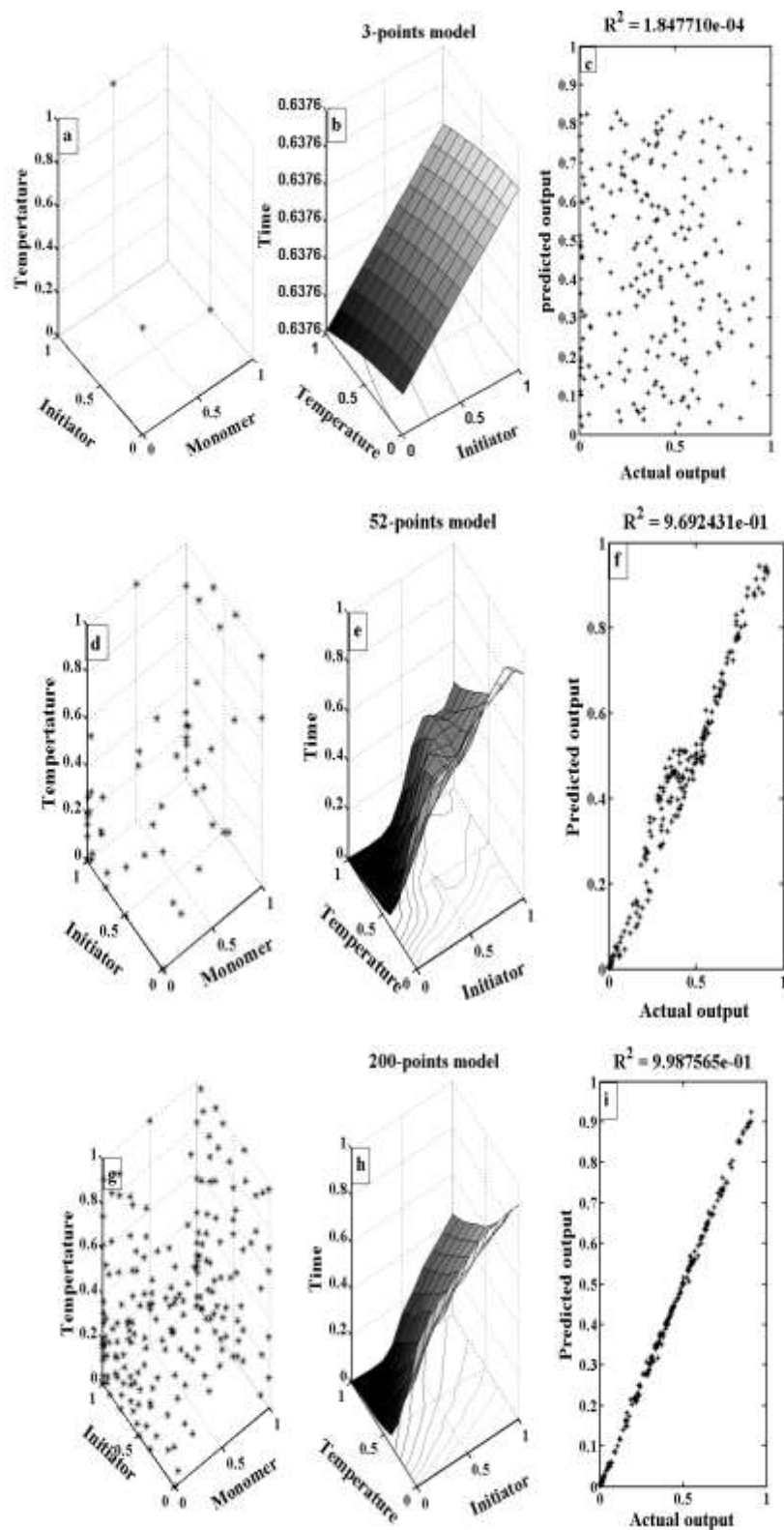


Figure 7.5: Evolution of Kriging model for polymerization time with starting 3 points (a. Input space b. surface plot c. parity plot) and Intermediate 52 points (d. Input space e. surface plot f. parity plot) and final 200 points (g. Input space g. surface plot i. parity plot)

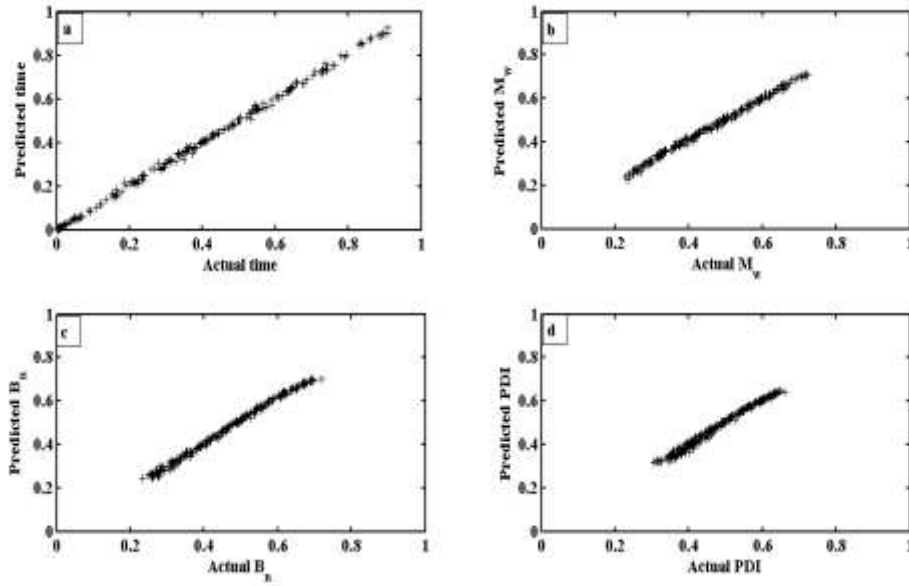


Figure 7.6: Validation results for different output variables using Kriging

The above validated surrogate models have been utilized next to conduct multi-objective optimization of various conflicting objectives to reduce the computational burden by the original first principle model. Fig. 7.7 displays PO solutions by the Kriging model and first principle model for the desired combination of three conflicting objectives. These Pareto fronts are quite close to each other. As indicated earlier, the PO solutions of the first principle model need 2800 function evaluations (equivalent to a run of 192 hours) in Intel(R) Xeon(R) CPU E5-2690 0 @ 2.90GHz (2 processors) 128 GB RAM machine whereas the PO solutions of the Kriging model need only 417 function evaluations (~85% savings in function evaluations). As compared to function evaluation using expensive model, the time required to solve the optimization problem using Kriging model is miniscule. There are multiple numbers of solutions in Fig. 7.7 which are all optimal or equally important (known as non-dominated solutions). Trade-off among solutions is clear as improvement in certain objective comes at the cost of deterioration in other objective. For example, to find a polymer of high  $M_w$  or high  $B_n$ , one has to compromise for more processing time. However, at the end of the optimization study, one has to choose only one solution as the solution of choice and this selection needs decision maker's knowledge about how to prioritize among various objectives [19]. Real coded NSGA-II provides the best feasible non-dominated solutions on the basis of optimization problem posed. In Fig. 7.7, the optimal sets of decision variable values  $[M, I, T]$  for the expensive model and Kriging model are different. Next, the expensive model is run for each of these PO solutions



obtained by Kriging model to measure the level of accuracy. This comparison is shown in Fig. 7.8, where the points in the 3-dimensional Pareto are projected upon the individual 2-dimensional planes to show the level of accuracy in prediction. For the above PO solutions, accuracy of the surrogate model has been assessed by calculating the relative % error. Most of the points are within 3% error, while few points provide more than 3% error. Similarly, the parity plots between the predictions of the four independent Kriging models and the first principle model with respect to the Kriging PO solutions are presented in the Figs. 7.9(a) – 7.9(d).

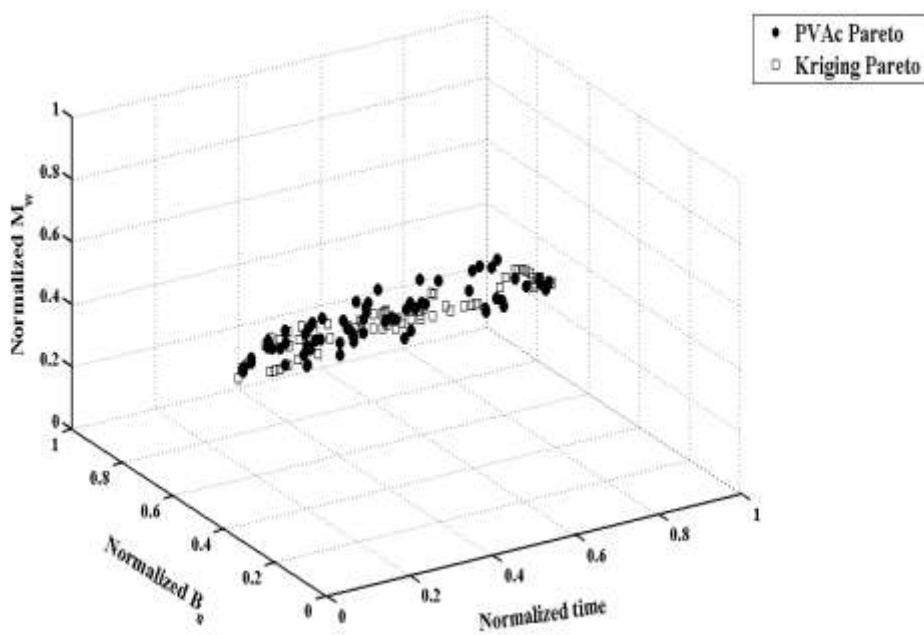


Figure 7.7: Pareto comparison of Kriging model with first principle model

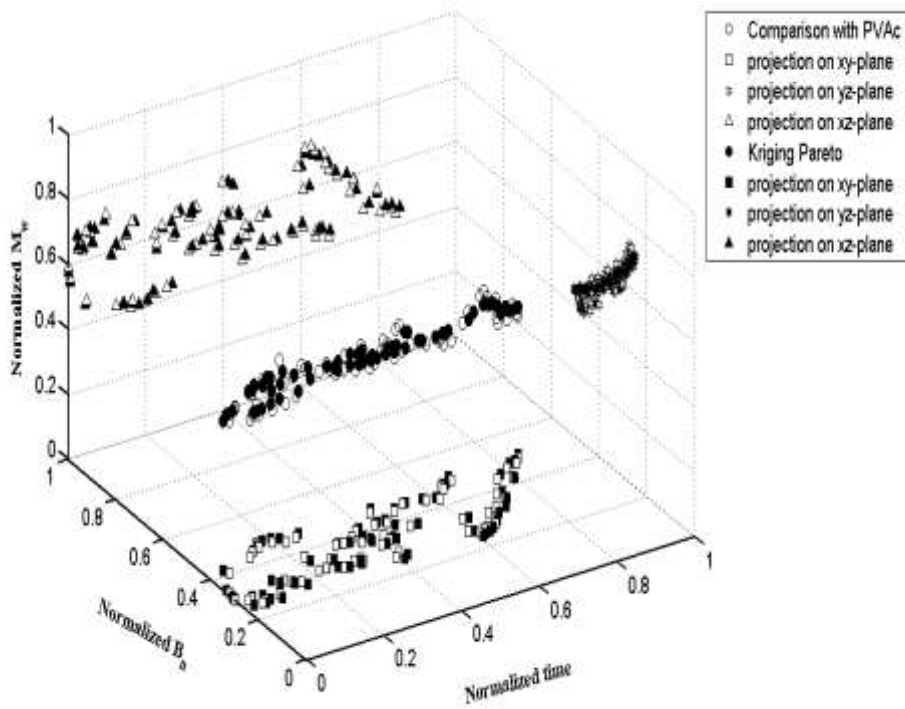


Figure 7.8: Comparison of non-dominated points projected on individual 2D plane.

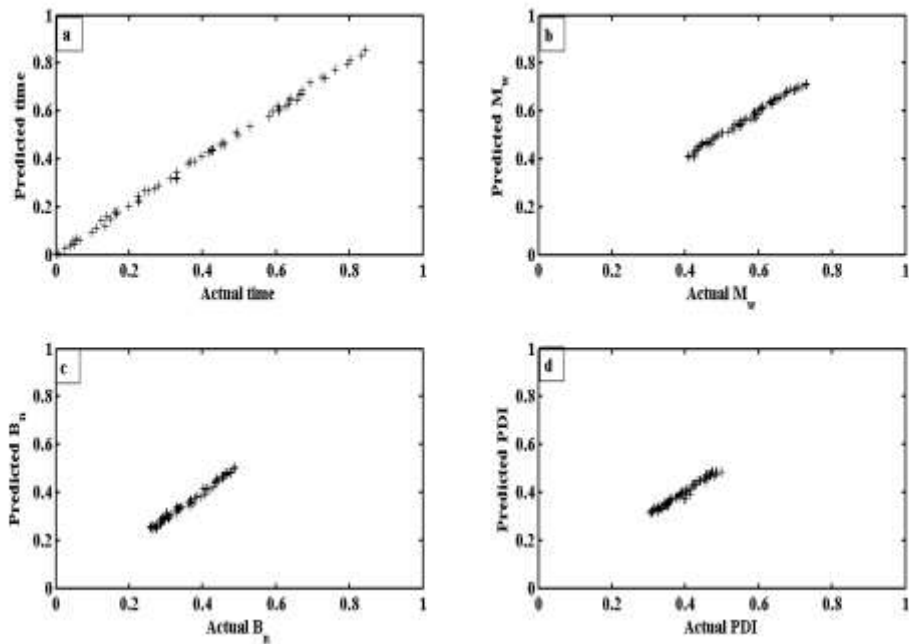


Figure 7.9: Predicted points by Kriging models obtained from NSGA II with the corresponding first principle

## 7.5 Conclusion

Simultaneous maximization of  $M_w$ ,  $B_n$  and minimization of gel point conversion time have been considered in this study with the addition of monomer, initiator and reaction temperature as decision variables. While genetic algorithm based evolutionary optimization is a preferred method of choice for solving this kind of problems, it requires high computational time with expensive first principle model. To handle this situation, original expensive first principle model has been replaced by high fidelity, parsimonious Kriging based surrogate model. These Kriging models are built incrementally; starting with a few number of sampling points, further sampling locations are decided based on the maximization of expected improvement criterion of the statistical model built. As more sampling points are added based on this criterion, quality of the model improves and this kind of model building continues till a desired accuracy in model building is achieved. Kriging assisted multi-objective optimization has provided faster execution time (~ 85% saving in function evaluations) as compared to the first principle model within reasonable accuracy.

# Chapter 8

## Conclusions and Future work

### 8.1 Conclusions

Significant contributions to multi objective optimization of branched polymers to find the optimal process conditions have been made in this research:

NSGA II has been utilized to find optimal process conditions for batch vinyl acetate polymerization process. Maximization of weight average molecular weight and number average degree of branching have been attained along with simultaneous minimization of gel point conversion time without violating the relevant process constraints (first optimization study). Monomer addition, initiator addition and reaction temperature are taken as decision variables within prescribed experimental bounds. Two multi objective optimization studies have been carried out. For the first optimization study, optimizer has provided wide range of initiator and temperature values to maximize branching and molecular weight. So, an operator can get many optimal choices to operate the reactor at different point in time based on the optimality criteria set. The second optimization case (maximization of live radical concentration and number average degree of branching in less gel point conversion time) results in another variety of solutions at relatively higher temperature range with higher live radical concentration. In short, looking at varying scenario faced by today's process operator, batch vinyl acetate polymerization process has been revisited with additional capability of controlling the degree of branching and optimum sets of operating conditions have been identified with a trade-off between conflicting process objectives for a range of temperatures.

For the first time, a mathematical model has been developed with a newly proposed kinetic mechanism by using two single site catalysts that produced long chain branched

polypropylene (isotactic back bone and atactic side chains) which can validate the experimental data in open literature [16]. The proposed model can predict the molecular properties such as molecular weight, PDI and grafting density by the tandem action of the two catalyst system with different cocatalyst to catalyst ratios, cocatalyst concentration, two catalysts ratio and the time gap between the two catalyst additions. Following important points are revealed out of this modeling exercise: (i) Molecular weight of the iPP copolymer is found to depend on the cocatalyst concentration (due to chain transfer reaction) and the cocatalyst/catalyst ratio (due to the bimolecular deactivation). (ii) Grafting density depends on the catalyst (2) addition time, ratio of the two catalysts and copolymerization time. (iii) If more time is allowed before the catalyst (2) addition, long chain branching content is increased in the copolymer due to accumulation of more amounts of aPP macromonomers in the reactor. (iv) By increasing the first catalyst to second catalyst ratio, more aPP macromonomers are grafted to the back bone of isotactic polypropylene because of the higher macromonomer concentration in the reactor.

Multi-objective optimization has been formulated for various conflicting objectives with relevant constraints using the above validated model. Maximization of iPP weight average molecular weight and grafting density have been attained along with simultaneous minimization of total polymerization time without violating the process constraints. Real coded NSGS II has been used to find the multi-objective Pareto optimal solution and corresponding operating conditions. Optimization routine provided wide variety of solutions in the entire terrain of search for this dual catalyst system. Two catalysts and one cocatalyst concentrations, time gap between the two catalyst additions and total polymerization time are used as decision variables. One of the objective functions, grafting density, strongly depends on the time gap between the two catalyst additions, ratio of the two catalysts and copolymerization time. The optimization exercise not only leads to a variety of competitive process choices but also shows improvement in process objectives as compared to the existing literature data. Solutions originating from different regions of the PO set were considered and the possible reasons for their occurrence were analyzed in detail in terms of reaction mechanisms proposed.

Genetic algorithm based evolutionary optimization is a preferred method of choice for solving the above kind of problems; it requires high computational time with expensive first principle model (eg. Simultaneous maximization of weight average molecular weight ( $M_w$ ), number average degree of branching ( $B_n$ ) and minimization of gel point conversion time for

bulk polymerization of vinyl acetate have been considered in this study with the addition of monomer, initiator and reaction temperature as decision variables.). To handle this situation, original expensive first principle model has been replaced by high fidelity, parsimonious Kriging based surrogate model. These Kriging models are built incrementally; starting with a few number of sampling points; further sampling locations are decided based on the maximization of expected improvement criterion of the statistical model built. As more sampling points are added based on this criterion, quality of the model improves and this kind of model building continues till a desired accuracy in model building is achieved. Kriging assisted multi-objective optimization has provided faster execution time (~ 85% saving in function evaluations) as compared to the first principle model within reasonable accuracy.

## **8.2 Future work**

Further elucidation of the kinetic mechanism behind the formation of long chain branched polypropylene is necessary via binary catalyst system is necessary. For this, more experimental data is necessary (for cross validation) to improve the kinetic mechanism. Conduction of further experimental study is necessary to solve the purpose. By doing so, prediction of atactic polypropylene (i.e. macromonomers) weight average molecular weight of the polymer with the experimental data can be improved. Experiments exploring very high grafting density are essential to know the possible limit of branching of polypropylene in bimetallic catalytic systems. Scarcity of available experimental data has left a clear possibility to improve the parameter estimation and subsequently widening the constraints to search for better process performances. In addition to that, investigating the individual classes, especially for highly branched cases can be taken as an important challenge, where more specific information, cause-effect relation can be revealed for the classes with higher LCBs. Uncertainty analysis of the estimated parameters is another area, which needs to be tackled inside the overall optimization frame work.

A more exhaustive model, which focuses the estimation beyond the experimental range, is necessary. This model is also referred as “tendency modeling”. It is a non-linear, lower order, dynamic model that approximates the kinetic relationships of a process using the experimental data along with basic knowledge of the process [91-93]. The model structure and parameters are updated as more data becomes available. The main purpose of the tendency model is to find a direction towards optimum. Model validation is an important

issue in tendency modeling because these are approximate models. If process-model mismatch is there, it will effect on the optimization of the process.

The results of the final optimization formulation can further be connected to the melt rheology and its direct relation to the polymer architecture to incorporate more practicality into the problem. A more exhaustive study of the extensional flow behavior of LCB PP prepared by this approach is necessary. An assortment of LCB PP with varying molecular weights and branching densities should be used to understand the relation among branching density, strain hardening and extensional viscosity.

# References

- [1] S. Thomas. Measurement and Modeling of Long Chain Branching. Ph.D. thesis, McMaster University, Canada, 1998.
- [2] J. A. Langston. Synthesis and Characterization of Long Chain Branched Isotactic Polypropylene via Metallocene catalyst and T-reagent. Ph.D. thesis, The Pennsylvania State University, USA, 2007.
- [3] Z. Ye. Synthesis, Characterization and properties of Novel Polyolefins by Single-site Catalysts. Ph.D. thesis, McMaster University, Canada, 2004.
- [4] W. -J. Wang, D. Yan, S. Zhu and A. E. Hamielec. Kinetics of Long Chain Branching in Continuous Solution Polymerization of Ethylene Using Constrained Geometry Metallocene. *Macromolecules* 31 (1998) 8677-8683.
- [5] D. Yan, W. -J. Wang, S. Zhu. Effect of long chain branching on rheological properties of metallocene polyethylene. *Polymer* 40 (1999) 1737-1744.
- [6] W. Weng, W. Hu, A.H. Dekmerzian and C.J. Ruff. Long Chain Branched Isotactic Polypropylene, *Macromolecules*, 35 (2002) 3838.
- [7] E. Kolodka, W. -J. Wang, P. A. Charpentier, S. Zhu, and A. E. Hamielec. Long-chain branching in slurry polymerization of ethylene with zirconocene dichloride/modified methylaluminoxane. *Polymer*, 41, (2000) 3985-3991.
- [8] E. Kolodka, W. -J. Wang, S. Zhu, and A. E. Hamielec. Copolymerization of Propylene with Poly(ethylene-co-propylene) Macromonomer and Branch Chain-Length Dependence of Rheological Properties. *Macromolecules*, 35 (2002) 10062-10070.
- [9] E. Kolodka, S. Zhu, and A. E. Hamielec. Synthesis and Characterization of Long-Chain-Branched Polyolefins with Metallocene Catalysts: Copolymerization of Ethylene with Poly (ethylene-co-propylene) Macromonomer. *Macromolecular rapid communications*, 24 (2003) 311-315.
- [10] T. Shiono, S.M. Azad and T. Ikeda. Copolymerization of Atactic Polypropene Macromonomer with Propene by an Isospecific Metallocene Catalyst, *Macromolecules*, 32 (1999) 5723-5727.



- [11] J.A. Langston, R.H. Colby, T.C. Mike Chung, Fumihiko Shimizu, T. Suzuki and M. Aoki. Synthesis and Characterization of Long Chain Branched Isotactic Polypropylene via Metallocene Catalyst and T-reagent, *Macromolecules*, 40 (2008) 2712-2720.
- [12] D. Graebing. Synthesis of Branched Polypropylene by a Reactive extrusion Process. *Macromolecules*, 35 (2002) 4602.
- [13] D. Auhl, J. Stange, H. Munstedt, B. Krause, D. Voigt, A. Lederer, U. Lappan and K. Lunkwitz. Long-Chain Branched Polypropylenes by Electron Beam Irradiation and Their Rheological Properties, *Macromolecules*, 37 (2004) 9465.
- [14] Z. J. A. Komon and G. C. Bazan. Synthesis of Branched Polyethylene by Tandem Catalysis. *Macromol. Rapid. Commun*, 22 (2001) 467-478.
- [15] R. F. de Souza and O. L. Casagrande. Recent Advances in Olefin Polymerization Using Binary Catalyst Systems. *Macromol. Rapid. Commun.*, 22 (2001) 1293-1301.
- [16] Z. Ye and S. J. Zhu, Synthesis of Branched Polypropylene with Isotactic backbone and atactic side chains by Binary iron and zirconium single-site catalysts. *Polym. Sci., Part A: Polym. Chem.* 41 (2003) 1152.
- [17] S. Paavola, T. Saarinen, B. Lofgren and P. Pitkanen. Propylene Copolymerization with Non-conjugated Dienes and  $\alpha$ -olefins using Supported Metallocene catalyst. *Polymer*, 45 (2004) 2099.
- [18] P. Pladis and C.Kiparissides. A comprehensive model for the calculation of molecular weight-long-chain branching distribution in free-radical polymerizations, *Chem. Eng Sci.*, 53 (1998) 3315.
- [19] K. Deb, *Multi-objective optimization using evolutionary algorithms*, Wiley, Chichester, 2001.
- [20] K. Mitra and S. Majumder. Successive approximate model based multi-objective optimization for an Industrial straight grate iron ore induration process using evolutionary algorithm. *Chem. Eng. Sci.*, 6 (2011) 3471-3481.
- [21] K. Mitra. Evolutionary Surrogate Optimization of an Industrial Sintering Process. *Materials and Manufacturing Processes*, 28 (2013) 768-775.
- [22] D. R. Jones A taxonomy of global optimization methods based on response surfaces. *Journal of Global Optimization*, 21 (2001) 345-383.
- [23] G, Dellino, P. Lino, C. Meloni and A. Rizzo. Kriging metamodel management in the design optimization of a CNG injection system. *Mathematics and Computers in Simulation*, 79 (2009) 2345-2360.

- [24] Li, M.; Li, G.; Azarm, S. A Kriging Metamodel Assisted Multi-Objective Genetic Algorithm for Design Optimization. *Journal of Mechanical Design*, 130 (2008) 031401-031410.
- [25] Li, M. An Improved Kriging-Assisted Multi-Objective Genetic Algorithm. *Journal of Mechanical Design* 133 (2011) 071008-071011.
- [26] M. Nagasawa and T. Fujimoto. Preparation, Characterization and Viscoelastic Properties of Branched Polymers. *Progress in Polymer Science*, Japan 3, (1972) 263.
- [27] M. Krajnc, I. Polijansek and J. Golob. Kinetic modeling of methyl methacrylate free-radical polymerization initiated by tetraphenyl biphosphine. *Polymer* 42, (2001) 4153-4162.
- [28] Simon P. Gretton-Watson, E. Alpay, Joachim H.G. Steinke and J.S. Higgins. Multi-functional monomer derived hyperbranched poly(methyl methacrylate): Kinetic modeling and experimental validation. *Chemical Engineering Science* 61, (2006) 1421-1433.
- [29] Keramopoulos and C. Kiparissides. Development of a Comprehensive Model for Diffusion-Controlled Free-Radical Copolymerization Reactions. *Macromolecules* 35, (2002) 4155-4166.
- [30] D.S. Achilias and C. Kiparissides. Development of a general mathematical Framework for Modeling Diffusion-Controlled Free-Radical Polymerization Reactions. *Macromolecules* 25, (1992) 3739-3750.
- [31] W. Zhou, E. Marshall and L. Oshinowo. Modeling LDPE Tubular and Autoclave Reactors. *Ind. Eng. Chem. Res.* 40, (2001) 5533-5542.
- [32] H. Tobita and K. Hatanaka. Branched Structure Formation in Free Radical Polymerization of Vinyl Acetate. *Journal of Polymer Science: Part B: Polymer Physics* 34, (1996) 671-681.
- [33] A. Chatterjee, K. Kabra and W.W. Graessley. Free-Radical Polymerization with Long Chain Branching: Batch Polymerizations of Vinyl Acetate in t-Butanol. *Journal of applied polymer science* 21, (1977) 1751-1762.
- [34] Timothy F. McKenna and A. Villanueva. Effect of Solvent on the Rate Constants in Solution Polymerization. Part II. Vinyl Acetate. *Journal of Polymer Science: Part A: Polymer Chemistry* 37, (1999) 589-601.
- [35] F. Teymour and J. D. Campbell. Analysis of the Dynamics of Gelation in Polymerization Reactors Using the "Numerical Fractionation" Technique. *Macromolecules* 27, (1994) 2460-2469.

- [36] Gurutze Arzamendi and Jose M. Asua, Modeling Gelation of Sol Molecular weight distribution in Emulsion Polymerization. *Macromolecules* 28(1995) 7479.
- [37] M. Chanda. Introduction to polymer science and chemistry, a problem solving approach. Taylor and Francis: 2006.
- [38] D. Meimaroglou, A. Krallis, V. Saliakas and C. Kiparissides. Prediction of the Bivariate Molecular weight-long chain branching distribution in highly branched polymerization systems using monte- carlo and sectional grid methods. *Macromolecules*, 40 (2007) 2224-2234.
- [39] S. Kumar and D. Ramkrishna. On the Solution of Population Balance Equations by Discretization-I. A Fixed Pivot Technique. *Chemical Engineering Science* 51, (1996) 1311-1322.
- [40] M. Asteasuain, C. Sarmoria and A. Brandolin. Recovery of molecular weight distributions from transformed domains. Part I. Application of pgf to mass balances describing reactions involving free radicals. *Polymer* 43, (2002) 2513-2527.
- [41] P. Deuffhardt, E. Hairer, Zugk, One step and extrapolation methods for differential-algebraic systems, *J. Numer. Math.* 51 (1987) 501.
- [42] M. Asteasuain, S. Pereda, M. H. Lacunza, P.E. Ugrin and A. Brandolin. Industrial High Pressure Ethylene Polymerization Initiated By Peroxide Mixtures: A Reduced Mathematical Model for Parameter Adjustment, *polymer engineering and science.* 41 (2001) 711-726.
- [43] D. Beigzadeh, J.B.P. Soares and T.A. Duever. Combined metallocene catalysts: an efficient technique to manipulate long-chain branching frequency of polyethylene, *Macromol. Rapid. Commun.* 20 (1999) 541.
- [44] H. Zou, F.M. Zhu, Q. Wu, J.Y. Ali and S.A. Lin, Synthesis of Long-Chain-Branched Polyethylene by Ethylene Homopolymerization with a Novel Nickel(II)  $\alpha$ -Diimine Catalyst, *J. Polym. Sci., Part A: Polym. Chem.* 43 (2005) 1325.
- [45] S. Mehdiabadi, J.B.P. Soares and A.H. Dekmezian. Production of Long-Chain Branched Polyolefins with Two Single-Site Catalysts: Comparing CSTR and Semi-Batch Performance. *Macromol. React. Eng.* 2 (2008) 529.
- [46] L.C. Simon and J.B.P. Soares. Monte Carlo Simulation of Long-Chain Branched Polyolefins Made with Dual Catalysts: A Classification of Chain Structures in Topological Branching Families. *Ind. Eng. Chem. Res.*, 44 (2005) 2461.
- [47] J.B.P. Soares and A.E. Hemielec. Bivariate chain length and long chain branching distribution for copolymerization of olefins and polyolefin chains containing terminal double-bonds. *Macromol. Theory Simul.* 5 (1996) 547.

- [48] S. Zhu and D. Li. Molecular weight distribution of metallocene polymerization with long chain branching using a binary catalyst system. *Macromol. Theory Simul.* 6 (1997) 793.
- [49] H. Yiannoulakis, A. Yiagopoulos, P. Pladis and C. Kiparissides. Comprehensive dynamic model for the calculation of the molecular weight and long chain branching distributions in metallocene-catalyzed ethylene polymerization reactors. *Macromolecules*, 33 (2000) 2757.
- [50] P. D. Iedema and H. C. J. Hoefsloot. A conditional Monte Carlo method to predict branched architectures from molecular weight and degree of branching distribution of polyethylene for single and mixed systems with a constrained geometry metallocene catalyst in continuous reactors. *Polymer*, 45 (2004) 6071-6082.
- [51] D. J. Read and J. B. P. Soares. Derivation of the Distributions of Long Chain Branching, Molecular Weight, Seniority, and Priority for Polyolefins Made with Two Metallocene Catalysts. *Macromolecules*, 36 (2003) 10037-10051.
- [52] J. B. P. Soares. Polyolefins with Long Chain Branches Made with Single-Site Coordination Catalysts: A Review of Mathematical Modeling Techniques for Polymer Microstructure. *Macromol. Mater. Eng.* 289 (2004) 70-87.
- [53] A. TSoukas, M. V. Tirrel and G. Stephanopoulos. Multiobjective Dynamic Optimization of Semibatch Copolymerization Reactors. *Chemical engineering science*, 37 (1982) 1785.
- [54] L. T. Fan, C. S. Landis, and S. A. Patel. In *Frontiers in Chemical Reaction Engineering*, L. K. Dorais wamy and R. A. Mashelkar, Eds., Wiley Eastern, New Delhi, 1984, p. 609.
- [55] K. Mitra, K. Deb and S. K. Gupta. Multiobjective Dynamic Optimization of an Industrial Nylon 6 Semibatch Reactor Using Genetic Algorithm. *J. Appl. Polym. Sci.*, 69 (1998) 69-87.
- [56] S. Raha, S. Majumdar and K. Mitra. Effect of Caustic Addition in Epoxy Polymerization Process: A Single and Multi-Objective Evolutionary Approach. *Macromolecular Theory and Simulations* 13, (2004) 152-161.
- [57] K. Mitra, S. Majumdar and S. Raha. Multiobjective Optimization of a Semibatch Epoxy Polymerization Process Using the Elitist Genetic Algorithm. *Ind. Eng. Chem. Res.* 43, (2004) 6055-6063.
- [58] S. Majumdar, K. Mitra and S. Raha. Optimized species growth in epoxy polymerization with real coded NSGA-II. *Polymer* 46, (2005) 11858-11869.

- [59] S. Majumdar, K. Mitra and G. Sardar. Kinetic Analysis & Optimization for the Catalytic Esterification Step of PPT Polymerization. *Macromolecular Theory and Simulations*, 14 (2005) 49-59.
- [60] K. Mitra and S. Majumdar. Selection of Catalyst for the Esterification Step of the PPT Polymerization Process. *Macromolecular Theory and Simulations*, 15 (2006) 497-506.
- [61] B. S. Sundaram, S. R. Upreti and A. Lohi. Optimal Control of Batch MMA Polymerization with Specified Time, Monomer Conversion, and Average Polymer Molecular Weights. *Macromolecular theory and simulations*, 14 (2005) 374-386.
- [62] S. R. Upreti, B. S. Sundaram and A. Lohi. Optimal control determination of MMA polymerization in non-isothermal batch reactor using bifunctional initiator. *European polymer journal*, 41 (2005) 2893-2908.
- [63] N. Agrawal, G. P. Rangaiah, A. K. Ray, and S. K. Gupta. Multi-objective Optimization of the Operation of an Industrial Low-Density Polyethylene Tubular Reactor Using Genetic Algorithm and Its Jumping Gene Adaptations. *Ind. Eng. Chem. Res.*, 45 (2006) 3182-3199.
- [64] K. Mitra. Genetic algorithms in polymeric material production, design, processing and other applications: a review. *International materials reviews*, 53 (2008) 275-297.
- [65] V. Bhaskar, S. K. Gupta and A. K. Ray. Multiobjective Optimization of an Industrial Wiped-Film Pet Reactor. *AICHE*, 46 (2000) 1046-1058.
- [66] R. B. Kasat, A. K. Ray and S. K. Gupta. Applications of genetic algorithm in polymer science and engineering. *Materials and Manufacturing processes*, 18 (2003) 523-532.
- [67] M. Ramteke and S. K. Gupta. Kinetic modeling and reactor simulation and optimization of industrially important polymerization processes: a perspective. *International Journal of Chemical Reactor Engineering*, 9(1) (2011) 1-54.
- [68] S. Datta and P. P. Chattopadhyay. Soft computing techniques in advancement of structural metals. *International Material Reviews*, 58(8) (2013) 475-504.
- [69] W. Paszkowicz. Genetic Algorithms, a Nature-Inspired Tool: A Survey of Applications in Materials Science and Related Fields: Part II. *Materials and Manufacturing Processes*, 28 (2013) 708-725.
- [70] P. Nain and K. Deb. A computationally effective multi-objective search and optimization techniques using coarse-to-fine grain modeling. In *Proceedings of the PPSN Workshop on Evolutionary Multiobjective Optimization 2002*.

- [71] Y. A. Jin. Comprehensive survey of fitness approximation in evolutionary computation. *Soft Computing*, 9 (2005) 3–12.
- [72] P. Bradshaw, G. A. Mizner and K. Unsworth. Calculation of compressible turbulent boundary layers on straight-tapered swept wings. *American Institute of Aeronautics and Astronautics Journal*, 14 (1976) 399–400.
- [73] R. Smith, B. Dike and S. Stegmann. Fitness inheritance in genetic algorithms. In *Proceedings of ACM Symposiums on Applied Computing*, Nashville, TN, February (1995) 345–350.
- [74] M. Farina. A neural network based generalized response surface multiobjective evolutionary algorithms. In *Congress on Evolutionary Computation*; IEEE Press: New York, (2002) 956–961.
- [75] Clarke, S.M., J. H. Griebisch and T. W. Simpson. Analysis of support vector regression for approximation of complex engineering analyses. *Journal of Mechanical Design*, 127 (2005) 1077–1087.
- [76] H. Nakayama, M. Arakawa and R. Sasaki. Simulation-based optimization using computational intelligence. *Optimization and Engineering*, 3 (2002) 201–214.
- [77] G. Meghabghab. Iterative radial basis functions neural networks as metamodels of stochastic simulations of the quality of search engines in the World Wide Web. *Information Processing and Management*, 37 (2001) 571–591.
- [78] J. A. Biles. Genjam: a genetic algorithm for generating jazz solos. In: *Proceedings of the International Computer Music Conference*, (1994) 131–137.
- [79] L. Bull. On model-based evolutionary computation. *Soft Computing* , 3 (1999) 76–82.
- [80] A. Ratle. Accelerating the convergence of evolutionary algorithms by fitness landscape approximation. In *Proceedings of Parallel Problem Solving from Nature*, V, Amsterdam, The Netherlands, September 27–30, (1998) 87–96.
- [81] Y. Jin, M. Olhofer and B. Sendhoff. A framework for evolutionary optimization with approximate fitness functions. *IEEE Transactions on Evolutionary Computation*, 6 (2002) 481–494.
- [82] V. Oduguwa and R. Roy. Multiobjective optimization of rolling rod product design using metamodeling approach. In: *Proceedings of the Genetic and Evolutionary Computation Conference*, Morgan Kaufmann, (2002) 1164–1171.
- [83] Y. F. Li, S. H. Ng, M. Xie and T. N. Goh. A systematic comparison of metamodeling techniques for simulation optimization in Decision Support Systems. *Appl. Soft Comput. J.*, 10 (2010) 1257–1273.

- [84] S. Hou, Q. Li, S. Long, X. Yang and W. Li. Multiobjective optimization of multi-cell sections for the crash worthiness design. *International Journal of Impact Engineering*, 35 (2008) 1355-1367.
- [85] M. Guedri, S. Ghanmi, R. Majed, and N. Bouhaddi. Robust tools for prediction of variability and optimization in structural dynamics. *Mechanical Systems and Signal Processing*, 23 (2009) 1123–1133.
- [86] G. Sun, G. Li, Z. Gong, X. Cui, X. Yang and Q. Li Multiobjective robust optimization method for drawbead design in sheet metal forming. *Materials and Design*, 31 (2010) 1917-1929.
- [87] B. K. Giri, F. Pettersson, H. Saxen and N. Chakraborti. Genetic Programming Evolved through Bi-Objective Genetic Algorithms Applied to a Blast Furnace. *Materials and Manufacturing Processes*, 28 (2013) 776-782.
- [88] T. Chen, K. Hadinotoa, Y. Wenjin Yana, Y. Ma. Efficient meta-modelling of complex process simulations with time–space-dependent outputs. *Computers and chemical engineering*, 35 (2011) 502-509.
- [89] D. R. Jones, M. Schonlau and W. Welch. Efficient Global Optimization of Expensive Black-Box Functions. *Journal of global optimization*, 13 (1998) 455-492.
- [90] G. Chi, S. Hu, Y. Yang and T. Chen. Response surface methodology with prediction uncertainty: A multi-objective optimisation approach, 90 (2012) 1235-1244.
- [91] D. Visser, R. van der Heijden, K. Mauch, M. Reuss, S. Heijnen. Tendency Modeling: A new approach to obtain simplified kinetic models of metabolism applied to *saccharomyces cerevisiae*, 2 (2000) 252-275.
- [92] J. Fotopoulos, C. Georgakis, H. Stenger. Effect of process-model mismatch on the optimization of the catalytic epoxidation of oleic acid using tendency models, 51 (1996) 1899-1908.
- [93] J. Fotopoulos, C. Georgakis, H. Stenger. Uncertainty issues in the modeling and optimization of batch reactors with tendency models, 49 (1994) 5533-5548.
- [94] J. M. Asua. *Polymer Reaction Engineering*, Blackwell publishing, UK, 2007.
- [95] A. Butte´, A. Ghielmi, G. Storti and M. Morbidelli. Calculation of molecular weight distributions in free-radical polymerization with chain branching. *Macromol. Theory Simul.*, 8 (1999) 498-512.
- [96] S. M. Walas. *Modeling with differential equations in chemical engineering*. Boston, USA. Butterworth-Heinemann; 1991.

- [97] A. Krallis and C. Kiparissides. Mathematical modeling of the bivariate molecular weight- long chain branching distribution of highly branched polymers. A population balance approach. *Chem. Eng. Sci.*, 62 (2007) 5304-5311.
- [98] P.D. Hustad, R.L. Kuhlman, E.M. Carnahan, T.T. Wenzel and D.J. Arriola. An exploration of the effects of reversibility in chain transfer to metal in olefin polymerization. *Macromolecules*, 41 (2008) 4081.
- [99] J.B.P. Soares and T.F.L. McKenna, *Polyolefin Reaction Engineering*, Wiley, 2012.
- [100] M. Atiqullah, H. Hammawa and H. Hamid. Modeling the solubility of ethylene and propylene in a typical polymerization diluent: some selected situations. *Eur. Polym.J.*, 34 (1998) 1511.
- [101] S. I. Sandler. *Chemical and Engineering Thermodynamics*, John Wiley and Sons, (1989).
- [102] B.L. Small and M. Brookhart. Polymerization of Propylene by a New Generation of Iron Catalysts: Mechanisms of Chain Initiation, Propagation, and Termination. *Macromolecules*, 32 (1999) 2120.
- [103] E. Ochoteco, M. Vecino, M. Montes and J.C. De la Cal. Kinetics and properties in metallocene catalysed propene polymerisations. *Chem. Eng. sci.*, 56 (2001) 4169.
- [104] S. Mehdiabadi and J.B.P. Soares. Ethylene Homopolymerization Kinetics with a Constrained Geometry Catalyst in a Solution Reactor. *Macromolecules*, 45 (2012) 1777.
- [105] S.T. Babik and G. Fink. Propylene polymerization with a bisiminepyridine iron complex: activation with  $\text{Ph}_3\text{C} [\text{B}(\text{C}_6\text{F}_5)_4]$  and  $\text{AlR}_3$ ; iron hydride species in the catalytic cycle. *J. Mol. Catal. A: Chem.*, 188 (2002) 245.
- [106] A. Mogilicharla, T. Chugh, S. Majumdar and K. Mitra. Multi-objective Optimization of Bulk Vinyl Acetate Polymerization with Branching. *Materials and Manufacturing Processes*, 29 (2014) 210-217.
- [107] R. L. J. Coetzer, J. P. Engelbrecht, J. C. Crause and D. K. J. Lin. Statistical Robustness Study for Kinetic Models. *Industrial Engineering and Chemistry Research*, 49 (2010) 2932-2942.



# List of publications

## Journal Papers

1. Anitha Mogilicharla, Tinkle Chugh, Saptarshi Majumdar and K. Mitra. Multi-Objective Optimization of Bulk Vinyl Acetate Polymerization with Branching. *Materials and Manufacturing Processes*, 29 (2014) 210-217.
2. Anitha Mogilicharla, Kishalay Mitra and Saptarshi Majumdar. Modeling of propylene polymerization with long chain branching, *Chemical Engineering Journal*, 246 (2014) 175-183.
3. Anitha Mogilicharla, Saptarshi Majumdar and Kishalay Mitra. Multi Objective Optimization of Long Chain Branched Propylene Polymerization. *Polymer Engineering and Science*, DOI 10.1002/pen.23977.
4. Anitha Mogilicharla, Prateek Mittal, Saptarshi Majumdar and Kishalay Mitra. Kriging Surrogate based Multi-objective Optimization of Bulk Vinyl Acetate Polymerization with Branching. *Materials and Manufacturing Processes*, DOI: 10.1080/10426914.2014.921709.

## Peer reviewed international conference proceedings:

1. Anitha Mogilicharla, Saptarshi Majumdar and K. Mitra. Modeling and Optimization of Propylene Polymerization with Branching, *Proceedings of European Symposium on Computer Aided Process Engineering (ESCAPE 24)*, June 15 – 18, Computer Aided Chemical Engineering, *Elsevier*, 33, 1435-1440.
2. Anitha Mogilicharla, Saptarshi Majumdar and K. Mitra. Kinetic Analysis and Optimization of Long Chain Branched Propylene Polymerization System, *IFAC'14*, Cape Town, August 2014, accepted.

## Conferences

1. Tinkle Chugh, Anitha Mogilicharla and Saptarshi Majumdar. Study of Branching in Batch Free Radical Polymerization of vinyl Acetate and Calculation of Molecular weight-Long Chain Branching Distributions, *TACEE*, BITS PILANI, PILANI CAMPUS.
2. Anitha Mogilicharla, Tinkle Chugh, Saptarshi Majumdar and Kishalay Mitra. Optimal Process Conditions for the Controlled Branching of Free Radical Polymerization: A Case Study, *Chemcon2012*, NIT Jalandhar.

3. Anitha Mogilicharla, Saptarshi Majumdar and Kishalay Mitra. Optimal process conditions for the controlled branching of polymers, ICNP-2012, Mahatma Gandhi University, Kottayam, Kerala.
4. Anitha Mogilicharla, Saptarshi Majumdar and Kishalay Mitra. Effect of live radical species in controlled branching of bulk free radical polymerization system: A multiobjective evolutionary approach, ACE 2013, IIT Roorkee.

**Under Preparation for Submission in International Journal:**

Optimal process conditions to increase particular branching for long chain branched propylene polymerization

# Appendices (Few Source Codes)

## Appendix A

### Fortran Code to solve ODEs (numerical fractionation) using RK technique

```
c -----  
c Program for solving ODEs  
c Based on the Runge Kutta method  
c -----
```

```
program nf  
  real kp,kfp,kfm,kft,ktd,ktc,ki,t  
  integer counter,r  
  integer i,j,k  
  common /ani/ counter  
  
  parameter (dist=0.1)  
  parameter (maxi=180000)  
  real B,xn,xw,y  
  dimension B(29),xn(8),xw(8),y(8)  
  real z  
  dimension z(8)  
  real w(8,200000),wt(200000)  
  external runge4,x,find_fact  
  open (unit = 1, file = "rungekutta2.txt")  
  
  B(1)=8.43      ! monomer  
  B(2)=0.001    ! initiator  
  B(3)=0.0      ! solvent  
  B(4)=0.0  
  B(5)=0.0  
  B(6)=0.0
```

B(7)=0.0

B(8)=0.0

B(9)=0.0

B(10)=0.0

B(11)=0.0

counter=1

do k=12,29

    B(k)=0.0

end do

do j=1,maxi

    t=j\*dist

    if(t.Le.Maxi) then

        call runge4(t,B,dist)

    if(B(1).LE. 1.686) then

        GO TO 40

    end if

end if

end do

40 r=7

    do i=1,3

        xn(i)=B(r)/B(r-1)

        xw(i)=B(r+1)/B(r)

        z(i)=1/((xw(i)/xn(i))-1)

        y(i)=(z(i)+1)/xw(i)

        r=r+3

    do j=1,200000,5

        A= find\_fact(nint (z(i)))

        w(i,j)=(y(i)\*(j\*y(i))\*\*z(i))\*exp(-j\*y(i))/ A

    end do

```

end do
      do j=1,200000,5
          wt(j)=(w(1,j)*B(7)+w(2,j)*B(10)+w(3,j)*B(13))/B(5)
          WRITE(1,*) j, wt(j)
      end do

```

```

close(1)
end

```

```

c -----

```

```

c Subroutine for runge kutta

```

```

c Input : tval, B, Step size

```

```

c -----

```

```

subroutine runge4(tval, B, step)
    integer i
    real tval
    real B(29)
    real h,step
    real t1(29),t2(29),t3(29)
    real k1(29),k2(29),k3(29),k4(29)
    real fval1,fval2,fval3,fval4
    h=step/2
    do i=1,29
        fval1 = x(tval,B,i)
        k1(i)=step*fval1
        t1(i)=B(i)+0.5*k1(i)
    end do
    do i=1,29
        fval2 = x(tval+h,t1,i)
        k2(i)=step*fval2
        t2(i)=B(i)+0.5*k2(i)
    end do
    do i=1,29
        fval3 = x(tval+h,t2,i)
        k3(i)=step*fval3
        t3(i)=B(i)+0.5*k3(i)

```

```

end do
do i=1,29
  fval4 = x(tval+step,t3,i)
  k4(i)=step*fval4
end do
do i=1,29
  B(i)=B(i)+(k1(i)+2*k2(i)+2*k3(i)+k4(i))/6.0
end do
return
end

```

c -----

c Function for calculating runge kutta

c Input : tval, B, p

c -----

```

function x(tval,B,p)
integer i,j,k,det
real sum1,sum2
integer p ,coun
real tval
real B
real R0,R1,R2,p0,p1,p2
real lam0
real B0,B1,B2
dimension R0(8),R1(8),R2(8),p0(6),p1(6),p2(6)
dimension B0(8),B1(8),B2(8)
dimension B(29)
real kp,kfp,kft,kfm,ktc,ktd,ki
integer n
real lval
common /ani/ coun
kp=500.0
kfp=0.50
kfm=0.09070
kft=0.0
ktd=0.0

```

ktc= 5970000.0

ki=0.00000118

lval=(2\*ki\*B(2))/(kct+ktc)

lam0= SQRT(lval)

R0(1)=(kfm\*B(1)+kft\*B(3)+kct\*lam0+ktc\*lam0)\*lam0/(kfm\*B(1)+  
& kft\*B(3)+(kct+ktc)\*lam0+kfp\*B(5))

R1(1)=(kp\*B(1)\*R0(1)+(kfm\*B(1)+kft\*B(3)+kct\*lam0+ktc\*lam0+  
& kfp\*B(5))\*lam0)/(kfm\*B(1)+kft\*B(3)+(kct+ktc)\*lam0+kfp\*B(5))

R2(1)=(2\*kp\*B(1)\*R1(1)+(kfm\*B(1)+kft\*B(3)+kct\*lam0+ktc\*lam0+  
& kfp\*B(5))\*lam0)/(kfm\*B(1)+kft\*B(3)+(kct+ktc)\*lam0+kfp\*B(5))

R0(2)=(kfp\*lam0\*(B(7)+B(10)))/(kfm\*B(1)+kft\*B(3)+(kct+ktc)\*lam0+  
& kfp\*B(5))

R1(2)=(kp\*B(1)\*R0(2)+kfp\*lam0\*(B(8)+B(11)))/(kfm\*B(1)+kft\*B(3)+  
& (kct+ktc)\*lam0+kfp\*B(5))

if((B(7).eq.0).OR.(B(6).eq.0).OR.(B(10).eq.0).OR.(B(9).eq.0))then

R2(2)=(kp\*B(1)\*(R0(2)+2\*R1(2)))/(kfm\*B(1)+kft\*B(3)+(kct+ktc)\*lam0  
& +kfp\*B(5))

else

R2(2)=(kp\*B(1)\*(R0(2)+2\*R1(2))+kfp\*lam0\*B(8)\*((2\*B(8)/B(7))-B(7)  
& /B(6)))+kfp\*lam0\*B(11)\*((2\*B(11)/B(10))-B(10)/B(9)))/(kfm\*B(1)  
& +kft\*B(3)+(kct+ktc)\*lam0+kfp\*B(5))

end if

if(p.eq.1) then

x=-kp\*lam0\*B(1)-kfm\*lam0\*B(1)

end if

if(p.eq.2) then

```

x=-ki*B(2)
end if
if(coun.eq.1) then
do k=3,8
  B0(k)=0.0
end do
do k=3,8
  B1(k)=0.0
end do
do k=3,8
  B2(k)=0.0
end do
end if
if(p.eq.3) then
x=-kft*lam0*B(3)
end if

if(p.eq.4) then
x=(kfm*B(1)+kft*B(3))*lam0+ktc*lam0*lam0/2+ktd*lam0*lam0
end if

if(p.eq.5) then
x=kp*B(1)*lam0
end if

if(p.eq.6) then
x=(kfm*B(1)+kft*B(3)+ktd*lam0)*R0(1)-kfp*lam0*B(7)+kfp*B(5)*R0(1)
& +ktc*R0(1)*R0(1)/2
end if

if(p.eq.7) then
x=(kfm*B(1)+kft*B(3)+ktd*lam0)*R1(1)-kfp*lam0*B(8)+ktc*R0(1)*
& R1(1)+kfp*B(5)*R1(1)
end if

```



```

if(p.eq.8) then
  if((B(7).eq.0).OR.(B(6).eq.0)) then
    x=(kfm*B(1)+kft*B(3)+ktd*lam0)*R2(1)+kfc*(R1(1)*R1(1)+R0(1)*
&      R2(1))+kfp*B(5)*R2(1)

  else
    x=(kfm*B(1)+kft*B(3)+ktd*lam0)*R2(1)-kfp*lam0*B(8)*((2*B(8)/
& B(7))-(B(7)/B(6)))+kfc*(R1(1)*R1(1)+R0(1)*R2(1))+kfp*B(5)*R2(1)
  end if
end if

if(p.eq.9) then
  x=(kfm*B(1)+kft*B(3)+ktd*lam0+kfp*B(5))*R0(2)-kfp*lam0*B(10)+kfc*
&      R0(1)*R0(2)
end if

if(p.eq.10) then
  x=(kfm*B(1)+kft*B(3)+ktd*lam0+kfp*B(5))*R1(2)-kfp*lam0*B(11)+
&      kfc*(R1(1)*R0(2)+R1(2)*R0(1))
end if

if(p.eq.11) then
  if((B(10).eq.0).OR.(B(9).eq.0)) then
    x=(kfm*B(1)+kft*B(3)+ktd*lam0+kfp*B(5))*R2(2)+kfc*(R2(2)*R0(1)
&      +2*R1(2)*R1(1)+R0(2)*R2(1))
  else
    x=(kfm*B(1)+kft*B(3)+ktd*lam0+kfp*B(5))*R2(2)-kfp*lam0*B(11)*
& ((2*B(11)/B(10))-(B(10)/B(9)))+kfc*(R2(2)*R0(1)+2*R1(2)*R1(1)+
&      R0(2)*R2(1))
  end if
end if

if(p.GE.12) then
  do i=3,8
    sum1=0.0
    sum2=0.0

```

```

do j=1,i-1
  sum1= sum1+ R0(j)
  sum2= sum2+R1(j)
end do
R0(i)=(kfp*lam0*B1(i))/(kfm*B(1)+kft*B(3)+(ktc+kt d)*lam0+
&      kfp*B(5))

R1(i)=(kp*B(1)*R0(i)+kfp*lam0*B2(i))/(kfm*B(1)+kft*B(3)+(ktc+
&      ktd)*lam0+kfp*B(5))
if((B1(i).eq.0) .OR.(B0(i).eq.0))      then
  R2(i)=kp*B(1)*(R0(i)+2*R1(i))/(kfm*B(1)+kft*B(3)+(ktc+kt d)*
&      lam0+kfp*B(5))

else
  R2(i)=(kp*B(1)*(R0(i)+2*R1(i))+kfp*lam0*B2(i)*((2*B2(i)/B1(i)
&      -(B1(i)/B0(i)))))/(kfm*B(1)+kft*B(3)+(ktc+kt d)*lam0+kfp*B(5))
end if

p0(i)=(kfm*B(1)+kft*B(3)+kfp*B(5)+kt d*lam0)*R0(i)-kfp*lam0*B1(i)+
&      ktc*R0(i)*sum1+ktc*R0(i-1)*R0(i-1)/2

p1(i)=(kfm*B(1)+kft*B(3)+kfp*B(5)+kt d*lam0)*R1(i)-kfp*lam0*B2(i)+
&      ktc*R0(i-1)*R1(i-1)+ktc*(R0(i)*sum2+R1(i)*sum1)

if((B1(i).eq.0) .OR.(B0(i).eq.0))      then
  p2(i)=(kfm*B(1)+kft*B(3)+kfp*B(5)+kt d*lam0)*R2(i)+ktc*(R1(i-1)
&      *R1(i-1)+R0(i-1)*R2(i-1))+ktc*(R2(i)*sum1+2*R1(i)*sum2+R0(i)
&      *sum2)
else
  p2(i)=(kfm*B(1)+kft*B(3)+kfp*B(5)+kt d*lam0)*R2(i)-kfp*lam0*
&      B2(i)*((2*B2(i)/B1(i)-(B1(i)/B0(i))))+ktc*(R1(i-1)*R1(i-1)
&      +R0(i-1)*R2(i-1))+ktc*(R2(i)*sum1+2*R1(i)*sum2+R0(i)*sum2)
end if
end do
det= p-11

```

```

n=3
do while(det.GT.3)
  det=det-3
  n=n+1
end do
if(det .eq. 1) then
  x= p0(n)
  else if (det .eq. 2) then
  x=p1(n)
  else if(det.EQ. 3)      then
  x= p2(n)
  end if
end if
  coun=coun+1
return
end

```

c -----

c Function for calculating factorial value

c Input : integer value

c Output: Output

c -----

```

function find_fact( m)
integer j
  find_fact =1
  do 10 j=2,m
    find_fact=find_fact*j
10  continue
end

```

## Appendix B

### Fortran Code to solve ODEs (partition according to number of branches) using LIMEX DAE solver

```
program rctngflows
implicit none
  double precision y(225), ys(225), h
  double precision Ropt(5), t_Begin, t_End
  double precision aTol, rTol, sum1(200000)
  integer n,r, i,i1,l, Iopt(30), IFail(3), IPos(225)
  double precision w(35,200000),wt(200000)
  real y1(35),z(35),xn(35),xw(35),xm(35),j
  real findfact
  double precision Bn,Bw,sigmasq(35),p,q,TT,TM,TI
  external Fcn, Jacobian,findfact

  n = 225          ! Total number of equations
  t_Begin = 0
  t_End = 10000
  h = 0
  aTol = 1e-5
  rTol = 1e-5

  c----- Initial Values -----

  y(1) = 12.0      ! Momomer
  y(2) = 0.0001    ! Initiator
  y(3) = 0.0       ! solvent
  y(4) = 0         ! zeroth moment live
  y(5) = 0         ! 1st moment live
  y(6) = 0         ! 2nd moment live
  y(7) = 0         ! zeroth moment dead
  y(8) = 0         ! 1st moment dead
  y(9) = 0         ! 2nd moment dead
```

```
do i=10, 225
  y(i)= 0
end do
do i=1,225
  ys(i) =0
end do
do i = 1, 10
  Iopt(i) = 0
end do
Iopt(8) = n
Iopt(9) = n
Iopt(10) = 1
Iopt(12) = 1
Iopt(13)= 1
Iopt(14)= 0
Iopt(15)=0
Iopt(16)=0
Iopt(17)=0
Iopt(18)=0

do i = 1, 5
  Ropt(i)=0
end do

do i = 1, 225
  IPos(i) = 0
end do

do i = 1, 3
  IFail(i) = 0
end do
open(unit=1,file='output.txt')
open(unit=101,file='output1.txt')
```

```

do while(t_Begin.lt.t_End)

    Bn=0.0

    call XLIMEX( n,Fcn, Jacobian, t_Begin, t_End, y, ys,
&              rTol, aTol, h, Iopt, Ropt, IPos, IFail)

    do i= 1, 20
        Bn=Bn+i*y(6*i+13)
    end do

    if(Bn .ge. 0.9) then

        go to 40
    end if
end do

40  r=14
    do i=1,9
        xn(i)=(y(r)+y(r-3))/(y(r-1)+y(r-4))
        xw(i)=(y(r+1)+y(r-2))/(y(r)+y(r-3))
        sigmasq(i)= ALOG(xw(i)/xn(i))
        xm(i)= ((y(r+1)+y(r-2))/(y(r-1)+y(r-4)))**0.5

        r=r+6
        do j=1,200000,5

            p= LOG(j)
            q= ALOG(xm(i))
            w(i,j)=(2*3.1428*j*j*sigmasq(i))**(-0.5)*
&  exp(-(p-q)**2/(2*sigmasq(i)))

            end do
        end do

```

```

do j=1,200000,1
  sum1(j)=0.0

end do
  do j=1,200000,5
    do i= 1, 9
      sum1(j)=sum1(j)+w(i,j)*y(6*i+7)/y(8)
    end do
    write(1,*) j, sum1(j)
  end do
close(1)
stop
end

```

```

c -----
Function for calculating LIMEX

```

```

c -----
subroutine Fcn(n, nz, t,y,f,b,ir,ic,FcnInfo)
implicit none

integer i,i1,i2,j,n, nz, ir(*),ic(*), FcnInfo
double precision t,y(*),f(*), b(*)
double precision kp,ktc,ktd,kfm,kfp,kdb,kd,kfs
double precision lam0(35),lam1(35),lam2(35)
double precision flam0(35),flam1(35),flam2(35)
double precision mu0(35),mu1(35),mu2(35)
double precision fmu0(35),fmu1(35),fmu2(35)
double precision sum,sum1,sum2,sum3,sum4,sum5,sum6
double precision sum7,sum8,sum9,sum10
real temp,fr
nz = 225          ! number of odes

```

```

c-----
c  kinetic constants
c-----

```

```

temp=80+273
fr=0.5

```

```

kp=4.2E9*exp(-6300/(1.98*temp))
kd=2.7E16*exp(-30000/(1.98*temp))
ktc=1.62E12*exp(-2800/(1.98*temp))
kfm=4.957E8*exp(-10480/(1.98*temp))
kfp=5.177E8*exp(-11440/(1.98*temp))
ktd=0.0
kdb=0.66*kp
kfs=0.0

```

! ODEs

```

f(1)= -kp*y(4)*y(1)
f(2)= -kd*y(2)
f(3)= -kfs*y(4)*y(3)
f(4)= 2*fr*kd*y(2)-(kfc+ktd)*y(4)*y(4)
f(5)= 2*fr*kd*y(2)-(kfm*y(1)+kfs*y(3))*y(5)+kp*y(1)*y(4)-(kfc+ktd)
&      *y(4)*y(5)+kfp*(y(4)*y(9)-y(5)*y(8))+kdb*y(4)*y(8)
  if(y(8) .eq. 0 .or. y(7) .eq. 0) then
f(6)= 2*fr*kd*y(2)-(kfm*y(1)+kfs*y(3))*y(6)+2*kp*y(1)*y(5)-
& (kfc+ktd)*y(4)*y(6)+kfp*(-y(6)*y(8))+kdb*(2*y(5)*y(8)+y(4)*y(9))
  else
f(6)= 2*fr*kd*y(2)-(kfm*y(1)+kfs*y(3))*y(6)+2*kp*y(1)*y(5)-
& (kfc+ktd)*y(4)*y(6)+kfp*(y(4)*
&((y(9)/(y(8)*y(7)))*(2*y(9)*y(7)-y(8)*y(8)))-y(6)*y(8))+
& kdb*(2*y(5)*y(8)+y(4)*y(9))
  end if

f(7)= (kfm*y(1)+kfs*y(3))*y(4)+(kfc/2+ktd)*y(4)*y(4)-kdb*y(4)*y(7)
f(8)= (kfm*y(1)+kfs*y(3))*y(5)+(kfc+ktd)*y(4)*y(5)-kdb*y(4)*y(8)
& -kfp*(y(4)*y(9)-y(5)*y(8))

  if(y(8) .eq. 0 .or. y(7) .eq. 0) then
f(9)= (kfm*y(1)+kfs*y(3))*y(6)+(kfc+ktd)*y(4)*y(6)-kdb*y(4)*y(9)
& +kfc*y(5)*y(5)+kfp*(y(6)*y(8))

  else

```



$$\begin{aligned}
f(9) &= (kfm*y(1)+kfs*y(3))*y(6)+(kfc+ktd)*y(4)*y(6)-kdb*y(4)*y(9) \\
&\& \quad +kfc*y(5)*y(5)-kfp*(y(4)*((y(9)/(y(8)*y(7))))* \\
&\& \quad (2*y(9)*y(7)-y(8)*y(8)))-y(6)*y(8)
\end{aligned}$$

end if

$$flam0(1)= f(10)$$

$$lam0(1)= y(10)$$

$$flam1(1)= f(11)$$

$$lam1(1)= y(11)$$

$$flam2(1)= f(12)$$

$$lam2(1)=y(12)$$

$$fmu0(1)=f(13)$$

$$mu0(1)=y(13)$$

$$fmu1(1)=f(14)$$

$$mu1(1)=y(14)$$

$$fmu2(1)=f(15)$$

$$mu2(1)=y(15)$$

$$\begin{aligned}
flam0(1) &= (kfm*y(1)+kfs*y(3))*y(4)+2*fr*kd*y(2)-(kfm*y(1)+kfs*y(3)+ \\
&\& \quad (kfc+ktd)*y(4)+kfp*y(8)+kdb*y(7))*lam0(1)
\end{aligned}$$

$$\begin{aligned}
flam1(1) &= kp*y(1)*lam0(1)+(kfm*y(1)+kfs*y(3))*y(4)+2*fr*kd*y(2)- \\
&\& \quad (kfm*y(1)+kfs*y(3)+(kfc+ktd)*y(4)+kfp*y(8)+kdb*y(7))*lam1(1)
\end{aligned}$$

$$\begin{aligned}
flam2(1) &= 2*kp*y(1)*lam1(1)+(kfm*y(1)+kfs*y(3))*y(4)+2*fr*kd*y(2)- \\
&\& \quad (kfm*y(1)+kfs*y(3)+(kfc+ktd)*y(4)+kfp*y(8)+kdb*y(7))*lam2(1)
\end{aligned}$$

$$\begin{aligned}
fmu0(1) &= (kfm*y(1)+kfs*y(3)+ktd*y(4)+kfp*y(8))*lam0(1)+kfc*lam0(1)* \\
&\& \quad lam0(1)/2-kfp*y(4)*mu1(1)-kdb*y(4)*mu0(1)
\end{aligned}$$

$$\begin{aligned}
fmu1(1) &= (kfm*y(1)+kfs*y(3)+ktd*y(4)+kfp*y(8))*lam1(1)+kfc*lam0(1)* \\
&\& \quad lam1(1)-kfp*y(4)*mu2(1)-kdb*y(4)*mu1(1)
\end{aligned}$$

if(mu0(1) .eq. 0 .or. mu1(1) .eq. 0) then

```

fmu2(1)=(kfm*y(1)+kfs*y(3)+ktd*y(4)+kfp*y(8))*lam2(1)+ktc*(lam0(1)
& *lam2(1)+lam1(1)*lam1(1))-kdb*y(4)*mu2(1)
else
fmu2(1)=(kfm*y(1)+kfs*y(3)+ktd*y(4)+kfp*y(8))*lam2(1)+ktc*(lam0(1)
& *lam2(1)+lam1(1)*lam1(1))-kdb*y(4)*mu2(1)-kfp*y(4)*mu2(1)*
& (2*mu2(1)*mu0(1)-mu1(1)*mu1(1))/mu1(1)*mu0(1)

```

```

end if

```

```

f(10)= flam0(1)
y(10)= lam0(1)
f(11)= flam1(1)
y(11)= lam1(1)
f(12)= flam2(1)
y(12)= lam2(1)
f(13)= fmu0(1)
y(13)= mu0(1)
f(14)= fmu1(1)
y(14)= mu1(1)
f(15)= fmu2(1)
y(15)= mu2(1)

```

```

i2=16

```

```

i1=16

```

```

do i=2,35

```

```

    lam0(i)=y(i2)

```

```

    lam1(i)=y(i2+1)

```

```

    lam2(i)=y(i2+2)

```

```

    mu0(i)=y(i2+3)

```

```

    mu1(i)=y(i2+4)

```

```

    mu2(i)=y(i2+5)

```

```

    flam0(i)=f(i2)

```

```

    flam1(i)=f(i2+1)

```

flam2(i)=f(i2+2)

fmu0(i)=f(i2+3)

fmu1(i)=f(i2+4)

fmu2(i)=f(i2+5)

i2=i2+6

sum = 0.0

sum1= 0.0

sum2= 0.0

sum3= 0.0

sum4= 0.0

sum5= 0.0

sum6= 0.0

sum7= 0.0

sum8= 0.0

sum9= 0.0

sum10=0.0

do j=1,i-1

sum=sum+lam0(j)\*mu0(i-j)

sum1=sum1+lam0(j)\*mu1(i-j)

sum2=sum2+lam1(j)\*mu0(i-j)

sum3=sum3+lam0(j)\*mu2(i-j)

sum4=sum4+lam1(j)\*mu1(i-j)

sum5=sum5+lam2(j)\*mu0(i-j)

end do

do j=1,i

sum6=sum6+lam0(j)\*lam0(i-j+1)

sum7=sum7+lam0(j)\*lam1(i-j+1)

sum8=sum8+lam0(j)\*lam2(i-j+1)

sum9=sum9+lam1(j)\*lam1(i-j+1)

sum10=sum10+lam2(j)\*lam0(i-j+1)

end do

flam0(i)= kfp\*y(4)\*mu1(i-1)+kdb\*sum-(kfm\*y(1)+kfs\*y(3)+

```

& (ktc+ktc)*y(4)+kfp*y(8)+kdb*y(7))*lam0(i)

flam1(i)=kp*y(1)*lam0(i)+kfp*y(4)*mu2(i-1)+kdb*(sum1+sum2)-
& (kfm*y(1)+kfs*y(3)+(ktc+ktc)*y(4)+kfp*y(8)+kdb*y(7))*lam1(i)

if(mu0(i) .eq. 0 .or. mu1(i) .eq. 0) then
flam2(i)=2*kp*y(1)*lam1(i)+kdb*(sum3+2*sum4+sum5)-
& (kfm*y(1)+kfs*y(3)+(ktc+ktc)*y(4)+kfp*y(8)+kdb*y(7))*lam2(i)
else
flam2(i)=2*kp*y(1)*lam1(i)+kdb*(sum3+2*sum4+sum5)-
& (kfm*y(1)+kfs*y(3)+(ktc+ktc)*y(4)+kfp*y(8)+kdb*y(7))*lam2(i)
& +kfp*y(4)*mu2(i)*(2*mu2(i)*mu0(i)-mu1(i)*mu1(i))/mu1(i)*mu0(i)
end if

fmu0(i)=(kfm*y(1)+kfs*y(3)+ktd*y(4)+kfp*y(8))*lam0(i)+ktc*sum6/2-
& kfp*y(4)*mu1(i)-kdb*y(4)*mu0(i)

fmu1(i)=(kfm*y(1)+kfs*y(3)+ktd*y(4)+kfp*y(8))*lam1(i)+ktc*sum7-
& kfp*y(4)*mu2(i)-kdb*y(4)*mu1(i)

c write(101,*) y(1),y(4),y(8),sum6
if(mu0(i) .eq. 0 .or. mu1(i) .eq. 0) then

fmu2(i)=(kfm*y(1)+kfs*y(3)+ktd*y(4)+kfp*y(8))*lam2(i)+ktc*(sum8/2+
& +sum9+sum10/2)-kdb*y(4)*mu2(i)

else

fmu2(i)=(kfm*y(1)+kfs*y(3)+ktd*y(4)+kfp*y(8))*lam2(i)+ktc*(sum8/2+
& +sum9+sum10/2)-kdb*y(4)*mu2(i)-kfp*y(4)*mu2(i)*(2*mu2(i)*
& mu0(i)-mu1(i)*mu1(i))/mu1(i)*mu0(i)

end if

y(i1)= lam0(i)

```

```
y(i1+1)= lam1(i)
y(i1+2)= lam2(i)
y(i1+3)= mu0(i)
y(i1+4)= mu1(i)
y(i1+5)= mu2(i)
```

```
f(i1)= flam0(i)
f(i1+1)= flam1(i)
f(i1+2)= flam2(i)
f(i1+3)= fmu0(i)
f(i1+4)= fmu1(i)
f(i1+5)= fmu2(i)
```

```
    i1=i1+6
end do
do i =1,225
    b(i) = 1
    ir(i) = i
    ic(i) = i
end do
return
end
subroutine Jacobian
return
end
```